IAEA TECDOC SERIES

IAEA-TECDOC-1865

Reliability of Advanced High Power, Extended Burnup Pressurized Heavy Water Reactor Fuels

Final Report of a Coordinated Research Project

IAEA
International Atomic Energy Agency

RELIABILITY OF ADVANCED HIGH POWER, EXTENDED BURNUP PRESSURIZED HEAVY WATER REACTOR FUELS

The following States are Members of the International Atomic Energy Agency:

AFGHANISTAN
ALBANIA
ALGERIA
ANGOLA
ANTIGUA AND BARBUDA
ARGENTINA
ARMENIA
AUSTRALIA
AUSTRIA
AZERBAIJAN
BAHAMAS
BAHRAIN
BANGLADESH
BARBADOS
BELARUS
BELGIUM
BELIZE
BENIN
BOLIVIA, PLURINATIONAL STATE OF
BOSNIA AND HERZEGOVINA
BOTSWANA
BRAZIL
BRUNEI DARUSSALAM
BULGARIA
BURKINA FASO
BURUNDI
CAMBODIA
CAMEROON
CANADA
CENTRAL AFRICAN REPUBLIC
CHAD
CHILE
CHINA
COLOMBIA
CONGO
COSTA RICA
CÔTE D'IVOIRE
CROATIA
CUBA
CYPRUS
CZECH REPUBLIC
DEMOCRATIC REPUBLIC OF THE CONGO
DENMARK
DJIBOUTI
DOMINICA
DOMINICAN REPUBLIC
ECUADOR
EGYPT
EL SALVADOR
ERITREA
ESTONIA
ESWATINI
ETHIOPIA
FIJI
FINLAND
FRANCE
GABON
GEORGIA
GERMANY
GHANA
GREECE
GRENADA
GUATEMALA
GUYANA
HAITI
HOLY SEE
HONDURAS
HUNGARY
ICELAND
INDIA
INDONESIA
IRAN, ISLAMIC REPUBLIC OF
IRAQ
IRELAND
ISRAEL
ITALY
JAMAICA
JAPAN
JORDAN
KAZAKHSTAN
KENYA
KOREA, REPUBLIC OF
KUWAIT
KYRGYZSTAN
LAO PEOPLE'S DEMOCRATIC REPUBLIC
LATVIA
LEBANON
LESOTHO
LIBERIA
LIBYA
LIECHTENSTEIN
LITHUANIA
LUXEMBOURG
MADAGASCAR
MALAWI
MALAYSIA
MALI
MALTA
MARSHALL ISLANDS
MAURITANIA
MAURITIUS
MEXICO
MONACO
MONGOLIA
MONTENEGRO
MOROCCO
MOZAMBIQUE
MYANMAR
NAMIBIA
NEPAL
NETHERLANDS
NEW ZEALAND
NICARAGUA
NIGER
NIGERIA
NORTH MACEDONIA
NORWAY
OMAN
PAKISTAN
PALAU
PANAMA
PAPUA NEW GUINEA
PARAGUAY
PERU
PHILIPPINES
POLAND
PORTUGAL
QATAR
REPUBLIC OF MOLDOVA
ROMANIA
RUSSIAN FEDERATION
RWANDA
SAINT LUCIA
SAINT VINCENT AND THE GRENADINES
SAN MARINO
SAUDI ARABIA
SENEGAL
SERBIA
SEYCHELLES
SIERRA LEONE
SINGAPORE
SLOVAKIA
SLOVENIA
SOUTH AFRICA
SPAIN
SRI LANKA
SUDAN
SWEDEN
SWITZERLAND
SYRIAN ARAB REPUBLIC
TAJIKISTAN
THAILAND
TOGO
TRINIDAD AND TOBAGO
TUNISIA
TURKEY
TURKMENISTAN
UGANDA
UKRAINE
UNITED ARAB EMIRATES
UNITED KINGDOM OF GREAT BRITAIN AND NORTHERN IRELAND
UNITED REPUBLIC OF TANZANIA
UNITED STATES OF AMERICA
URUGUAY
UZBEKISTAN
VANUATU
VENEZUELA, BOLIVARIAN REPUBLIC OF
VIET NAM
YEMEN
ZAMBIA
ZIMBABWE

The Agency's Statute was approved on 23 October 1956 by the Conference on the Statute of the IAEA held at United Nations Headquarters, New York; it entered into force on 29 July 1957. The Headquarters of the Agency are situated in Vienna. Its principal objective is "to accelerate and enlarge the contribution of atomic energy to peace, health and prosperity throughout the world''.

IAEA-TECDOC-1865

RELIABILITY OF ADVANCED HIGH POWER, EXTENDED BURNUP PRESSURIZED HEAVY WATER REACTOR FUELS

FINAL REPORT OF A COORDINATED RESEARCH PROJECT

INTERNATIONAL ATOMIC ENERGY AGENCY
VIENNA, 2019

COPYRIGHT NOTICE

For further information on this publication, please contact:

Nuclear Fuel Cycle and Materials Section
International Atomic Energy Agency
Vienna International Centre
PO Box 100
1400 Vienna, Austria
Email: Official.Mail@iaea.org

Printed by the IAEA in Austria
March 2019

IAEA Library Cataloguing in Publication Data

Names: International Atomic Energy Agency.
Title: Reliability of advanced high power, extended burnup pressurized heavy water reactor fuels / International Atomic Energy Agency.
Description: Vienna : International Atomic Energy Agency, 2019. | Series: IAEA TECDOC series, ISSN 1011–4289 ; no. 1865 | Includes bibliographical references.
Identifiers: IAEAL 19-01220 | ISBN 978–92–0–101319–4 (paperback : alk. paper)
Subjects: LCSH: Fuel burnup (Nuclear engineering). | Nuclear fuels. | Pressurized water reactors.

FOREWORD

Proven natural uranium fuel bundle designs have been used for decades for most pressurized heavy water reactors (PHWRs). However, there has been a need to operate these fuel bundles at extended burnup for reasons such as savings on fuel cycle costs, reductions of spent fuel volume, synergy with light water reactor fuel strategies and increased refuelling intervals. Extended burnup operation in PHWRs is possible with use of advanced fuel cycles such as slightly enriched uranium, reprocessed uranium, plutonium doped uranium oxide and thorium based fuels.

In parallel with high burnup fuels, modifications in current bundle design are of interest for examining margin recovery in ageing reactors. Large overpower trip margins established at the beginning of life are reduced steadily over time. If no action is taken, the reactor may need to be operated at a reduced power to ensure enough operating margin to trip. Local power peaks (i.e. end flux peaking, refuelling ripples) make the situation worse. Advanced fuel design is one of the various options for enhancing operational and safety margins.

All countries with operating PHWRs have invested significant effort in developing advanced fuels for extended burnup and for enhanced operational and safety margins in PHWRs. Some of these countries show significant progress in this area in terms of industrial efforts, while others lag behind. The present publication reports on the work undertaken as part of a coordinated research project entitled Reliability of High Power, Extended Burnup and Advanced PHWR Fuels. The project, carried out from 2014 to 2018, was aimed at encouraging and sharing research on the challenges encountered when deploying advanced fuels for extended burnup and for enhanced operational and safety margins.

The IAEA wishes to thank all the project participants and their Member States, and in particular those who contributed to the preparation of this publication. The IAEA officers responsible for this publication were U. Basak and K. Sim of the Division of Nuclear Fuel Cycle and Waste Technology.

EDITORIAL NOTE

This publication has been prepared from the original material as submitted by the contributors and has not been edited by the editorial staff of the IAEA. The views expressed remain the responsibility of the contributors and do not necessarily represent the views of the IAEA or its Member States.

Neither the IAEA nor its Member States assume any responsibility for consequences which may arise from the use of this publication. This publication does not address questions of responsibility, legal or otherwise, for acts or omissions on the part of any person.

The use of particular designations of countries or territories does not imply any judgement by the publisher, the IAEA, as to the legal status of such countries or territories, of their authorities and institutions or of the delimitation of their boundaries.

The mention of names of specific companies or products (whether or not indicated as registered) does not imply any intention to infringe proprietary rights, nor should it be construed as an endorsement or recommendation on the part of the IAEA.

The authors are responsible for having obtained the necessary permission for the IAEA to reproduce, translate or use material from sources already protected by copyrights.

The IAEA has no responsibility for the persistence or accuracy of URLs for external or third party Internet web sites referred to in this publication and does not guarantee that any content on such web sites is, or will remain, accurate or appropriate.

CONTENTS

1. INTRODUCTION

1.1. BACKGROUND

Presently, 45 pressurized heavy water reactors (PHWRs[1]) are operating in seven countries using mainly natural uranium (NU) fuel. These reactors operate with a fuel discharge burnup of approximately 7000 MWd/tU. The fuel designs, fabrication facilities, reactor operation and spent fuel management are tailored to these conditions.

Many advanced fuels are under consideration for application in PHWRs. Most of these fuels involve higher burnups than those obtained with NU. To achieve high burnups, the fissile content of the fuel is increased as compared to NU. This may lead to high initial power and consequently an increase in the defect probability. Modifications to fuel design and/or refueling scheme may be required. Some of the Member States are working on slightly enriched uranium (SEU), reprocessed uranium, thorium and plutonium-doped uranium oxide (MOX) fuels for PHWRs.

In India, besides using NU fuel bundles, the aforementioned materials have been designed, fabricated and loaded in commercial reactors. Thorium-based fuel bundles have been loaded as part of initial fuel charges for flux flattening for new units. Mixed oxide fuel bundles and 0.9% SEU fuel bundles have been loaded as lead fuel assemblies in operating units. Fuel elements with different MOX types were also loaded in research reactors for test irradiation. In Romania, experimental fuel elements containing thorium and SEU were tested in a research reactor. In Canada, advanced fuels such as SEU, MOX, reprocessed uranium and thorium have also been tested in research reactors and in a power reactor. In China, natural uranium equivalent (NUE) fuel has been demonstration-irradiated in a power reactor. The NUE fuel consisted of a mixture of reprocessed uranium and depleted uranium and was equivalent with NU in nuclear aspects. Atucha-1 in Argentina is operating with a full core loading of an advanced fuel cycle since the year 2000. An increase of the uranium enrichment from natural uranium to 0.85% U-235 in this reactor increased the average discharge burnup of the fuel from 5900 MWd/tU to more than 11 000 MWd/tU. The main consequence of this improvement is an important reduction of the fuel consumption and spent fuel volume and thus to improve the fuel economy.

Extended burnup fuels also pose new challenges to existing fuel design and manufacturing techniques. Fuel reliability issues at extended burnups include, but are not limited to, release of gaseous and volatile fission products, changes of microstructure, excessive pellet-cladding interaction (PCI), build-up of internal gas pressure, fuel swelling, degradation of thermal-physical properties of fuel, cladding corrosion and stress corrosion cracking (SCC), etc. Some experimental observations of PHWR fuel behaviors at extended burnups are described in [1]. Attention is also required for the performance of fuels under off-normal and accident conditions. Similar issues have been addressed for light water reactor (LWR) fuel and fuel assemblies since the discharge burnup of LWR fuels is much higher than that of PHWR fuels. PHWR fuel characteristics, for horizontal channel type, are quite different from LWR fuel characteristics with respect to thin cladding thickness, high linear element rating (LER), high

[1] It is necessary to clarify that as most of the PHWRs in operation are of the horizontal channel type (i.e. CANDUs and Indian PHWRs), the considerations of this reports are referred to this type of reactors unless otherwise specified. The vertical channel type PHWRs include Atucha-1 and -2 reactors, both operated in Argentina.

centreline temperature, absence of plenum volume, on-power refueling, etc., which all could affect fuel performance. This indicates that technical basis for PHWR fuels need to be extended if high burnup is to be pursued.

In parallel with high burnup fuels, modifications in current bundle design have been perused for margin recovery in ageing reactors. In horizontal channel type PHWRs (i.e. CANDUs), large overpower trip margins are established at the beginning of life. Over time, as the reactor ages, certain conditions degrade from the beginning of life. As a result, the overpower trip margins are reduced steadily over time. If no action is taken, the reactor may need to be operated at a reduced power to ensure enough operating margin to trip. Local power peaks (i.e. end flux peaking, refueling ripples) will make the situation worse. Advanced fuel design is considered as an option among required actions.

With this background, the Coordinated Research Project (CRP) entitled Reliability of High Power, Extended Burnup and Advanced PHWR Fuels was launched by the IAEA in May 2014 to provide a platform for PHWR countries to develop and share research work on resolving the challenges in deploying extended burnup and advanced fuels in PHWRs.

Five partners actively participated in this CRP: three Research Agreements were signed with Canada (Royal Military College of Canada), India (Bhabha Atomic Research Centre (BARC)) and Korea (Korea Atomic Energy Research Institute (KAERI), and two Research Contracts were signed with Argentina (National Commission on Atomic Energy (CNEA)) and Romania (Institute for Nuclear Reactor (INR)).

1.2. OBJECTIVE

The objective of this publication is to provide a comprehensive summary of the technical work carried out under the CRP entitled Reliability of High Power, Extended Burnup and Advanced PHWR Fuels, and to provide an overview of Member States' approaches[2] to mitigate challenges that are encountered in achieving reliability, sustainability and safety with advanced PHWR fuels. These challenges include: fuel performance degradation; insufficient availability of operating experience at high burnup and margin erosion by ageing.

1.3. SCOPE

This CRP was intended to encourage the development and sharing of research work on mitigating the challenges in deploying advanced fuels for extended burnup and power recovery in PHWRs. Specifically, the following items were analyzed:

- Fuel concepts[3] for higher burnup (design, materials and fabrication);
- Life limiting aspects of extended burnup;
- Fuel concepts[3] leading to enhanced operational and safety margins.

1.4. STRUCTURE

This report is organized into four main sections.

---

[2] Commercial activities are not included.

[3] The term 'fuel concepts' is referred to 'viable fuel design options' to achieve higher burnup or enhanced operational and safety margins.

Section 1, given here, provides a brief introduction.

Section 2 describes fuel concepts that can be considered for extended burnup PHWR fuels. Specifically, the following subjects are dealt with:

- Design options to improve element ratings, fission gas release (FGR) and resistance to PCI-induced fuel failure;
- Adequacy of advanced fuel materials;
- Improvement of analysis tools;
- Experimental database at extended burnup.

Section 3 describes fuel concepts that can be considered to enhance operational and safety margins. Specifically, the following subjects are dealt with:

- Design options to enhance the critical heat flux of fuel bundles;
- Design options to mitigate local power peaking.

In Section 4, outcomes from Sections 2 and 3 and future challenges are described.

In Section 5, a summary of the CRP is presented.

Description of Sections 2 and 3 is supported by five Annexes that provide details of this CRP study.

2. FUEL CONCEPTS FOR HIGHER BURNUP

2.1. OVERVIEW

Advanced fuel concepts for PHWR high burnup have been proposed based on operational experiences, literature review, design analysis using computer codes, irradiation tests and associated results from post irradiation examinations (PIEs).

Slightly enriched uranium (SEU) has been mainly considered for achieving the extended discharge burnup. In the Argentine Atucha-1 PHWRs (vertical channel type PHWRs), an increase of fuel enrichment from NU to 0.85% U-235 has increased the discharge burnup to approximately twice of the typical NU fuel burnup. Based on the good operating experience with 0.85% SEU fuel, it is planned to increase the enrichment of the Atucha-2 fuels to extend the fuel discharge burnup to approximately 13 000 MWd/tU. Evidently, additional advantages of SEU utilization have been the reduction of spent fuel volume and refueling frequency.

Burnup increase will affect the operation of the nuclear power plants, which will restrict power ramps in fuel bundles at high burnup. Some design improvements have been considered to mitigate issues related to high burnup.

Thorium based fuel cycle could be a viable option for burnup extension in CANDUs (horizontal channel type PHWRs). In this CRP study, a thorium based fuel has been selected for assessment in line with the following criteria:

- Bringing sustainability to PHWR nuclear fuel cycles;
- Enhancing safety and reliability by utilizing its good thermal properties;
- Enhancing proliferation resistance.

A 43-element bundle design has been selected as the carrier for the thorium based fuel. The discharge burnup could be extended to three times the typical NU burnup. The suitability of using the selected thorium based fuel in a CANDU core has been preliminarily examined from various aspects including reactor physics comparability, manufacturability and in-reactor fuel performance. The in-reactor fuel performance has been supported by an irradiation test and associated results from PIEs, with supplementary analysis using fuel analysis codes. Legacy issues of fuel performance at extended burnups have also been investigated via an irradiation of UO_2 fuel during a prolonged period in a power reactor, followed by PIEs.

2.2. IMPROVEMENTS FOR ELEMENT RATING, FISSION GAS RELEASE AND RESISTANCE TO PELLET-CLADDING INTERACTION INDUCED FAILURE

2.2.1. Bundle design for low element rating

2.2.1.1. Bundle design improvement for CANDUs

Excessive fission gas release (FGR) and a significant accumulation of gas pressure in the fuel element have been identified as a showstopper for high burnup operation of a CANDU fuel. In this CRP study, the 43-element fuel bundle has been selected as the carrier of advanced fuel material (i.e. $(Th,U)O_2$, refer to Section 2.3.1) considered for extended burnup. The maximum LER in a 43-element bundle is 20% lower than that of a reference 37-element bundle (hereafter called 37R bundle) [2], reducing the consequences of most design-basis accidents. The lower LER is achieved by adding extra elements and using larger-diameter elements in the two center rings and smaller-diameter ones in the outer two rings.

Since the 43-element bundle design has been qualified for use, following extensive irradiation tests at the material test reactor and demonstration irradiations in power reactors [2]–[4], it is technically feasible to select the 43-element bundle design as the carrier of the advanced fuel material for high burnup in CANDUs.

2.2.1.2. Bundle design improvement for Atucha reactors

The Atucha type bundle designs have not been significantly changed for high burnup, except for some structural materials, ductility adjustment of cladding material and use of SEU. In the fuel elements, the plenum has been increased to provide more volume for fission gases released. The ductility of the cladding material was increased to reduce the fuel rod susceptibility to PCI failure on power ramps [5]. Detailed description of the Atucha-type fuel bundle designs can be found in [6].

In Atucha-1, the maximum LER is managed by the optimized in-core fuel management strategy (refer to Section 2.3.2).

2.2.2. Pellet design improvements for low fission gas release

The increase of fuel discharge burnup requires an increase of fuel enrichment and a reduction of the release of fission gases during the irradiation. For normal operations, FGR is affected by grain sizes in the pellets due to increase in the diffusion length of fission gas atoms. The large grain size in the pellets can be achieved by several means, for example, as listed below:

- Use of additives;

- Changes in sintering conditions;
- Use of heat treated U_3O_8 powder.

Pros and cons of these means have been investigated mainly via literature survey. The following results were obtained (see Annex I for details):

- Among several additive candidates (Cr_2O_3, TiO_2, Nb_2O_5, Al_2O_3), the use of 0.05 wt.% of chrominium oxide (Cr_2O_3) is proposed as a first option for consideration. The use of Cr_2O_3 (0.05 wt.%) would increase the average grain size to 30 – 40 microns, without requiring significant changes in the current industrial manufacturing process;
- Changes in the sintering process, as described in Annex I, may allow to obtain large grain sizes. Changes in sintering conditions are not feasible in current industrial plants mainly due to high costs;
- U_3O_8 seeds improve the distribution of particle sizes and facilitate the formation of large grains. Its fabrication does not need significant changes in the manufacturing process. A sintering temperature of 325°C is proposed.

The benefits of having a large grain size is expected to diminish with high LER, at which columnar grains can be formed in the pellet, and high pellet density, based on limited Canadian experience [7] on irradiation performance of large-grained UO_2 fuel.

2.2.3. Cladding design improvements for enhanced resistance to pellet-cladding interaction induced failure

At extended burnup under normal operating conditions, PHWR fuel elements may become more susceptible to PCI-induced fuel failures at power ramps. Under these operating conditions, stress corrosion cracking (SCC) is known as the major failure mechanism. Several new cladding materials and internal coatings that can mitigate this susceptibility have been examined (see Annex I for details). These studies are the basis for Lead Test Assembly (LTA) programme to evaluate the new materials. The details of this study are described in Annex I.

Two approaches are considered as design measures to mitigate PCI-induced fuel failures.

2.2.3.1. Internal coatings

The graphite coating DAG-154 is commonly used in CANDUs. The protection against PCI-SCC is achieved mainly because of its ‘getter’ property, as the carbon absorbs iodine in the form of a complex stabilized zirconium iodide.

At greater demands on ramp powers and higher burnup, the siloxane coating is known to have a better performance against fuel failures. The poly-siloxane coating is an attractive option for CANDU fuels, and new coating technologies have been developed [8].

In case of long fuel elements like in the vertical channel type PHWRs, the application and control of non-metallic coatings is difficult. An alternative option is the use of Zr-liner as it is used for boiling water reactors [9].

An LTA programme has been proposed in Argentina. It would include the following steps:

- Processes adaptation and qualification for new coatings and liners;

- Fabrication of fuel rods for irradiation tests in research reactors;
- Post-irradiation inspection including:
  - External visual inspection looking for cladding failures or other abnormalities
  - Internal characterization of the microstructure of the coating, especially in the zones of PCI
  - Bonding and thickness control
  - Chemical analysis
  - Mechanical properties testing on irradiated samples.

At the end of the irradiation an on-line sipping and post-irradiation inspection would be performed.

2.2.3.2. New cladding materials

The use of new cladding materials to mitigate the PCI-SCC fuel failure has also been reviewed. The result indicated that for PHWR conditions there is no need to replace the current cladding material.

2.3. ADVANCED FUEL MATERIALS

2.3.1. $(Th,U)O_2$ fuel in CANDUs

The technical basis of using $(Th,U)O_2$ fuel for high burnup in a CANDU reactor has been examined from various aspects, including comparability on reactor physics results (with fuel management consideration), manufacturability and in-reactor performance of fuel bundle. These results are described in the following subsections.

2.3.1.1. Reactor physics analysis

Mixed oxide of UO_2 and ThO_2 (hereafter called $(Th,U)O_2$ fuel) has been selected in Romania for this CRP study, taking into account thorium potential benefits of large abundance (three times higher than uranium), desirable thermal properties and proliferation resistance. Fuel compositions have been preliminarily determined in line with the following considerations:

- Target discharge burnup - approximately three times the typical NU fuel burnup;
- Flat radial power distribution for the core;
- Large depletion of U-235;
- Proliferation resistance - less contents of fissile plutonium isotopes remain in the spent fuel.

For simulation exercises, a total of 72 cases have been generated by various combinations of the following three parameters:

- Pellet density in the range of 9.0 – 9.6 g/cm^3;
- U-235 enrichment in the range of 5 – 10 wt%;
- Th/U weight ratio: in the range of 60/40 – 70/30 %.

Lattice analysis was performed (refer to Annex V for details). Sixty simulation cases with U-235 enrichments ≥ 6 wt.% showed discharge burnups exceeding 20 000 MWd/t. The fuel was assumed to be discharged when the cell multiplication factor became less than 1, thus defining the bundle end of life. Then, in the fresh fuel, the overall U-235 concentration per heavy

element (HE) was estimated to be 1 – 4 wt.%. The fuel pellets in the fuel bundle were assumed to have a uniform composition.

Figure 1 shows the fractional ring powers across the bundle radius at discharge. From the figure,

- C37 indicates the 37-NU fuel element bundle;
- C43 indicates the 43-NU fuel element bundle;
- T43 caz 14 indicates the 43-element bundle with 40% UO_2 (6 wt.% U-235) – 60% ThO_2 fuel (9 g/cm^3 density);
- T43 caz 55 indicates the 43-element bundle 30% UO_2 (5 wt.% U-235) – 70% ThO_2 fuel (9.6 g/cm^3 density).

DRAGON [10] and WIMS [11] computer codes were used in this study. Results from each code were compared to ensure consistency (see Table 1 and Fig.1).

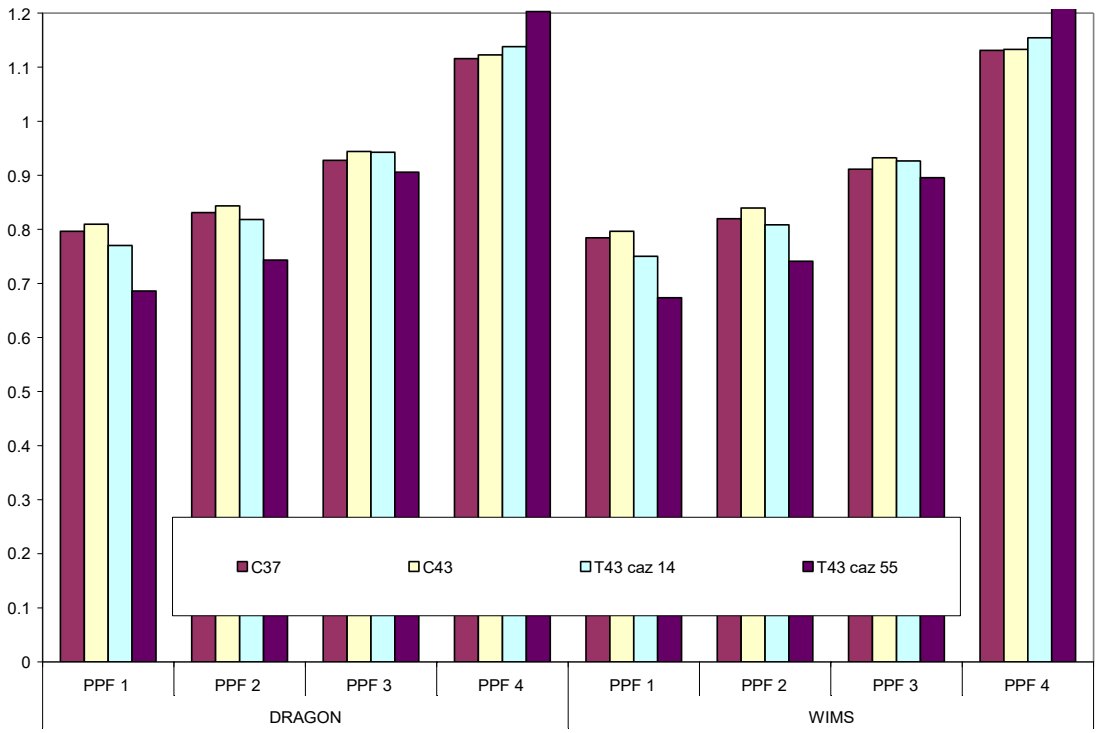

FIG.1. Radial power distributions at the end of life of fuel bundles.

The most balanced (caz 14) and the most unbalanced (caz 55) were selected to be represented. The analysis showed that at the discharge burnup the radial power distribution in the bundle becomes less flat when the Th/U ratio increases, leading to higher power at the outer ring for the same bundle geometry. This will slightly increase the maximum LER of the (Th,U)O_2 outer element compared to UO_2 fuel in the 43-element bundle (e.g. 5–9 %). PPF1 – PPF4 indicate the relative powers on the centre, inner, intermediate and outer rings, respectively.

Similar to the UO_2 fuel, the void reactivity of (Th,U)O_2 fuel becomes slightly more positive with burnup. However, it is less than the UO_2 fuel, especially at the beginning of the bundle life. The void effect increases with burnup due to presence of U-233. Overall, the lattice characteristics of (Th,U)O_2 fuel are comparable to those of NU fuel.

TABLE 1. RADIAL POWER DISTRIBUTIONS AT END OF LIFE

Case	*Code used*	*Density (g/cm^3)*	*UO_2 (%)*	*Enrichment (U-235, %)*	*Maximum burnup (MWd/t-HE)*	*PPF1*	*PPF2*	*PPF3*	*PPF4*
C37	DRAGON	0	100	0.71	6534	0.796	0.831	0.928	1.116
C43	DRAGON	0	100	0.71	6431	0.810	0.844	0.944	1.123
T43 caz 14	DRAGON	9	40	6	> 20 000	0.770	0.818	0.943	1.138
T43 caz 55	DRAGON	9.6	30	5	5263	0.686	0.743	0.906	1.203
C37	WIMS	0	100	0.71	7062	0.785	0.820	0.911	1.131
C43	WIMS	0	100	0.71	6976	0.796	0.839	0.933	1.133
T43 caz 14	WIMS	9	40	6	> 20 000	0.750	0.809	0.927	1.154
T43 caz 55	WIMS	9.6	30	5	5786	0.674	0.741	0.896	1.212

The isotopic concentrations at the discharge burnup were also analyzed. As an exercise, the 43-element bundle with 30% UO_2 (10 wt.% U-235) – 70% ThO_2 fuel (9.8 g/cm^3 density) was illustrated as an example. The results are summarized below in comparison with the 37-NU fuel element bundle case:

- To assess the fuel consumption, the amounts of uranium isotopes were estimated at the end of life as percentage of initial fuel mass. For the considered thorium based fuel, the values were 28.1% for U-235 and 98.5% for U-238 in percentage of initial mass, while for the 37-NU fuel element bundle the values were 37.2% and 98.9%, respectively. When these values were converted into absolute values, the remaining U-235 fraction in the thorium fuel bundle was estimated to be around 1.12 wt.%, while in the NU fuel bundle it was estimated to be around 0.03 wt.%. The high concentration of the residual U-235 implies the necessity of subsequent cycles for enhancing the fissile utilization;

- The thorium based fuel contained less amount of plutonium isotopes (i.e. 20% as compared to 57% for the NU) at the end of life, which demonstrates proliferation resistance of the thorium based fuel.

Core follow analysis up to 950 full power days (FPDs) was also done with the following assumptions:

- Two-bundle-shift in the central core region and four-bundle-shift in the outer core region;
- Two compositions were considered in the bundle:
  - Case 4, 43-element bundle with 40% UO_2 (5 wt.% U-235) – 60% ThO_2 (9.6 g/cm^3 density)
  - Case 64, 43-element bundle with 30% UO_2 (8 wt.% U-235) – 70% ThO_2 (9.6 g/cm^3 density).

As shown in Table 2, the maximum bundle power and the maximum channel power of the thorium based fuel core were higher than those of NU fuel in the 37R bundle. The maximum element power and its increase were comparable to those obtained for the NU fuel element in the 37R bundle.

For both thorium based fuel cases, the P_{max} appeared to be below the power-ramp failure threshold, while the ΔP exceeded the other threshold for power-ramp failures (Figure 2

illustrates power-ramp induced fuel failure assessments for 40% UO_2 (5 wt.% U-235) – 60% ThO_2 fuel case).

TABLE 2. CORE FOLLOW PARAMETRS

Parameter / Case	*Case 4*	*Case 64*	*NU*
Full power days (FPDs)	950	950	950
Bundle consumption	5176	2520	16240
Bundles / FPD	5.4	2.6	17.1
Average Burnup (MWd/kg-HE)	13.9	17.0	6.0
Maximum bundle power (kW)	1080	1,089	914
Maximum channel power (kW)	7264	7112	7100
P**max**, Maximum LER (kW/m)	55.9	55.8	56.4
ΔP, Maximum element power boost (kW/m)	36.5	35.4	38.2

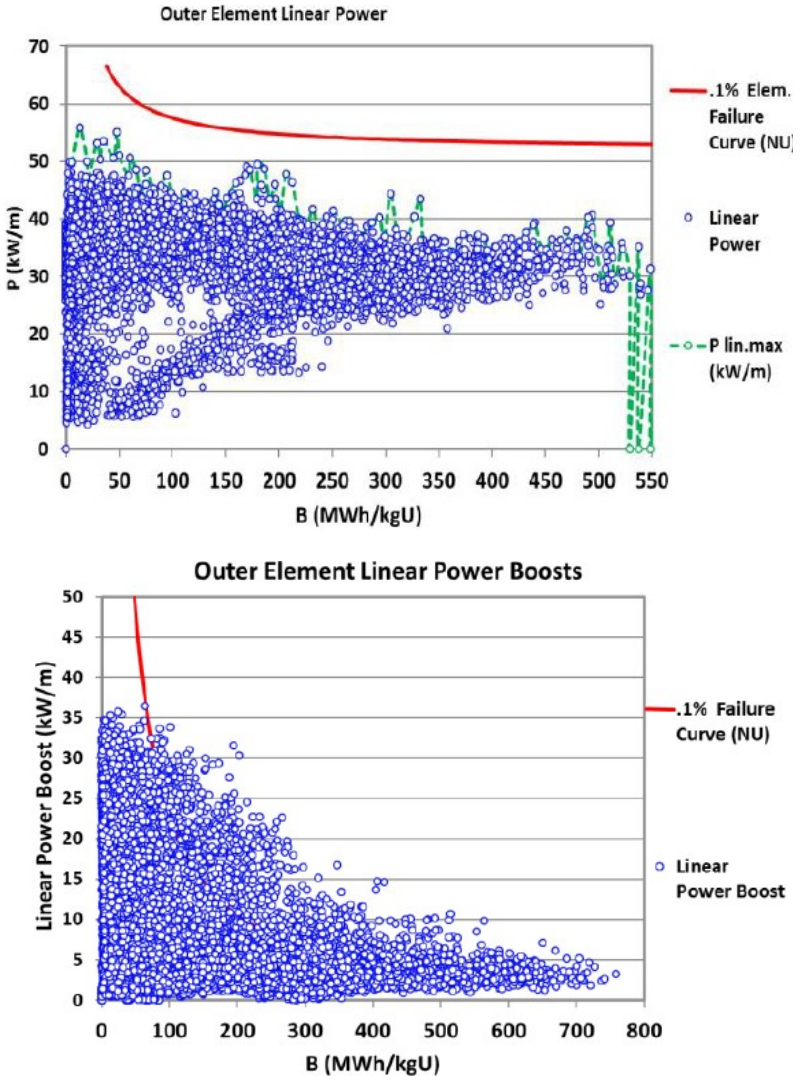

FIG.2. Power-ramp induced fuel failure assessments for 40% UO_2 (5 wt.% U-235)-60% ThO_2 fuel for maximum power (upper) and power increase (lower).

Since a fuel is considered to be failed only when both thresholds are exceeded [12], no failures of the thorium based fuel is expected to take place during power ramps in the reactor. It is noted, however, that these thresholds are those of NU fuel elements, and the assessments in Fig.2 are preliminary. Anyway, taking into account that the thermal conductivity of ThO_2 is higher than that of UO_2, the use of actual UO_2 linear power and power-ramp thresholds for $(Th,U)O_2$ fuel seems to be appropriate.

2.3.1.2. Fabricability

Part 1: Powder preparation

For the fabrication of $(Th,U)O_2$ fuel powder, the mechanical mixing method was adopted (see Fig. 3). Since both ThO_2 and UO_2 form a continuous series of solid solutions, a simple mixing and milling of these powders followed by cold pressing and sintering provides a quick and economical method for preparing a homogenous ThO_2-UO_2 powder.

ThO_2 and UO_2 powder were first blended or milled in proper portion to achieve the desired compositions, briquetted and calcinated in hydrogen to form partial ThO_2-UO_2 solid solutions. The calcinations briquettes were then crushed, comminuted, repressed into pellets and sintered. The technological flux used for the mechanical mixing method is presented in Fig. 3.

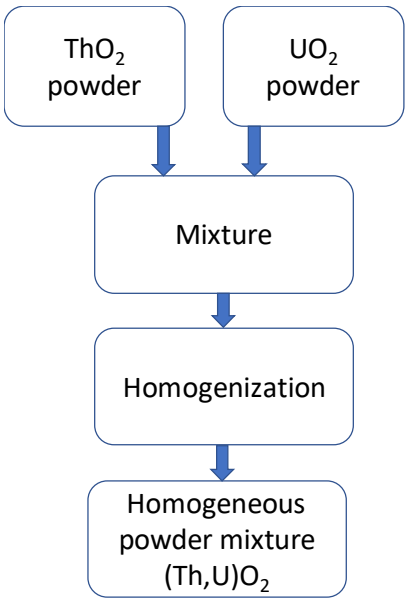

FIG.3. Flow diagram of mixing oxides of thorium and uranium powder using the mechanical mixing method.

Part 2: Pelleting process

The fabrication of fuel pellets by powder-pellet route involves conditioning of the powder to obtain the desired characteristic, mixing of the two different powder materials to obtain the desired mixed oxide fuel composition, pre-compaction and granulation to improve the flow ability of powder, and final compaction and sintering at high temperatures to get high density fuel pellets. The following lists important steps for pelleting:

- Pressing of the pre-compacted granules to form green pellets of the mixed thorium and uranium oxide to achieve a bulk density of ~6 g/cm^3;
- Dimensional control of the green pellets through bilateral pressing using a mechanical hydraulic press;
- Sintering of the green pellets to a final density of 9–9.5 g/cm^3.

Sintering is the normal process used for densification, recrystallization and thermal activation of free agglomerates. During sintering process, the conglomerate powder is strengthening by the formation of solid bonds between particles as well as diminishing unstable state of crystalline lattice system.

Sintering of the pellets was conducted in a furnace (located at the Materials Department of Institute for Nuclear Reactor -ICN) using the following parameters:

- Heating speed: 3-4^{o}C/minute;
- Levels:
  - 864 ± 25^{o}C for 45 minute
  - 1,680 ± 25^{o}C for 2 hour
  - 1,740 ± 25^{o}C for 2 hour;
- Cooling speed: 8 - 10^{o}C/minute;
- Dynamics atmosphere on H_2.

Figure 4 shows a temperature-time diagram for sintering of the green pellets of $(Th,U)O_2$.

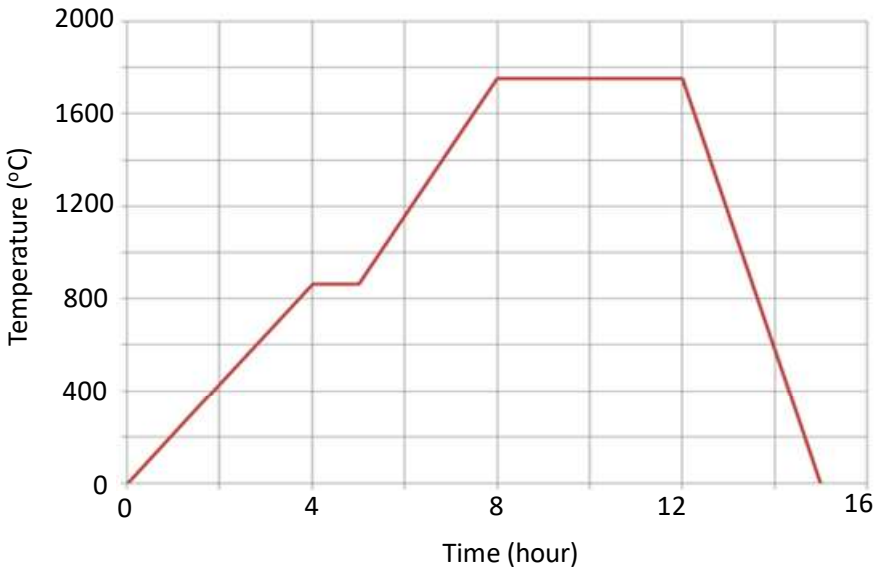

FIG.4. Sintering conditions for green pellets.

After sintering, the pellets were visually and dimensionally examined for compliance with technical specifications.

The homogeneous mixtures of thorium and uranium oxides were pressed using a bilateral machine with pneumatic control. The optimum compaction pressure was between 300 - 450

MPa. Under 190 MPa the powder has not been pressed, above 450 MPa the compacts would separate into planes with various densities.

Part 3: Fuel element fabrication

Figure 5 shows the overall process to fabricate a fuel element with $(Th,U)O_2$ pellets (A23) for an irradiation test at a material test reactor. The overall process includes the fabrication of Zircaloy components, Zircaloy sheath, $(Th,U)O_2$ powder and pellets, and the fuel element.

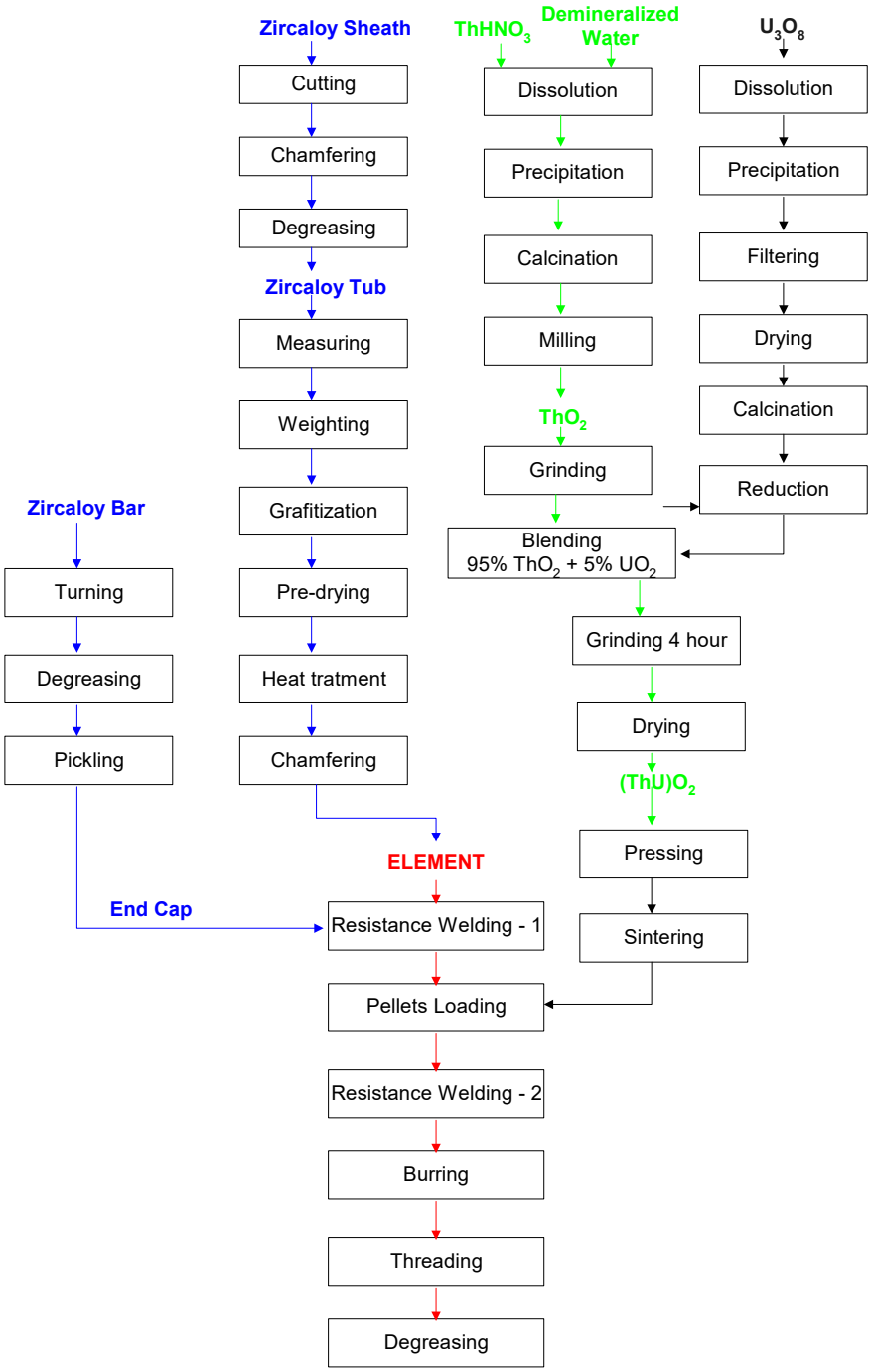

FIG.5. Technological flowchart for obtaining experimental fuel rod A23.

2.3.2. SEU fuel in Atucha reactors

Reactor physics studies have been performed using computer codes for fuel management calculations in Atucha-1 [13]. Refueling simulations were performed for a 6–12 months period, which facilitates some final adjustments to be made.

To develop fuel management strategies for the transition and equilibrium cores, it was decided not to modify the inlet nozzles for the coolant that were defined for the natural uranium core. The burnup zones and fuel movement were adjusted to ensure that channel power limits and PCI prevention criteria could be met.

The neutronic studies have confirmed the adequacy of the refueling strategy with the following results:

- Data to estimate the NU and SEU refuelling requirements for the subsequent years;
- Fuel bundle power and burnup histories that are representative of the transition core;
- A decreasing trend of the reactor maximum power with the use of SEU fuel in the core due to flattening of the axial power distribution. This could be achieved without any change of reactivity control mechanisms.

2.4. EXPERIMENTAL DATABASE AT EXTENDED BURNUP

Irradiation tests and associated PIEs are necessary to support proposed fuel concepts for high burnup. Technical insights are provided via reviewing such experimental data. Showstoppers for high burnup are also identified. These experimental data are critical to support the development and validation of fuel codes applicable to high burnup.

Two irradiation tests and associated PIEs are described in the subsequent sections. The selected thorium based fuel was fabricated and irradiated for a power-ramp test in a research reactor. In addition, a UO_2 fuel has been continuously irradiated in a power reactor for a prolonged period to achieve approximately three times the typical NU fuel burnup. This irradiation test was intended to understand PHWR fuel performance at an extended burnup.

2.4.1. $(Th,U)O_2$ fuel irradiation and post irradiation examination

In-reactor performance of UO_2-ThO_2 fuel was supported by irradiations tests, with supplementary analysis using computer codes as reported here. For comparison, a reference UO_2 fuel was irradiated under similar operating conditions. A power ramp test was also performed in a research reactor. Details are described in Annex V.

2.4.1.1. Test elements

The following two test elements were fabricated and irradiated in the TRIGA research reactor, Pitesti, Romania:

- Test element A23 – a fuel element containing $(Th,U)O_2$ fuel pellets;
- Test element A24 – a fuel element containing UO_2 pellets.

Test element A24 is to provide reference information that could be compared with test element A23. Table 3 presents the technical specifications for these test elements.

TABLE 3. TEST FUEL ELEMENT SPECIFICATIONS

Design parameters	*Test fuel element*	
	A23	*A24*
Pellet outer diameter (mm)	12.15	12.15
Pellet length (mm)	~13	~13
Fuel material	UO_2-ThO_2	UO_2
U-235 enrichment (wt.%)	5.0	5.0
Pellet density (g/cm^3)	9.7	10.5
Pellet grain size (µm)	-	9.4
Cladding inner diameter (mm)	12.22	12.22
Cladding wall thickness (mm)	0.41	0.41
Diametral gap with graphite coating (mm)	0.06	0.06

2.4.1.2. Irradiations

The (Th,U)O_2 experiments were conducted in the C1 irradiation device of the TRIGA research reactor. The operating pressure was 10.7 MPa. The maximum cladding temperature measured from thermocouples mounted on the outside surface of the cladding was ~324 °C for both fuel elements.

Irradiation conditions are summarized in Table 4. Corresponding power histories are shown in Fig.6.

TABLE 4. SUMMARY OF IRRADIATION CONDITIONS

Test Fuel Element	*Linear Power (kW/m) at:*		*Burnup (MWh/kg-HE)*
	Pre-ramp	**Ramped Power (7 days)**	
A23	33	51	189.2
A24	41	63	207.8

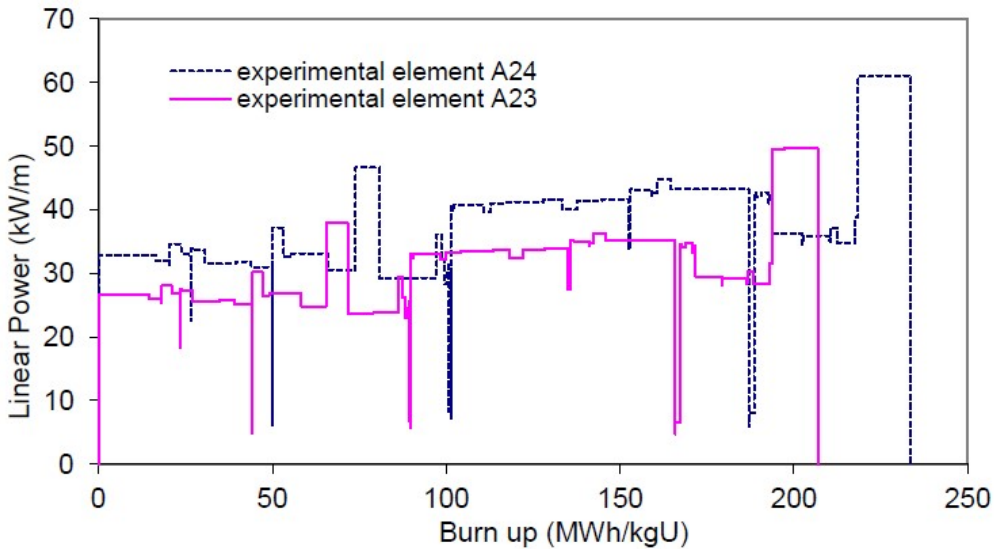

(Note. Burnup conversion : 100 MWh/kgU = 100 x 0.024 MWd/tU)

FIG.6. Irradiation histories of test fuel elements A23 and A24.

2.4.1.3. Post irradiation examinations

The following PIEs were performed in a hot cell:

- Non-destructive examinations: visual examinations, profilometry, axial gamma scanning and eddy-current testing.
- Destructive examinations: puncturing, measurements of fission gas volume and compositions, element void volume, chemical burnup determination, metallography and ceramography, and mechanical tests.

The visual examination showed an intact fuel element, without any damage found on the sheath surface. Along, on the entire element length, circumferential ridges and distinct ridges at both ends near endcaps can be seen (Fig.7).

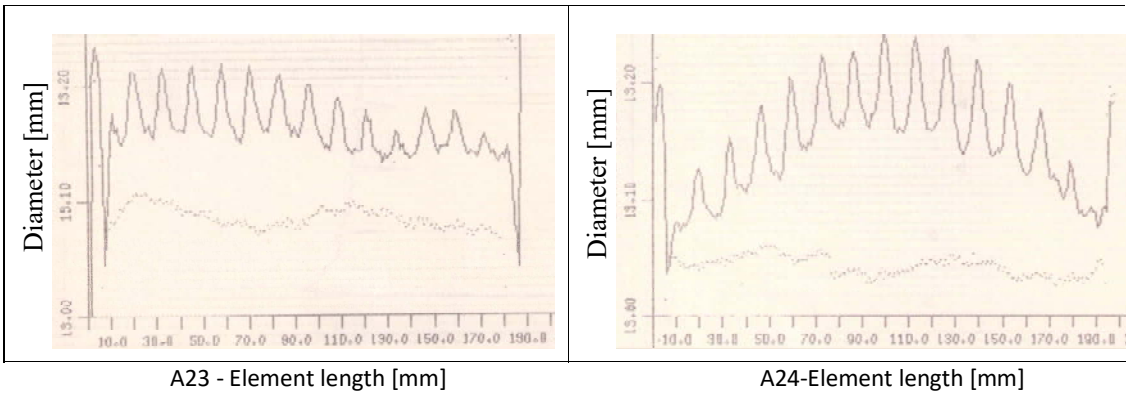

FIG.7. Sketches of cladding deformation profile after irradiation.

Before irradiation the outer mean diameter was 13.054 mm, and after irradiation the mean value increased to 13.167 mm. Important measurements done during the PIEs are presented in Table 5.

TABLE 5. POST IRRADIATION EXAMINATION RESULTS OF TEST FUEL ELEMENTS

Test Fuel Element	*Element bow (mm)*	*Axial elongation (mm)*	*Cladding oxide layer (µm)*		*Residual cladding strain (%)*		*Ridge height†(µm)*	*Gas release volume‡ (cm3)*
			Outside	*Inside*	*Mid-pellet*	*Pellet-pellet interface*		
A23	0.08	0.12	3 – 9	1 – 4	0.6	0.9	30	5.5
A24	0.05	0.10	5 – 26	3 – 6	0.7	0.7	35	15.9

† Average value at the middle length region;

‡ at STP (standard temperature and pressure) condition.

Overall, A23 and A24 test elements showed similar results for element bow, cladding elongation, cladding strain at pellet midplane and ridge height on the cladding. A23 test element showed lower gas released that might be due to lower element ratings and higher thermal conductivity of the thorium based fuel.

Figure 8 shows cross-sectional areas of both elements. A23 test element showed circumferential cracking and few radial cracks in the pellet, while A24 test element showed

radial cracks in the pellet. A23 test element did not show microstructural changes, while A24 test element showed microstructural changes in the central region of the pellet. This result indicated that A24 fuel element experienced higher centreline temperature.

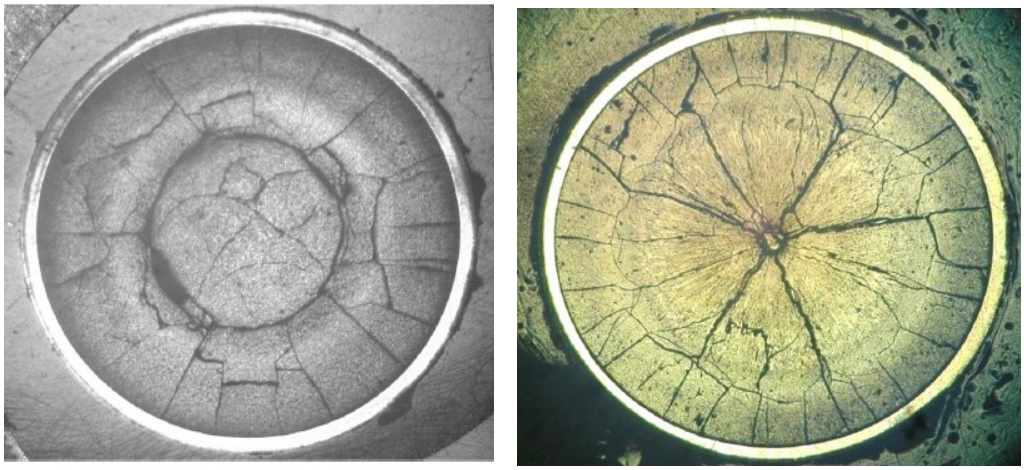

FIG.8. Microstructural features of test element A23 (left) and A24 (right).

2.4.2. Extended burnup irradiation of UO_2 fuel and post irradiation examination

Several NU fuel bundles were irradiated for extended periods in power reactors in India. PIE on two of those bundles, irradiated to ~15 000 MWd/tU and ~22 000 MWd/tU, respectively, were performed. Detailed PIE results of one of these two fuel bundles (No. 145530) are presented in this section, in terms of fuel restructuring, fuel swelling, fission gas release, cladding corrosion, strain and ductility, etc. Details of the extended burnup irradiation and PIE results are described in Annex III.

2.4.2.1. Description of experiments

The irradiated fuel bundle was a typical 19-element containing NU pellets. The bundle was irradiated in the channel O-8 at the 6th string location of the Kakrapara Atomic Power Station Unit 2. The fuel bundle accumulated around three times the typical discharge burnup (22,263 MWd/tU) over the residence period of ~1000 days. The maximum LER was 53.6 kW/m (see Fig.9 that shows the bundle power history).

At the hot cell, various non-destructive and destructive tests were carried out. These include visual examinations, leak tests, diameter measurement at different axial locations, ultrasonic tests, gamma scanning, puncturing and fission gas release measurements, microscopic examinations and mechanical properties tests of the cladding were carried out.

2.4.2.2. Results and discussion

Circumferential parallel lines at regular intervals (ridges) with discoloration were observed during visual examination along the length of the outer fuel elements. The distance between these lines was measured to be consistent with the length of the pellets. The ridge height on the outer fuel element cladding was found to be 40 μm maximum. It is noted that no ridges on the fuel cladding have been observed from 19-element fuel bundles irradiated to the typical NU fuel burnup.

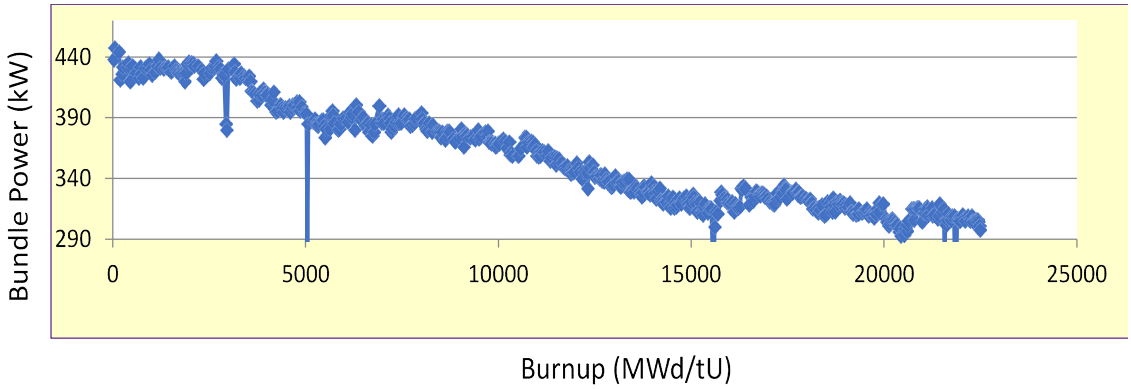

FIG.9. Irradiation history of fuel bundle 145530 loaded at the 6th bundle postion in the channel O-8.

Cladding strain at mid-pellets of the outer fuel elements was measured to be ranged between 0.06% and 0.6%, which is consistent with the measured strains of Canadian fuel element at an extended burnup of ~32 000 MWd/tU [1], without fuel failures.

Fractional release of fission gases and associated gas pressure from the outer ring elements were measured to be 13.66 % and 3.4 MPa, respectively, under ambient conditions. High gas release is attributed from pellet cracking and high temperatures (estimated based on microstructure changes in the pellet).

Pellet dishes in the outer elements were observed to have been filled due to thermal expansion at high centreline temperature.

A grain of UO_2 taken from the central region of the fuel section revealed the formation of large bubbles and a wide coverage by channels on the grain faces as compared to small bubbles observed in low burnup fuels (see Fig.10). Large numbers of white precipitates of metallic fission products containing Mo, Ru, Tc, Rh, Pd were also observed on the grain faces.

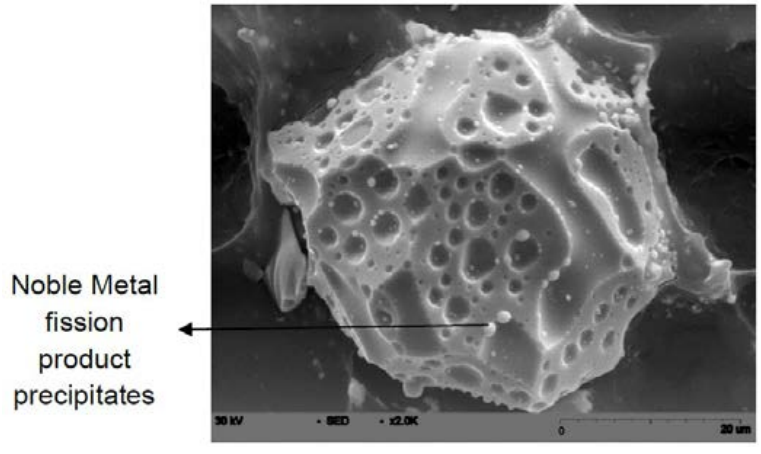

FIG.10. Grain from the centre of the fuel section of outer fuel element showing fission gas bubbles, channels and metallic fission products on the surface.

Few hydride platelets were observed in the cladding from the outer ring fuel element; most of the platelets were present towards the outer surface of the cladding. The average hydrogen content in the cladding from outer fuel element was ~38 ppm.

Transverse tensile properties of the cladding estimated from ring tension tests showed a total circumferential elongation of around 5-7% at 25ºC. The total elongation increased up to 22% at 300ºC. There was an increase in strength and a decrease in ductility of the cladding due to irradiation effects (see Fig.11). At room temperature, the increase in minimum strength and decrease in maximum ductility were about 30% and 85%, respectively.

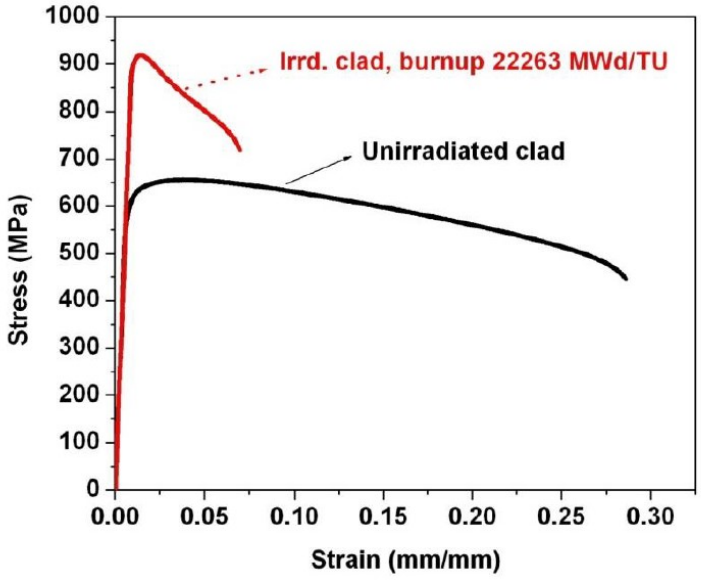

FIG.11. Typical engineering stress-strain diagrams for the unirradiated and irradiated cladding specimens at the ambient temperature.

2.5. IMPROVEMENT OF ANALYSIS TOOLS

2.5.1. Design analysis code for (Th,U)O_2 fuel in 43-element bundle

The ROFEM code [14] is a fuel element behavior analysis code for normal operating conditions using the finite element method. For the analysis of (Th,U)O_2 fuel, the following properties and correlations have been incorporated:

- Theoretical density;
- Ratio between metal and oxide mass;
- Melting temperature;
- Plasticity threshold temperature;
- Thermal conductivity;
- Thermal expansion coefficient.

The improved code has been preliminary validated by comparing with experimental measurements of A23 test element (see Table 6). Based on these preliminary results, the code is used to assist the design of next test elements in a research reactor.

2.5.2. Design analysis codes for SEU fuel elements in Atucha reactors

FRCC[4] and BACO [15] codes have been used for the assessment of FGR, internal gas pressure and thermal mechanical behavior of the SEU fuel elements in Atucha reactors. BACO was also used to assess fuel failures during ramp conditions. The validation exercises of these codes have been performed within the frame work of this CRP.

TABLE 6. COMPARISON BETWEEN ROFEM CODE CALCULATIONS AND A23 TEST ELEMENT MEASUREMENTS

Parameter	*ROFEM Calculations*	*Experimental Measurements*
Burnup (MWh/Kg-HE)	207.03	189.2
Volume of gas release (cm^3)	3.6	5.5
Internal pressure (MPa)	0.478	0.57
Residual deformation at mid-pellet (%)	0.97	0.9
Ridge height (μm)	22.3	30
Axial elongation (mm)	0.114	0.12

The codes were preliminary validated by comparing with experimental measurements obtained from IAEA's FUMEX-II cases [19]:

- CASE 7 – REGATE: Measurements on FGR and cladding diameter during and after a transient at ~47 GWd/tU burnup, and
- CASE 14 – RISØ-3 AN3: Measurements on FGR, internal gas pressure and fuel centreline temperature at ~37 GWd/t-UO_2 burnup.

The validation exercises also included the comparison with typical power histories that led to PCI-SCC failures in Atucha-1. The details of the validation exercise are described in Annex I.

Based on these preliminary results, the codes are used to assist the design of the lead test elements for irradiation in a research and Atucha reactors.

3. FUEL CONCEPTS LEADING TO ENHANCED OPERATIONAL AND SAFETY MARGINS

3.1. OVERVIEW

As an alternative fuel option to compensate for the eroded thermal margin in the aged CANDU reactors, fuel concepts to enhance the critical heat flux (CHF) of the bundle have been examined.

[4] FRCC is an internal code used by CNEA.

Generally, the following three principles are considered to enhance the CHF of the bundle:

(a) Less coolant to by-pass region;
(b) More coolant to bundle interior;
(c) More coolant mixing in bundle interior.

Principle (a) can be accomplished by an increase of the bundle diameter. Since dryout takes place in the central region of the 37R bundle (reference 37-element bundle), the increase of the bundle diameter by using taller bearing pads than the existing design may not be an effective method to enhance the CHF. Instead, an increase of the outer ring pitch circle radius may affect the CHF. Principle (b) can be accomplished by either using the centre element with a reduced diameter or increasing the inner ring pitch circle radius. In this CRP study, therefore, a modification of fuel element arrangement (i.e. increase of pitch circle radii) in the bundle was considered as a viable option to enhance the CHF.

Power ripples during refueling transients need to be managed. The use of burnable neutron absorbers (BNAs) in CANDU fuel design is considered to improve operating margin (by removing fueling transients) while at the same time providing safety margin (by mitigating end flux peaking during a loss-of-coolant accident).

3.2. CONCEPTS TO ENHANCE CRITICAL HEAT FLUX

Configuration of subchannels and pitch circle radii of a 37R bundle are shown in Fig.12 and Table 7, respectively. The radii of the inner, intermediate (sometimes call middle) and outer rings of a 37R bundle were modified while keeping the minimum separations between fuel elements. Such ring radii modifications of a fuel bundle can impact on CHF or dryout power of a fuel bundle. The subchannel analysis was done using ASSERT code [16]. Detailed analysis results are described in Annex IV. In this section, generalized results based on analysis results for 3.3% crept pressure tube and the inlet temperature of 262°C are described.

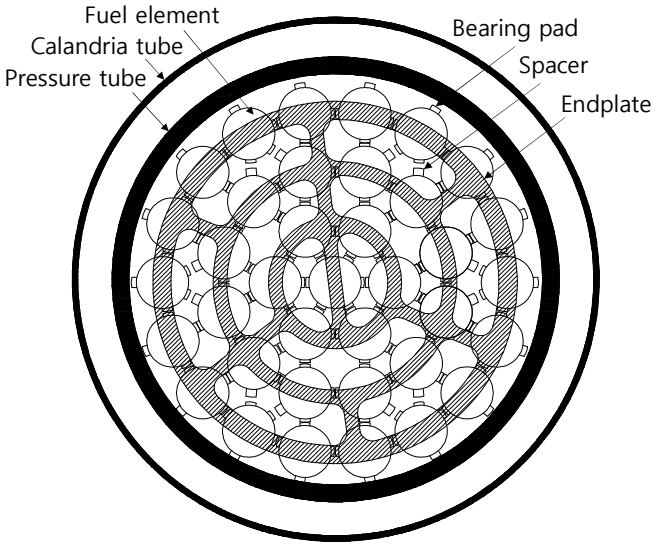

FIG.12. Cross-sectional View of the reference 37-element fuel bundle in pressure tube.

TABLE 7. RING RADII OF THE REFERENCE 37-ELEMENT BUNDLE

Ring identification	*Ring radius, mm*	*No. of elements*
Centre	0.0	1
Inner	14.88	6
Intermediate	28.75	12
Outer	43.33	18

3.2.1. Inner ring pitch circle modification

Inner ring pitch circle radius was increased up to 0.5 mm from the reference case for subchannel sensitivity analysis. All other ring radii remained unchanged. The general trends observed for the case of 3.3% crept channel and the inlet temperature of 262ºC are as follows:

- Most of the first CHF occurrence locations in the modified bundle geometry moved to the intermediate subchannels from the central subchannels which was the original location of the first CHF occurrence pf the 37R bundle;
- The dryout power ratio increased with increased inner ring radius (Fig.13).

3.2.2. Intermediate ring pitch circle modification

Intermediate ring pitch circle radius was increased up to 0.5 mm from the reference case for subchannel analysis. Inner ring radius was fixed to be 15.18 mm and outer ring radius remained unchanged.

Dryout power ratios for the intermediate ring modifications in terms of the 3.3% crept pressure tube are shown in Fig.14. Dryout power ratios for the intermediate ring modification were similar with inner ring modifications case. The locations of the first CHF occurrence moved from the central subchannel to the other subchannels depending on flow conditions.

3.2.3. Outer ring pitch circle modification

Outer ring pitch circle radius was increased up to 0.5 mm from the reference case for subchannel analysis. Inner and intermediate ring radii were fixed to be 15.18 mm and 29.25 mm, respectively.

Dryout power ratio for the outer ring modification in terms of the 3.3% crept pressure tube were shown in Fig.15. Dryout power ratios are significantly increased in a monotonic manner as the outer ring radius is increased. The maximum dryout power ratios were found at the maximum outer ring radius.

3.2.4. Summary

Modifying pitch circle radii within the current bundle specifications can enhance dryout power by redistribution of subchannel enthalpy and changing CHF location. The outer ring radius has the most significant impact on the dryout power enhancement with enlarged central flow area of the fuel bundle.

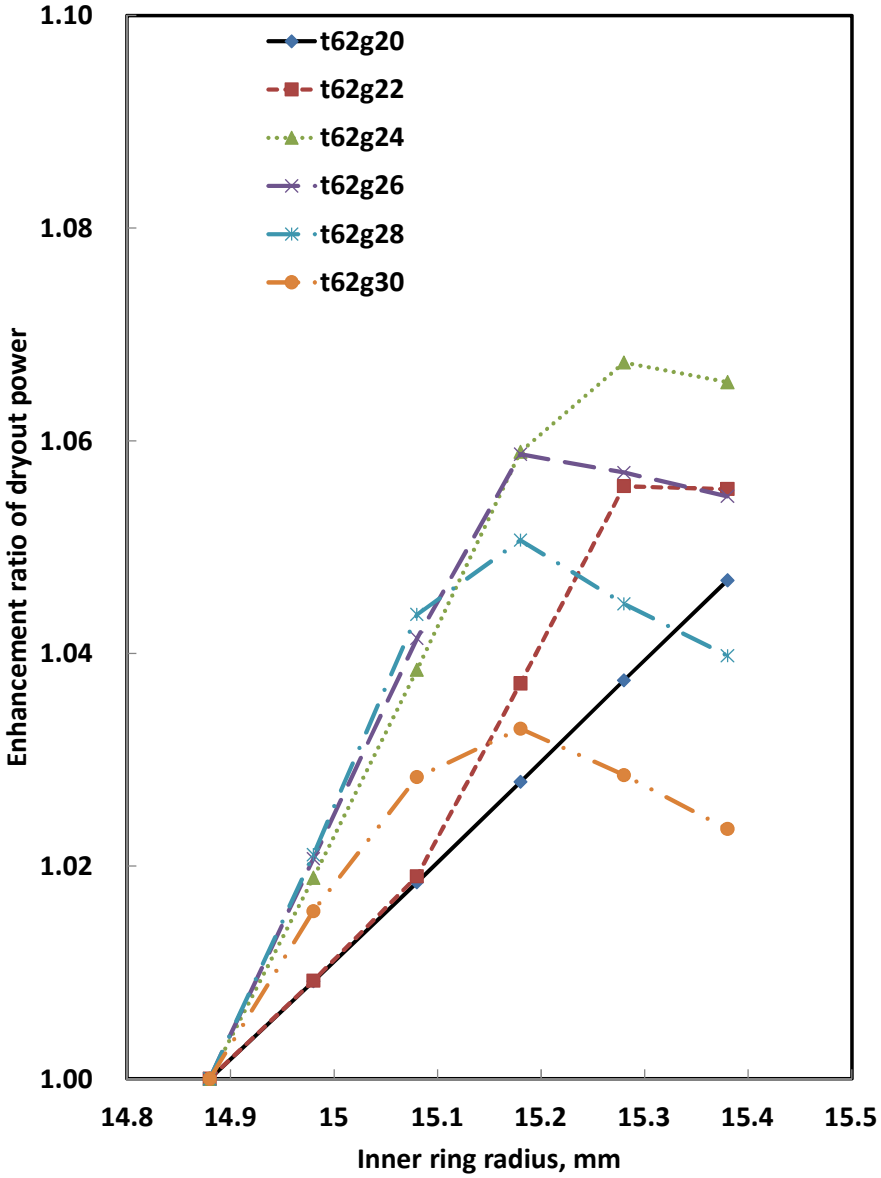

FIG.13. Enhancement of dryout power for a 37R fuel bundle with inner ring modification for 3.3% crept pressure tube and the inlet temperature of 262°C.

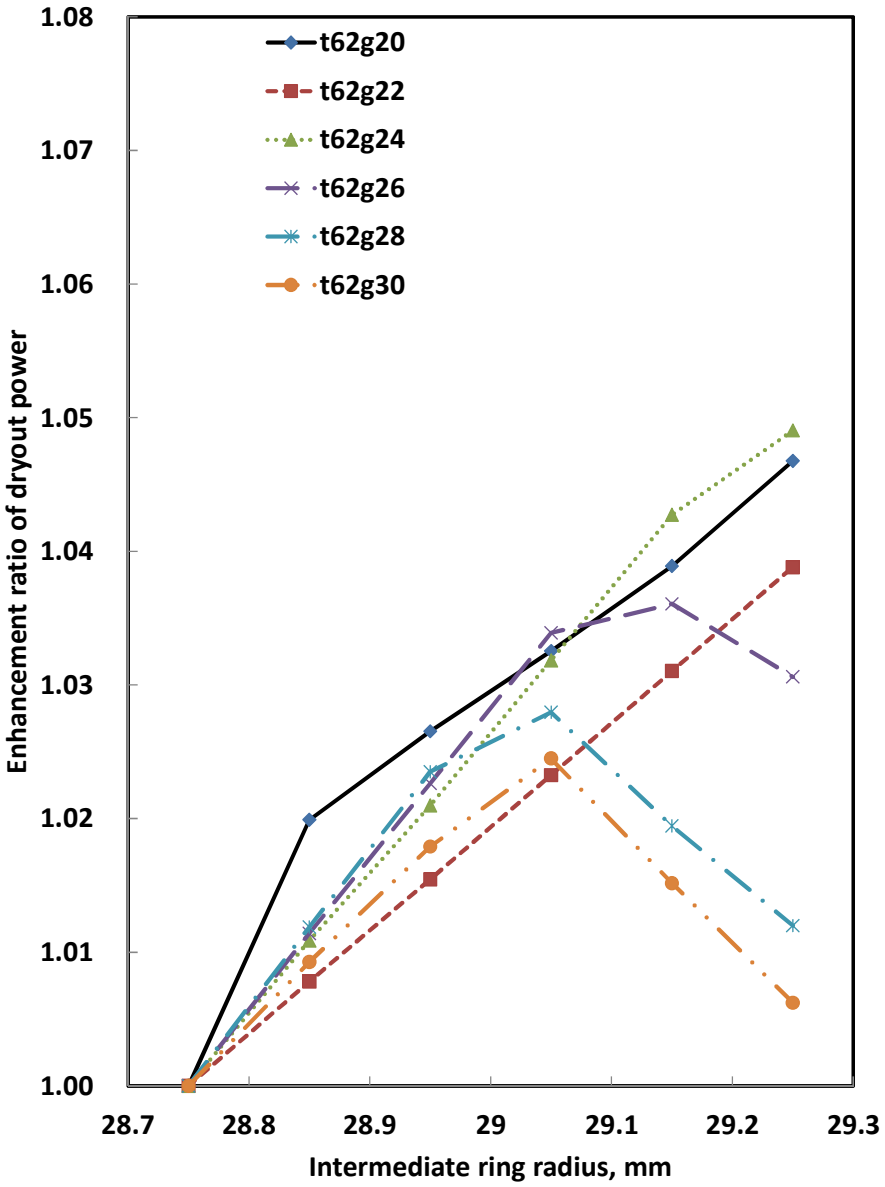

FIG.14. Enhancement of dryout power for a 37R fuel bundle with intermediate ring modification for 3.3% crept pressure tube and the inlet temperature of 262°C.

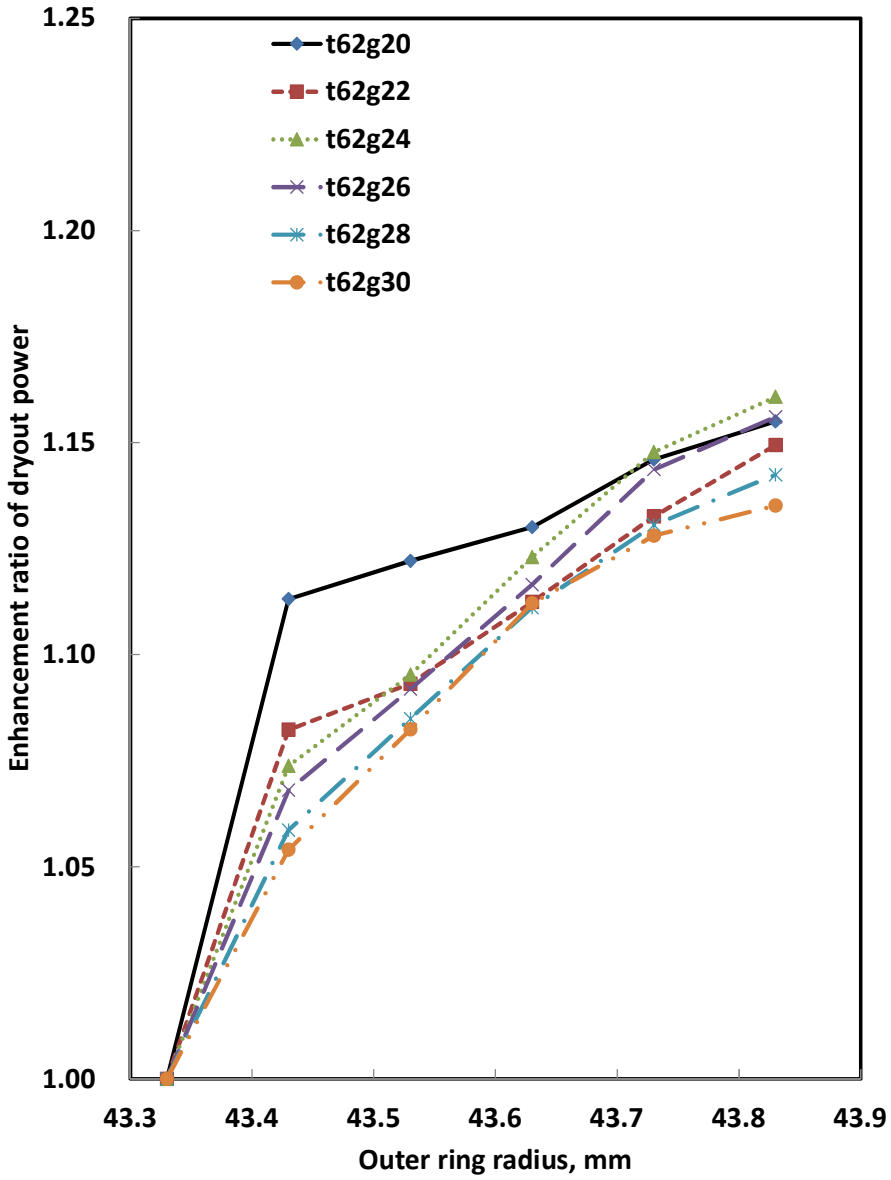

FIG.15. Enhancement of dryout power for a 37R fuel bundle with outer ring modification for 3.3% crept pressure tube and the inlet temperature of 262°C.

3.3. CONCEPTS TO MITIGATE LOCAL POWER PEAKING

3.3.1. Background

These power ripples often bring channel operating parameters very close to a neutron overpower protection trip setpoint and require immediate zone reactivity control system actions. With the added effects of heat transport system aging, where the trip margin is already tight, xenon-free effects and plutonium production in the NU fuel could potentially lead to a temporary power derating following a CANDU reactor fueling operation. Therefore, a significant operating safety margin is needed to account for these refueling power ripples, which has a large impact on fuel and physics, and reactor operation.

It is anticipated that adding small amounts of burnable neutron absorbers (BNAs) in the CANDU fuel elements could mitigate the fueling transient and lower the reactivity/power peak due to the plutonium production in fresh fuels.

3.3.2. Analysis methodology

A detailed description of the analysis tools could be found in Annex II.

Lattice-burnup calculations using WIMS-AECL 3.1 [11] was used to demonstrate that ~180 mg (~9 ppm) of Gd_2O_3 and ~1000 mg (~50 ppm) of Eu_2O_3 could be used to tailor the trend in the evolution of the reactivity of the CANDU NU fuel to a more optimal shape. The core-following analyses were carried out using RFSP-AECL [17] for various mixtures of BNAs. MCNP 6.1 [18] was used to simulate the addition of a small amount of neutron absorbers strategically at the bundle ends to mitigate end flux peaking.

3.3.3. Design approach and results

This study was performed in four parts:

Part 1: A literature review revealed that gadolinium, boron, europium and samarium are commonly used as BNAs in power reactors (see references [II-8]–[II-11] of Annex II). A parametric study was conducted using WIMS-AECL 3.1 and MCNP 6. Gadolinium oxide (Gd_2O_3) is clearly more efficient and its impact on fuel burnup is negligible. Europium oxide (Eu_2O_3) and boron oxide (B_2O_3) are longer-lived BNAs. Results indicated that the optimal amount of B_2O_3 and Eu_2O_3 were 35 mg 125 mg, respectively. This will bring the mean maximum channel power down by 20 kW with the liquid zone controller (LZC) at ~20% and with no impact on discharged burnup.

Part 2: The core-following study for each respective BNA fuel was conducted using a generic set of refueling history, which was created using the reference 37-NU fuel element bundle. Table 8 demonstrates the effects of refueling a fresh core with BNA fuels, imparted over 400 FPDs of normal operation, using a reference fueling scheme. Reductions in the maximum channel and bundle powers, the average discharge burnup of fuels, the channel power peaking factor, the radial form factor and the LZC levels were evident.

Using the reference fueling scheme, keeping the LZC level at approximately 20 to 25% and targeting the same average discharge burnup, a mixture of 150 mg Gd_2O_3 /125 mg Eu_2O_3 or 150 mg Gd_2O_3 /35mg B_2O_3 was recommended in this study to mitigate refueling power ripples and low the Pu-peak.

The behavior of a 37-element fuel bundle undergoing a degraded coolant conditions during a loss-of-coolant accident was also simulated. The AECL-WIMS code was used to conduct an analysis of the infinite multiplication factor for four cases, as illustrated in Table II-4 of Annex II. For fuel containing 150mg Gd_2O_3 and 125mg Eu_2O_3, reductions in reactivity under a typical degraded coolant condition were 56.57 mk and 0.803 mk for fresh fuel and fuel after 45 FPD, respectively. This comparative study provided an additional safety-related argument in favor of industry implementation of this design.

TABLE 8. AVERAGED RESULTS FROM 400 FPDs OF CORE FOLLOWING USING SIX DIFFERENT BNA FUELS

	Regular NU (control)	***120mg Gd_2O_3***	***150mg Gd_2O_3***	***150mg Eu_2O_3***	***300mg Eu_2O_3***	***120mg Gd_2O_3 & 300mg Eu_2O_3***	***150mg Gd_2O_3 & 300mg Eu_2O_3***
Mean exit burnup (MW-h/kgU)	169	169	169	169	169	169	169
Average peak channel power (kW)	6717	6707 (-10)	6704 (-13)	6673 (-44)	6632 (-85)	6624 (-93)	6623 (-94)
Mean CPPF	1.13	1.12	1.12	1.11	1.12	1.12	1.12
Average peak bundle power (kW)	821	820	819	814 (-7)	809 (-12)	809 (-12)	809 (-12)
Mean RFF	1.22	1.21	1.21	1.21	1.2	1.2	1.2
Mean average LZC level	45%	40%	40%	30%	19%	17%	17%
Mean maximum LZC level	92%	88%	88%	78%	53%	49%	49%

Part 3: An end flux peaking model using MCNP 6 was developed. The predicted peaking factors were compared with data obtained from ZED-2 experiments and a similar model performed with DRAGON 3.03a using the 89-group. While the MCNP 6.1 model used the more up to date ENDF/B-VII.1 library. The results were summarized in Table II-5 of Annex II. One could see that the model done in MCNP was able to accurately predict the peaking factors of each fuel ring.

Figure 16 below illustrated the effect of europium within an end pellet and its adjacent pellet on end flux peaking. Comparing with the no absorber case, end flux peaking was mitigated significantly.

MCNP 6.1 was also developed as a 3D-tool to simulate the addition of a small amount of neutron absorbers strategically at the bundle ends.

Part 4: Results indicated that the reference fueling scheme that is currently used with this CANDU model is quite robust. The salt-and-pepper approach (see Fig.II-7 of Annex II) has demonstrated that the fueling frequency, and thus the demand on temperamental fueling machines could be potentially reduced. As indicated in Table II-7 of Annex II, the LZC level was increased by 12%, instead of decreased by 25%, even with the presence of 150 mg Gd_2O_3 and 125 mg Eu_2O_3.

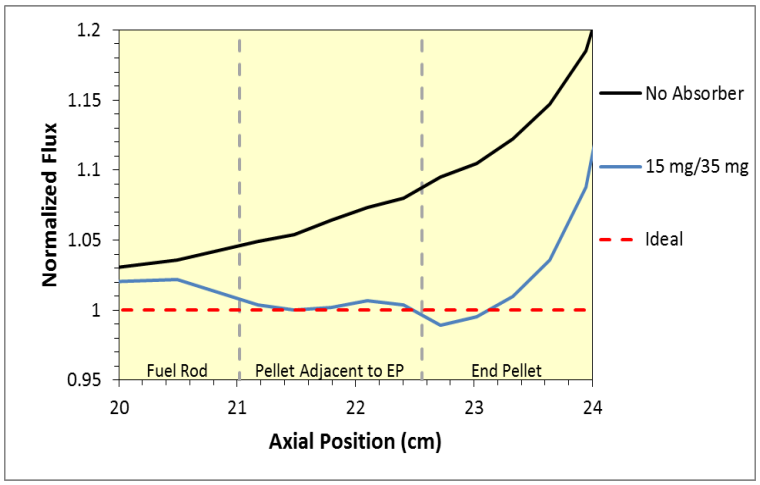

FIG. 16. Comparing the ideal europium trials with the case of having no absorber.

4. OUTCOME AND FUTURE CHALLENGES

4.1. OUTCOME

Advanced fuel bundles for PHWR are proposed here to achieve an extended discharge burnup compared with a typical NU burnup and/or to provide an alternative fuel option for use to recover margin loss in the aged reactors. In the following subsections, detailed results on the design concepts of the advanced fuel bundles and supporting information, which were obtained from this CRP, are summarized.

4.1.1. Fuel concepts for higher burnup

Operational experience in Atucha-1 reactor (vertical channel type PHWR) supported that 0.85% SEU fuel allows to increase the discharge burnup to about twice the typical NU burnup without requiring any modification of reactor control mechanisms. By means of using the optimized fuel management strategy in the core of Atucha-1, the maximum LERs could be maintained at an appropriate level with which the integrity of the fuel element is not likely to be threatened at the extended discharge burnup. For CANDUs, the advanced fuel bundle design with increased subdivisions has been considered as the preferable option to reduce the maximum LERs. In this CRP study, the 43-element bundle design has been chosen by Romania as the carrier of the advanced fuel material for high burnup fuel.

Several fuel performance parameters are identified as life limiting factors that may impose burdens to high burnup operation. The life limiting factors could be affected by LERs. At the high level of extended discharge burnup (e.g. three times the typical NU fuel discharge burnup), specific design measures may need to be provided in addition to the reduction of LERs. Through a literature survey, the large grain sized pellet has been proposed as a viable design to reduce the fission gas release and associated internal gas pressure in the fuel element. Internal coating with poly-siloxane or zirconium liner on the inside surface of the cladding has been proposed to prevent PCI-induced fuel failures. The final selection of a coating material will require additional experimental evidences.

A mixed oxide of UO_2 and ThO_2 in the 43-element fuel bundle has been selected and investigated to confirm whether the material is adequate for use as the high burnup fuel in CANDUs. Various aspects including: manufacturability, neutronics characteristics, thermal mechanical behavior in the reactor were investigated. Reactor physics analysis indicated that the characteristics of the $(Th,U)O_2$ fuel were comparable with the uranium fuel in terms of the radial power distribution and the reactivity feedback due to coolant void. The $(Th,U)O_2$ fuel elements were preliminarily assessed not to be failed due to power ramps during refueling, based on thresholds that are used for the NU fuel elements.

A $(Th,U)O_2$ and UO_2 fuel elements were irradiated under similar irradiation conditions (to a typical NU fuel burnup) in the research reactor. Specifically, the $(Th,U)O_2$ fuel element experienced slightly lower pre-ramp power, power increase and discharge burnup than the UO_2 fuel element. Overall, thermal mechanical behavioral results (e.g. cladding strains) between two test elements were similar; however, the UO_2-ThO_2 fuel element showed FGR three time lower than the UO_2 fuel element. This might be attributed to a combination of high thermal conductivity, different microstructural changes and slightly different operating conditions of the $(Th,U)O_2$ fuel element.

In parallel, high burnup features were investigated by PIE campaigns on a 19-NU fuel element bundle irradiated to around three times the typical NU burnup in an Indian PHWR. There were no fuel failures in the bundle. Excessive PCI was recognized by the formation of ridges in the highly irradiated fuel cladding, while no ridges on the fuel cladding have been observed from 19-element fuel bundles irradiated to the typical NU fuel burnup. The amount of fission gases released was much high, indicating that specific design improvement(s) may need to be incorporated for a possible reduction of FGR. Tensile properties of the irradiated cladding showed a strong influence of irradiation.

As a support to the development of design concepts of advanced fuel bundles for extended discharge burnup, fuel performance analysis codes have been improved to extend their modelling capabilities to cover the thorium based fuel element and phenomena under the extended burnup conditions.

4.1.2. Fuel concepts leading to enhanced operational and safety margins

Providing alternative fuel options to recover the eroded thermal margin in aged CANDUs was of primary interest in this CRP study. Geometric sensitivity study was performed, using a subchannel analysis code, for all pitch circle radii of the reference 37-element bundle without changing the fuel element sizes. Increasing pitch circle radii within the current bundle specifications was found to be effective in enhancing dryout power by changing critical heat flux location and redistribution of subchannel enthalpy. The outer ring radius had the most significant impact on the dryout power enhancement with enlarged central flow area of the fuel bundle. An increase of the outer ring radius together with an increase of the inner ring radius seem a viable option for the enhancement of the dryout power. The enhancement appeared to be great in the highly crept pressure tube.

End flux peaking and refueling ripples in CANDUs have significant impact on the operating margin of the reactor. In aged reactors, it would become a potential issue that impacts the operation of the reactor. Use of burnable absorbers would advance further fuel design and management optimization that might potentially offer a more reliable and convincing solution to manage the adverse impact of aging on safety and performance of operating reactors.

Through design exercises using reactor physics analysis computer codes, an optimized design of the burnable absorbers has been proposed.

4.2. FUTURE CHALLENGES

Design concepts for advanced fuel bundles to achieve an extended discharge burnup compared with a typical NU burnup and/or to provide an alternative fuel option for use to recover margin loss in the aged reactors have been proposed. These are based on preliminary studies only to direct desirable directions for further development or optimization. Fabrication of prototype bundles for in-reactor and out-reactor tests are necessary in future.

5. SUMMARY OF CRP RESULTS

There is an increasing interest among the Member States to introduce advanced fuels and extend the discharge burnup of fuel bundles in PHWRs for better resource utilization and improved economics. There is also an on-going issue to recover eroded margin in the aged reactors. This CRP was intended to encourage the development and sharing of research work on resolving the challenges that may be encountered in deploying new fuel concepts for higher burnup and for the recovery of margin loss in the aged reactor. This overall objective has been successfully achieved by sharing and exchanging specific data and information on specific research objectives among five participating countries.

Advanced fuel concepts for high burnup and to enhance operational and safety margins in PHWRs have been proposed, based on literature review, analyses using computer codes, irradiation tests and associated PIEs and current operating experience. Although results are preliminary, they are sufficient to provide directions for further development or optimization.

REFERENCES

[1] FLOYD, M.R., "Extended Burnup CANDU Fuel Performance", Proceedings of the 7th International Conference on CANDU Fuel, Kinston, Ontario, Canada, 23-27 September 2001.

[2] INCH, W.W., ALAVI, P., "CANFLEX Mk-IV Qualification Program and Readiness for Implementation", Proceedings of the 7th International Conference on CANDU Fuel, Kinston, Ontario, Canada, 23-27 September 2001.

[3] JUN, J.S., JING, J.Y., CHO, M.S., SUK, H.C., KIM, Y.B., SEO, H.B., "The Demonstration Irradiation of the CANFLEX-NU Fuel Bundle in Wolsong NGS 1", Proceedings of the 9th International Conference on CANDU Fuel, Belleville, Ontario, Canada, 18-21 September 2005.

[4] SIM, K.S., PALLECK, S.J., DORIA, F.J., CHARCRABORTY, K., LEUNG, L.K.H., CHOW, H., HE, Z., FLOYD, M.R., LAU, J.H.K., DUNCAN, J., "Design and Qualification of CANFLEX Low-Void Reactivity Fuel Bundle", Proceedings of 2008 Water Reactor Fuel Performance Meeting, Seoul, Korea, 19-23 October 2008.

[5] ALVAREZ, L., CASARIO, J., FINK, J., PEREZ, R., HIGA, M., "Extended burnup with SEU fuel in Atucha-1 NPP", Technical and Economic Limits to Fuel Burnup Extension (Proceedings of a Technical Committee Meeting held in San Carlos de Bariloche, Argentina, 15-19 November 1999), IAEA-TECDOC-1299, IAEA, Vienna (2002), 181-192.

[6] BUSSOLINI, A.A. et al, "Status of Fuel Engineering Activities on Extended Burnup Fuel for the Argentine Fleet of PHWRs", Pressurized Heavy Water Reactor Fuel: Integrity, Performance and Advanced Concepts (Proceedings of the Technical Meetings held in Bucharest, 24-27 September 2012, and in Mumbai, 8-11 April 2013), IAEA-TECDOC-CD-1751, IAEA, Vienna (2014).

[7] HASTINGS, I. J., Effect of Initial Grain Size on Fission Gas Release from Irradiated Fuel, AECL-8124, Atomic Energy of Canada Limited, Chalk River, Ontario (1983).

[8] FERRIER, G.A., FARAHANI, M., METZLER, J., CHAN, P.K., CORCORAN, E.C., Mitigating the Stress Corrosion Cracking of Zircaloy-4 Fuel Sheathing - Siloxane Coatings Revisited, ASME J of Nuclear Engineering and Radiation Science **2** (2016) 21004.

[9] COX, B., Pellet-Clad Interaction (PCI) Failures of Zirconium Alloy Fuel Cladding – A Review, Journal of Nuclear Materials **172** (1989) 249.

[10] MARLEAU, G., A User Guide for DRAGON.06k, Report IGE-174 (Revision 9), Institute de Genie Nucleaire, Ecole Polytechnique de Montreal, Canada (2011); http://www.polymt.ca

[11] JONKMANS, G., WIMS-AECL User's Manual, Version 3.1, Atomic Energy of Canada Limited, Chalk River, Ontario (2006).

[12] PENN, W.J., WOOD, J.C., LO, R.K., CANDU Fuel Power Ramp Performance Criteria, Nuclear Technology **34** (1977) 249.

[13] FINK, J.M. et al, "Overview of the SEU Project for Extended Burnup at the Atucha-I NPP Four Years of Operating Experience", Technical and Economic Limits to Fuel Burnup Extension (Proceedings of a Technical Committee Meeting held in San Carlos de Bariloche, Argentina, 15-19 November 1999), IAEA-TECDOC-1299, IAEA, Vienna (2002), 170–180.

[14] IONESCU, D.V., Improvement of ROFEM Fuel Behavior Code for Simulation the Comportment of Mixed Oxide of Thorium and Uranium Fuel, Report 10000/2013, Institute for Nuclear Reactor, Romania (2013).

[15] HARRIAGUE, S. et al, BACO (Barra Combustible) - A Computer Code for Simulating a Reactor Fuel Rod Performance, Nuclear Engineering and Design **56** (1980) 91.
[16] CARVER, M.B., KITELEY, ZOU, J.C., JUNOP, S.V., ROWE, D.S., Validation of the ASSERT Subchannel Code: Prediction of Critical Heat Flux in Standard and Nonstandard CANDU Bundle Geometries, Nuclear Technology **112** (1995) 299.
[17] SHEN, W., RFSP-IST Version REL_3-04: Theory Manual, SQAD-06-5058, CANDU Owners Group (2006).
[18] BROWN, F.B., "MCNP - A General Monte Carlo N-Particle Transport Code: Overview and Theory, Version 5 Volume 1, Los Alamos National Laboratory (2003).
[19] INTERNATIONAL ATOMIC ENERGY AGENCY, Report of the Coordinated Research Project 2002-2007: Fuel Modelling at Extended Burnup (FUMEX-II), IAEA-TECDOC-1687, IAEA, Vienna (2012).

ANNEX I: DEVELOPMENT OF IMPROVEMENTS FOR THE ARGENTINE PHWR FUELS TO INCREASE THE RELIABILITY AT EXTENDED BURNUP AND OTHER OPERATING CONDITIONS

A Summary Report of Research Contract with National Commission for Atomic Energy (CNEA), Argentina

I-1. BACKGROUND

Argentina is carrying on an advanced cycle with increased burnup in the Atucha-1 nuclear power plant (NPP) since 1995. An increase of the U-235 enrichment from natural uranium (NU) to 0.85% allowed increasing the average discharge burnup of the fuel from 5900 MWd/tU to more than 11 000 MWd/tU. The main consequence of this improvement is an important reduction of the fuel consumption and a positive impact on the reduction of the cost of power generation. A detailed fuel design analysis was performed by the National Commission on Atomic Energy (CNEA) to evaluate the behavior of the fuel in the new operating conditions and to define initial design modifications to reduce the impact of the changes in the response of the fuel in such new conditions.

Currently a SEU fuel design for use in Atucha-2 is under development at CNEA [I-1]. The discharge burnup of the Atucha-2 SEU fuel will be higher than that of the Atucha-1 SEU fuel. Due to the extended discharge burnup, the plant operation will be limited to stay within power ramps which fuel assemblies can withstand without failure.

Fuel analysis that supports the operational limits are associated with cladding materials, fuel behavior during power ramps and a buildup of internal gas pressure in the fuel element due to the increase of fission gases released from the fuel pellets.

As a participant of this CRP, CNEA is expected to define a set of potential improvements of the fuel for Atucha type PHWRs to increase the reliability at extended discharge burnup. The specific topics to be addressed with the potential design optimizations included:

- life limiting aspects of higher burnup fuels;
- operational margins and reliable calculation tools to verify these margins;
- fuel resistance to high burnup conditions, power ramps and eventual accident situations.

The development of the potential improvements also included aspects to facilitate application at industrial stage and the feasibility of demonstration irradiations.

This Annex describes the activities that were performed by CNEA under the framework of the CRP on Reliability of Extended Burnup and Advanced PHWR Fuels.

I-2. IMPROVEMENTS ON COMPUTATIONAL CALCULATION

At CNEA, fuel element behavior analysis under normal operating conditions is performed using an internally-developed computer code, named FRCC. FRCC is the fuel analysis code to simulate the thermo-mechanical behavior of Atucha-1 and Atucha-2 fuel elements. FRCC has been used since 1980s for supporting design changes and design verifications of Atucha-1

and Atucha-2 fuel elements. As specific examples, this computer code has been successfully used as design tool in following projects:

- implementation of SEU in Atucha-1;
- incremental increase of uranium mass in Atucha-1;
- Atucha-2 fuel design using natural uranium;
- design studies to implement SEU in Atucha-2.

The first activity related with FRCC was to determine if this code predicts correctly the fuel behavior beyond the current burnup level. Irradiations information available in the literature were used to achieve this objective.

The second step was to evaluate code predictions for Atucha-1 and Atucha-2 fuels for power ramps at high burnup exceeding the NU burnup. For the fuel performance analysis under power ramp conditions, FRCC is coupled with BACO, which is another code developed by CNEA.

I-2.1. Code validation at high burnup

Two power-ramp test cases conducted at high burnup were chosen from IAEA FUMEX-II exercises [I-2] and used for a validation exercise of FRCC code.

I-2.1.1. FUMEX II Case 7 – REGATE: fission gas release and cladding diameter during and after a transient at a burnup of 47 GWd/tU

The test fuel element was a segmented fuel, following a base irradiation to a burnup of 47.11 GWd/tU in a commercial pressurized water reactor. The test fuel element was power- ramped in the SILOE material test reactor. The available data, measured before and after the ramp, includes fission gas released (FGR), burnup and cladding outer diameter.

Table I-1 shows a comparison between code calculations and experimental measurements on burnup and FGR. Code predictions on FGR are higher than measured values for both the base irradiation and the power ramp.

TABLE I-1. FRCC CODE VALIDATION - CALCULATIONS VS MEASUREMENTS FROM CASE 7 - REGATE

Case	***Base irradiation***		***Ramp***		***FGR ratio (Ramp/Base)***
	Burnup (GWd/tU)	***FGR (%)***	***Burnup (GWd/tU)***	***FGR (%)***	
Experimental measurements	47.11	1.5	47.5	9.3-10.2	6.8
FRCC calculations	48.61	3.07	49.27	16.2	5.3

I-2.1.2. FUMEX II Case 14 – Risø-3 AN3: fission gas release, internal gas pressure and fuel centreline temperature at a burnup of 37GWd/tUO₂

This case consists of a re-fabricated and instrumented test fuel element from a fuel base-irradiated up to 40.4 GWd/tU in Biblis-A PWR. The test fuel element was power-ramped in the test reactor DR3 at Risø under PWR conditions [I-3].

The available information, before and after ramp, include fission product generation, fission gas release (FGR) and internal gas pressure. During the bump test, fuel centreline temperature and internal hot pressure were also measured. Two types of ramps were simulated for the bump test: a full ramp and a simplified one step ramp, as shown in Fig.I-1.

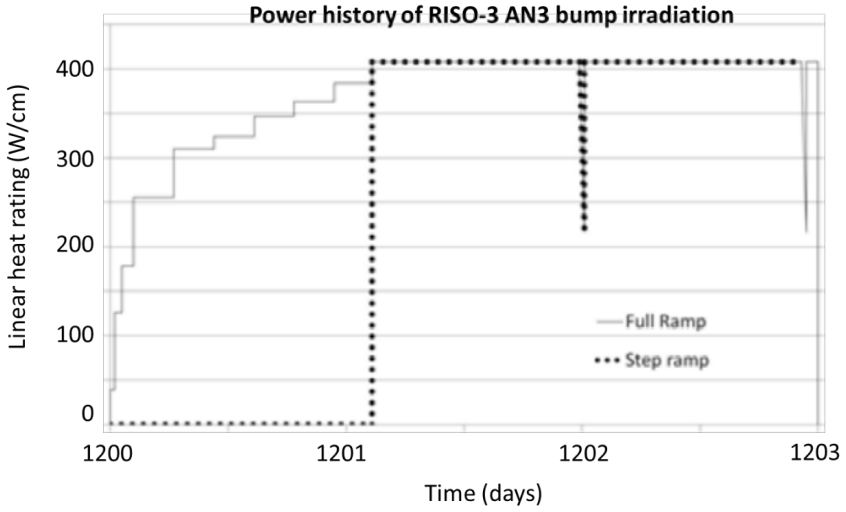

FIG. I-1. Different types of ramps used for FRCC simulation of Risø-3 AN3 Case.

Table I-2 shows a comparison of code calculations and experimental measurements on burnup, fission product generation, FGR and an internal gas pressure buildup. FGR after a transient was underpredicted for either a full or a step ramp. The prediction was better with a step ramp model. Figure I-2 shows fuel centreline temperature results for the simplified ramp history.

Table I-2. FRCC CODE VALIDATION - CALCULATIONS VS MEASUREMENTS FROM CASE 14 – RISO-3 AN3

		Base irradiation				***After bump test***		
		Burnup (GWd/tU)	***Pressure (Bar)***	***FGR (%)***	***FPG† (N cm³)***	***Burnup (GWd/tU)***	***FGR (%)***	***FPG (N cm³)***
Measurements		40.4	25.7	0.2	383	41.2	35.5	207.20
FRCC calculations	Full ramp	41.17	25.2	2.49	381	41.37	8.41	202.10
	Step ramp					41.31	26.39	201.79

† Fission product generation.

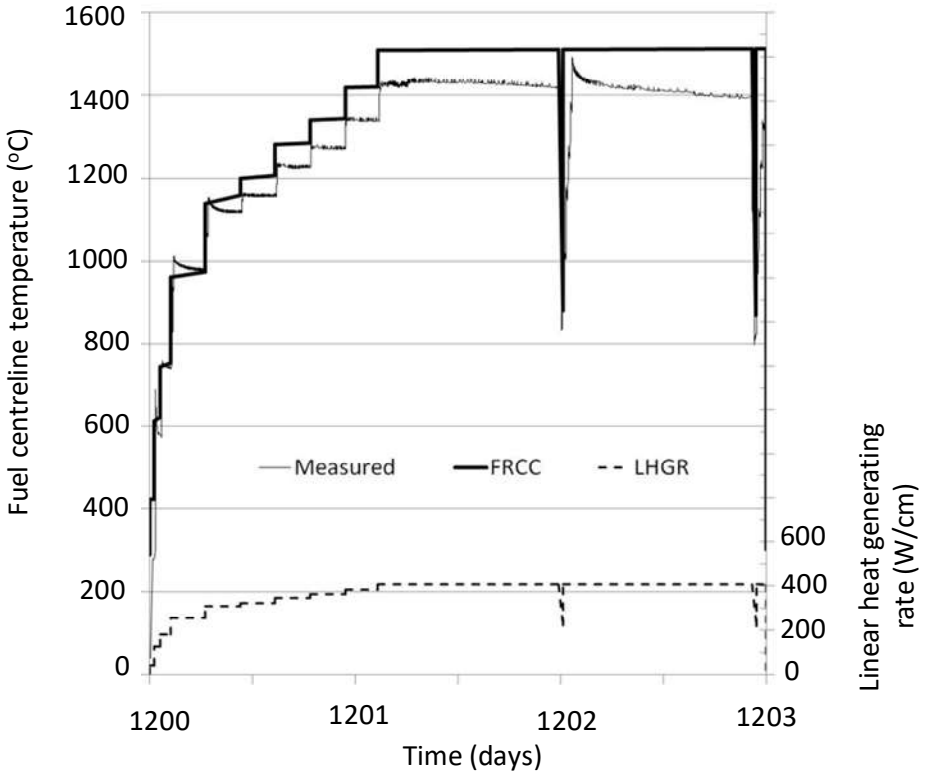

FIG.I-2. Fuel centreline temperature (measured vs calculated) for RISO-3 AN3.

I-2.2. Pellet-cladding interaction analysis

I-2.2.1. Computer codes and models

Pellet-cladding interaction (PCI) analysis with fuel analysis computer codes is based on interference criteria. The hypotheses assumed were:

- Fuel pellet is a rigid body that can expand freely without consideration of cladding contact pressure;
- Once pellet and cladding have the same diameter (gap closure), the clad adopts pellet diameter. In case pellet diameter decreases (e.g.: lower linear heat generation rating - LHGR), the gap can open again;
- Acceptable limits of cladding deformation imposed by pellet are defined for two types of interaction:
  - transient
  - long term interaction.

To improve the computational capabilities, FRCC code is coupled with a simplified BACO code (BACO-U) in this CRP. The BACO code [I-4] is another code developed in CNEA for thermo-mechanical fuel rod behavior under operation.

The main differences between FRCC and BACO-U are summarized in Table I-3.

TABLE I-3. MAIN DIFFERENCES BETWEEN THE FRCC AND BACO-U CODES

FRCC	***BACO-U***
Several densification models are available. The model is selected according to simulation requirements.	A fixed model is used.
Irradiation enhanced creep of the cladding is accounted for.	A fixed model chosen from bibliography is used.
Fuel is considered as a rigid body and the cladding follows its deformation.	Fuel deformation by clad contact pressure is calculated.
PCI limits are defined in terms of clad strain.	Clad Hoop stress is used as the limiting parameter regarding PCI.
Maximum internal gas pressure and maximum fuel centreline temperature values are obtained using maximum pellet-clad gap as input data.	Maximum internal gas pressure is calculated using the nominal pellet-clad gap as input data Maximum fuel centreline temperature is obtained using the maximum pellet-clad gap.

I-2.2.2. PCMI analysis for ATUCHA fuel elements

The maximum allowed LHGR on a power transient (plant start-up, refueling, fuel reshuffling) is a function of the local burnup and the pre-conditioning power. The last one is considered only for refueling and reshuffling. Both parameters are continuously calculated for all the fuel assemblies in the core.

If a power increase is higher than the calculated limit, the plant operator is allowed to do a fast ramp up to the maximum allowed power. After that point, the remaining power increase should be done at a slow rate to avoid PCI failures. The application of this requirement impacts on the operation at extended burnup: Atucha-1 with natural uranium (NU) may reach full power from a start up after 28 hours. With a SEU core the time to reach full power is more than 35 hours.

The PCI prevention criteria in Atucha-1 and Atucha-2 use the same limits regardless of the small differences in fuel rod geometry (Table I-4).

TABLE I-4. FUEL ELEMENT GEOMETRY FOR PELLET-CLADDING INTERACTION ANALYSIS

Fuel element design parameter	***Atucha-1***	***Atucha-2***
Fuel diameter (mm)	10.63	11.58
Minimum Fuel-Clad gap (mm)	0.13	
Clad internal diameter (mm)	10.76	11.71

Maximum hoop stress for the PCI analysis during power ramps in Atucha-1 and Atucha-2 fuel elements are calculated using the BACO-U. The fuel elements are divided in 10 axial segments, where the segment 1 is the lower end of the fuel assembly (coolant inlet). Atucha-1 and Atucha-2 fuels have typical cosine axial power distribution and the average LHGR in both cores is 23.2 kW/m.

This study includes the effect of a power ramp after a steady state base irradiation. The same power histories were applied to Atucha-1 and Atucha-2 fuel elements. These power histories consist of a base irradiation with a typical LHGR distribution (average or high power) up to a target burnup and then a power transient up to a higher hypothetical value in segment 7 (the axial power distribution is equal to base irradiation) – see Table I-5. On BACO-U, for calculation purposes, the time to reach the final power level is 0.01 days. On the other hand, FRCC does not have an explicit time input, but the ramp is divided in a given number of steps to calculate the FGR during the transient. There are in total 28 power histories for each computer code (7 burnups, 2 types of FR and 2 base irradiation power).

TABLE I-5. POWER HISTORIES

Power history parameters	***Rod average value***	***Max. LHGR (Segment 7)***
Medium power (core average) (W/cm)	232	290
High power (W/cm)	406	509
Local burnup before the ramp (MWd/kgU)	0.0 7.8 11.8 15.7 19.6 23.5 27.5	

For each ramp, there are two points of interest that were considered in the comparison: hard contact (gap closure) and cladding strain of 1% (PCMI limit in transient).

Figure I-3 shows the calculated LHGR at ramp that generate hard contact between the pellet and the cladding.

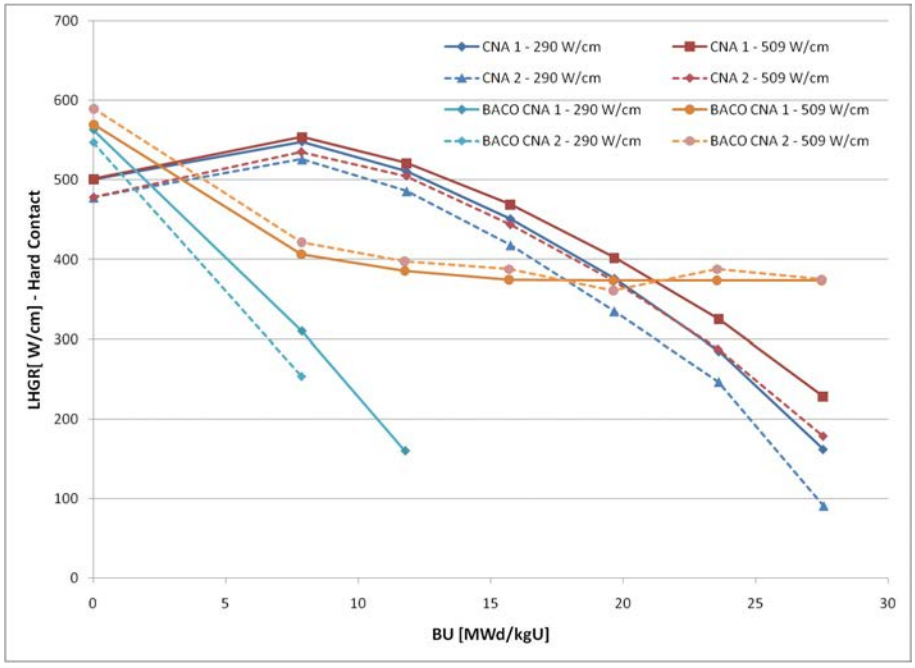

FIG.I-3. LHGR at ramp for gap closure vs. Burnup.

I-2.2.3. PCI-SCC: Real Atucha-1 Case

On June 1985 ten fuel elements of Atucha-1 with NU failed after a power cycle. At that time, the neutronic calculations were performed considering only 1/3 of the core. After this event a new neutronic code was developed for full core calculation [I-5]. More accurate analysis of power distribution proved that axial power profiles with high local LHGR led to fuel failures

by SCC. Figure I-4 shows the core positions with failed fuels. The channel J24 had the highest LHGR during the transient. The fuel had an average burnup of 2.87 GWd/tU and a preconditioning power of 39.3 kW/m. During the transient, the maximum LHGR achieved was 71.1 kW/m at segment 3. This failed fuel was modeled with a simplified power history considering previous irradiation data and the ramp was introduced as a fast transient.

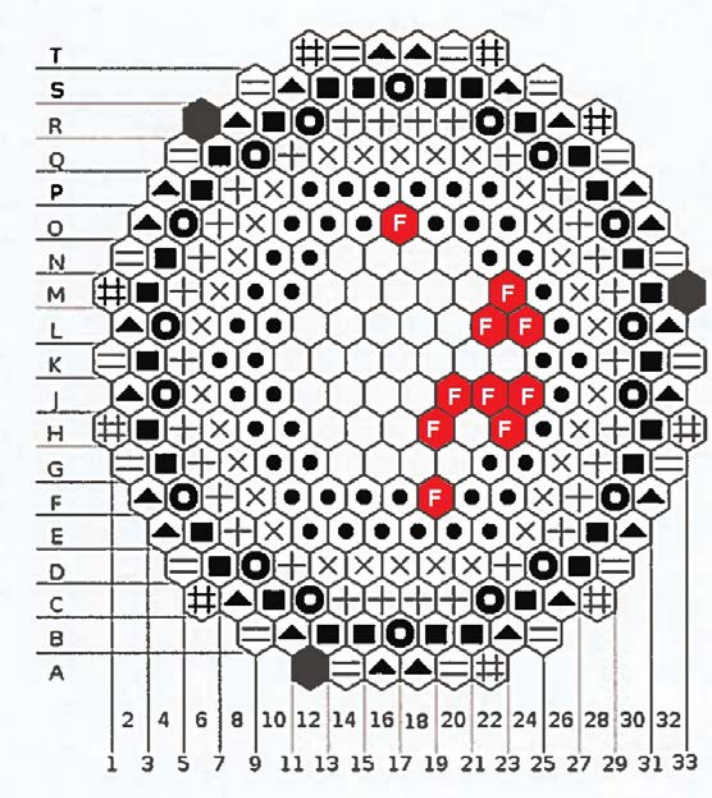

FIG.I-4. Atucha-1 reactor core showing channels with failed fuels (F) after the 1985 event.

The calculated cladding strain in segment 3 at 71.1 kW/m was 0.61 % DCM (medium clad diameter) by FRCC and 0.41 % DCM by BACO-U. These results are below 1 % limit for PCMI. BACO-U shows a maximum hoop stress of 207 MPa, which is higher than the SCC limit of 170 MPa (Fig.I-5).

I-3. IMPROVEMENTS ON CLADDING MATERIALS AND COATINGS

I-3.1. Synopsis

Advanced fuel cycles involving higher burnups are proposed for the existing PHWRs. One of the main concerns in the new high burnup conditions is the occurrence of failures associated to PCI-SCC. This subsection discusses effects of different cladding materials and internal coatings to improve resistance to PCI-SCC failures. A Lead Test Assembly (LTA) program for final evaluation of new materials is being planned.

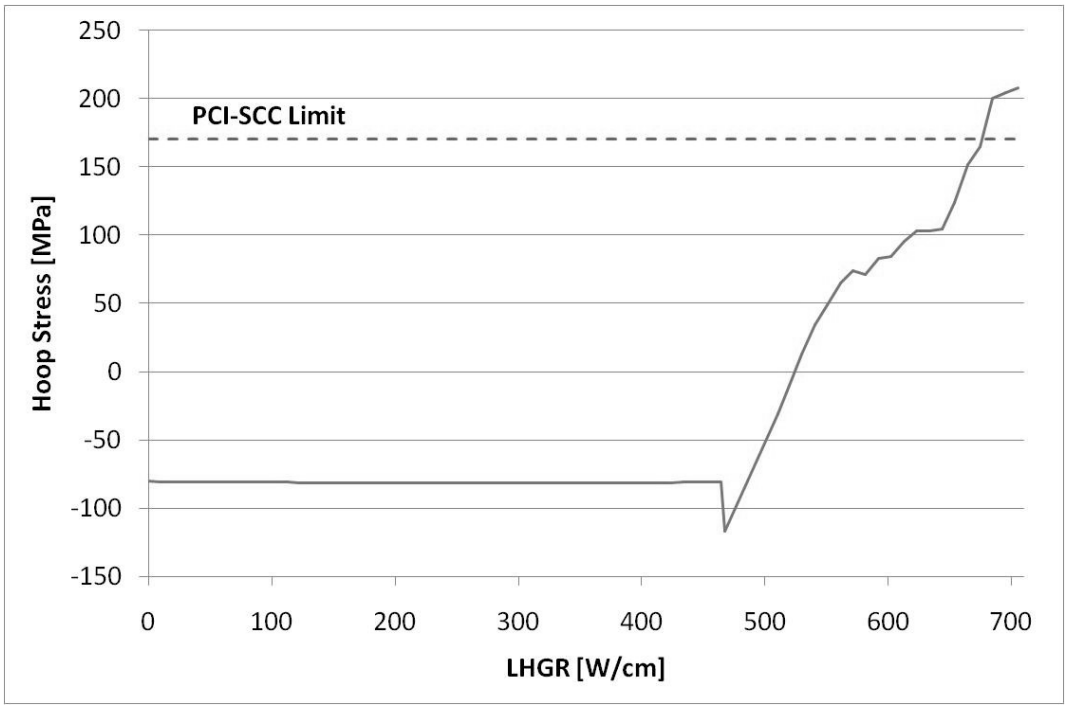

FIG.I-5. Fuel failure analysis: hoop stress vs. LHGR – Segment 3.

I-3.2. Solutions against PCI-SCC fuel failures

Pellet-cladding interaction-stress corrosion cracking (PCI-SCC) occurs due to three main factors: localized high stresses in the cladding produced by the interaction with the expanded pellet, the presence of SCC agents such as Iodine and Cesium at high burnup, for fission products release from the pellet and a susceptible material to SCC, such as, zirconium alloys. This type of fuel failure is more relevant at high burnup. The most common solutions to improve the performance of PHWR fuels against such failures are divided in two groups.

I-3.2.1. Internal coatings

For a prevention of power-ramp induced failure in CANDU fuel elements, use of internal coatings with graphite or siloxane is considered as the best solution so far [I-6]. The graphite coating DAG-154 is commonly used in this type of reactors and this solution has being used in fuels fabricated in Argentina for the Embalse NPP (CNE) since the beginning of the 80's. The protection against PCI-SCC is achieved mainly because the 'getter' property of the coating as the carbon absorbs iodine in the form of a complex stabilized zirconium iodide [I-7].

It was shown that at greater demands on power ramps and at higher burnups, the siloxane coating has better performance against fuel failures [I-8]. Siloxane coating has not been used because its coating thickness and hydrocarbon content are issues that still need to be controlled. Recent studies indicate that these problems could be solved using poly-siloxane coating that is recently being developed [I-9].

Comparing the coating alternatives, the main advantage of the graphite coating is that it has been widely use in CANDU fuels. The poly-siloxane, however, has shown a better aptitude as getter for SCC agents and adhesion on the sheath, which is important for long term performance.

In Atucha-1 and Atucha-2 fuel elements, the application and control of non-metallic coatings is unpractical so far. The current solution for long fuel rods (boiling water reactors) is an internal coating of pure Zr (i.e. Zr-liner) applied by coextrusion. The inner layer of pure zirconium has more ductility and therefore a better performance against PCI failures.

I-3.2.2. Improved cladding materials

Another option considered to improve the resistance of the fuel rods to the PCI-SCC phenomenon is to replace the cladding material.

In the 90´s the failures by PCI and I-SCC in LWRs were the driving forces to find an alloy that was immune to such failures. It was found that one of the alloying elements that improve resistance to I-SCC is the Nb. Several countries developed and applied commercially this type of alloys. The main driving forces for those developments were to improve the corrosion resistance at very high burnups.

Some alloys have shown good performance in PWR with good service experience regarding corrosion, creep and corrosion at high temperatures [I-10]. Considering that new cladding materials do not necessarily increase the reliability in the performance of the PHWR fuel elements on power ramps, the conclusion from CNEA is that a change on cladding material is not required to extend the irradiation level of PHWR fuels. Changing of the material is also not required to improve the corrosion resistance of the PHWR fuels, because the burnup level at extended cycles is considerably lower than the current final burnups of PWR fuels.

I-3.3. Road map for improvements implementation

As part of these studies, an implementation program was designed to evaluate the performance of poly-siloxane coatings and to implement it on the fabrication line. This program includes both out-of-pile and in-pile tests using fuel elements and fuel assemblies. Conditions for these tests have been established based on design critical service conditions of PHWRs in Argentina at extended burnup.

I-3.3.1. Test conditions for Atucha-1 & Atucha-2 fuel elements

To define test conditions for Atucha-1 and Atucha-2 fuel elements, several operating conditions have been considered. As mentioned before, in 1985 fuel elements of Atucha-1 failed after a power cycle. The conditions in which those fuels had failed were selected for the evaluation of new coatings and new materials for Atucha type fuel elements. Those conditions are summarized in Table I-6.

TABLE I-6. PROPOSED TEST CONDITIONS FOR ATUCHA-1 AND -2 FUEL ELEMENTS

Average burnup (MWd/tU)	*Conditioning level (W/cm)*	*Power increase (W/cm)*	*Maximum power (Ramp terminal level) (W/cm)*	*Maximum ramp rate (W/cm.h)*
2785	394	317	711	200

I-3.3.2. Test conditions for EMBALSE fuel elements

Test conditions for Embalse fuel elements were obtained from design documentation of this NPP. Two tests conditions were selected. The maximum power was 10% above the design

value for power ramps. Two cases of burnup (medium and high) were considered. Tests conditions are summarized in Table I-7.

TABLE I-7. TEST CONDITIONS FOR EMBALSE FUEL ELEMENTS

	Average burnup (MWd/Tu)	***Conditioning level (W/cm)***	***Power increase (W/cm)***	***Maximum power (Ramp terminal level) (W/cm)***
Medium burnup	4167	490	115	605
High burnup	11 667	395	100	495

I-3.3.3. Future irradiation tests capabilities in Argentina

Currently, Argentina is building a multipurpose Research Reactor (RA-10), which is expected to be finished in the year 2020. This reactor will include a facility to allow the irradiation of materials and fuels. It will include a separate loop for irradiation tests of fuel rods. The RA-10 will allow two modes of testing: fuel performance evaluation under high burnup and transients under power ramps.

I-3.3.4. Lead Test Assembly (LTA) program

Considering poly-siloxane as the selected coating material, a lead test Assembly (LTA) program for introducing PHWRs fuels in Argentina is being proposed. The LTA program should have the following steps:

Step 1: Processes adaptation for new materials

After the, the small-scale manufacturing tests and characterization, the process adaptation for industrial production needs to be developed. The. To set up the process, several controls need to be done, such as residual hydrogen, adherence and thickness. The first one is critical for the evaluation of the feasibility of the use of poly-siloxane coating.

Step 2: Process qualification

A qualification program will provide information to assess the quality of the products and to demonstrate the fulfillment of the specified requirements. Process qualification will be based on the experience with the graphite coating.

Step 3: Fuel elements for irradiation tests in a material test reactor

Tests conditions for each of the two types of PHWRs in Argentina were described previously in this work.

Step 4: Post-irradiation inspection

The objective of the fuel test is to qualify a new coating for reactor application. The post irradiation inspection will include:

- external visual inspection looking for cladding failures or other abnormalities;
- internal characterization of the coating, especially in the zones of PCI;

- adhesion and thickness measurements;
- chemical analysis for checking the behavior of the coating as a getter for fission products;
- hydrogen distribution within the cladding;
- mechanical properties testing on irradiated cladding.

Step 5: Program for LTA insertion in NPPs

Three fuel channels will be selected for LTA irradiations. Maximum power levels and time at irradiation will be considered. The LTA will include 1/3 of the external fuel rods that contain the proposed coating. These fuel rods will be equally distributed in the external ring of the fuel assembly. The remaining fuel rods of the fuel assembly will have graphite coating.

Step 6: Online sipping and post-irradiation inspection of LTA

The Argentine PHWRs have different designs but there are some common characteristics such as: on-line refueling, fuel shuffling and in-pool facilities for the visual inspection of irradiated fuel. Atucha-1 and Atucha-2 NPPs have on-line sipping detection system in the refueling machine and Embalse NPP has on-line defective fuel detection systems and in-pool sipping to confirm the defectiveness in case of failure. Removal of experimental fuel rods from the LTA and hot cell examination is also possible.

Step 7: Validation of fuel assembly

If the result of the first LTAs irradiation is successful, the final step of the program will be the irradiation of new LTAs completely fabricated with the proposed design improvements. Once the new designs and the manufacturing processes are qualified, a full core implementation will follow.

I-4. IMPROVEMENTS ON FUEL PELLETS

Some potential improvements of fuel pellet designs were also studied to increase the reliability of PHWR fuel at extended burnup.

The increase of fuel discharge burnup may require a minimization of the release of fission products during the irradiation. It is generally accepted that at typical power levels of water cooled reactors FGR is affected by the grain size of the pellets. The rate of FGR decreases due to increased length for diffusion of gas atoms in large-grained pellets. The increased grain size in pellets can be achieved via:

- use of additives,
- changes in sintering conditions,
- use of heat treated U_3O_8 powder, or
- changes in fuel pellets manufacturing process.

I-4.1. Additives

A method to increase the grain size in the pellet is to use low concentrated dopants (e.g. Cr_2O_3, Al_2O_3) in UO_2 powder. The thermos-physical properties of fuel pellets such as enthalpy, thermal expansion, etc. may be affected by such additives.

From literature survey, it was found that due to the use of dopants (e.g. Cr_2O_3, Al_2O_3, TiO_2, Nb_2O_5), grain size and porosity in sintered pellets increased. Sintering densities were not the same for all the test cases; in some of them, the density increased with use of additives and in others it decreased, indicating that sintering density depends on the types of additive and UO_2 powder used.

For Argentina PHWR fuels, the appropriate grain size would be targeted in a range of 30 to 40 microns. Since the target grain size is not extremely large, in principal, it can be achieved by any of additives studied. To avoid any changes in the industrial manufacturing process and based on the international experience on using Cr_2O_3 as additive in PWR fuels, the use of 0.05 wt.% Cr_2O_3 is the preferred option in this study.

Once the additive was defined, the impact of the use of chromia on UO_2 properties was considered. The properties analyzed included: fuel enthalpy, heat capacity, thermal conductivity [I-11], thermal expansion [I-12], diffusivity coefficient [I-13], Young's modulus and Poisson's ratio [I-14]. As a result, it was concluded that the incorporation of chromia in the amount proposed would not affect the physical properties of fuel pellets. Therefore, the properties of doped UO_2 with a small amount of chromia are considered the same as pure UO_2.

The use of chromia (0.05 wt%) would not cause significant changes in the current industrial manufacturing process, because the additive should be incorporated in the homogenization step. Since the amount of chromia to be aggregated is small, it is recommended to perform a MasterMix prior to homogenization. The MasterMix consists of mixing the additive with a small amount of UO_2 powder to achieve good homogeneity and then incorporate this mixture into the homogenizer (Fig.I-6).

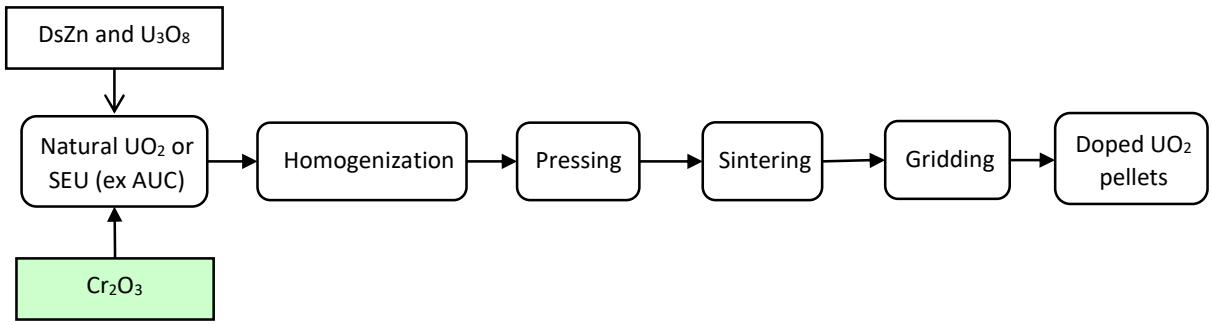

FIG.I-6. Schematic representation of an industrial process adaptation for doped pellets.

I-4.2. Sintering conditions

A high sintering temperature and a long sintering time allow reaching high densities and large grain sizes. Nevertheless, these sintering conditions will increase manufacturing cost. Keeping this in mind, several manufacturing methods have been developed using different sintering conditions seeking to obtain the same benefits.The low temperature sintering was proposed to obtain large grained UO_2 fuel pellets. This technology implements a two-stage (or more stages) pellet sintering process and a change at the sintering atmosphere. Harada [I-15] introduced a three-stage sintering process than achieves grain sizes three times larger than that of pellets sintered in reducing atmosphere of H_2 at 1750 °C (8 μm). Other researches [I-16] developed a sintering process which consists of four stages (CO_2-air-CO_2-H_2). They demonstrated that the time of the second stage influences sintered density and grain size.

The low temperature sintering technology allows obtaining the desired grain growth but the industrial implementation requires big changes on an existing fabrication line and its practical application is less feasible.

I-4.3. Heat-treated U_3O_8 powder

U_3O_8 powder is an additive commonly used in the manufacture of fuel pellets. Generally, this powder is obtained by oxidation of suitable rejections of sintered pellets, reducing the scrap in the manufacturing process of fuel pellets. So, the reuse of those pellets implies an economic benefit. Generally, the amount of U_3O_8 added to UO_2 powder is not higher than 10 wt%.

The industrial process carried out in Argentina to obtain U_3O_8 powder is the conventional method which involves the oxidation of scrap of UO_2 pellets in air at about 400 °C. The use of this decrease the density of UO_2 pellets because of the very low sintering activity of the U_3O_8 powder compared with the UO_2 powder. In addition, the grain size and the open porosity are degraded in some extension. The use of U_3O_8 powder improves the strength of green pellets, reducing chipping and end-capping defects [I-17]. So, this process does not accomplish the sintered density and grain size required for development of nuclear fuel for high burn-up.

Many works that deal with different heat-treatments of the recycled U_3O_8 or the use of additives to the U_3O_8 to improve U_3O_8 powder sintering activity and achieve a large grain UO_2 pellet have been published.

In [I-18], [I-19], a heat-treatment after the oxidation of the scraps of UO_2 pellets are proposed. The U_3O_8 powder obtained was heat-treated for 4 hours at 1000-1500 °C. U_3O_8 particles bonded together into particles consisting of many crystals. These particles were reduced in size mechanically to increase its sintering activity. This process resulted in a decrease in the number of crystals per particle. These U_3O_8 particles are referred as 'U_3O_8 seeds'. It was found that the seeds of 5 μm heat-treated at 1300 °C for 4 h and added in a quantity of 4 %, were more effective to increase grain size and reach a maximum of 20 μm. Besides they observed that as the content of U_3O_8 seed increases, the sintered density of UO_2 pellets decreases and that there is a seed content that would maximize the grain size.

Another process to obtain U_3O_8 powder of controlled morphology was developed by Kang, K.W. et. al [I-20] to fabricate large-grained UO_2 fuel pellets. Through this process the surface area of the U_3O_8 powder is two times larger than the initial U_3O_8. The same authors also investigated the effect of Al-doping in the grain size and the density of UO_2 pellets, and found that a surface area of about 1.2 m^2/g acts as a grain-enlarging promoter more effectively.

An optimized process for rejected UO_2 pellets was proposed in [I-21]. Through lowering the oxidation temperature at 350 °C, U_3O_8 powder with a small particle size and high surface area than those prepared by the conventional method (7-8 μm) were obtained. The UO_2 pellets containing this powder may duplicate the grain size. In addition, the sintered density of the UO_2 pellets was maintained. Other researchers developed the oxidizing process at 325, 350 and 450 °C in air [I-22], and revealed that the measured surface area of U_3O_8 powder oxidizing at 325 °C is twice than those treated at 450 °C. In addition, they found that the sintering density drop is considerably mitigated in pellets fabricated with low-temperature-oxidized U_3O_8 powder.

All the different methodologies exposed above achieve the increase in grain size of UO_2 pellets. Moreover, none of them implies severe changes in the infrastructure of the

manufacture plant. In particular, for the method of lowering the oxidation temperature, it is only necessary to change the setting temperature of the oven.

As a conclusion of this study, an oxidation temperature of 325 °C (Fig.I-7) could be selected as first option to improve the performance of our nuclear fuels without significant changes in U_3O_8 powder production.

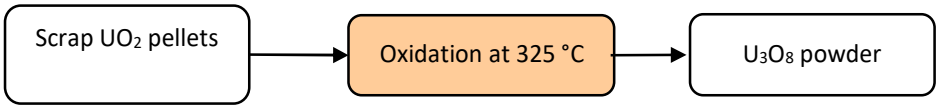

FIG.I-7. Schematic process to obtain improved U_3O_8 powder.

I-4.4. Changes in the manufacturing process

The characteristics of UO_2 powder depend on powder preparation method [I-23]. The industrial UO_2 ex-AUC powder has good sinterability and flowability properties. These characteristics allow direct processing in an automatic press. Ex-ADU powder should be prepressed and granulated before pressing due to lack of flowability. It has been proposed in this study to consider the AUC powder to similar pre-compacting and granulating steps with ADU powder. The objective of this proposal was to evaluate if this preparation of such powder may result in an improvement in the quality of the fuel pellets for the PHWRs.

Several tests were performed to evaluate the effect of pre-pressing and granulating ex-AUC powder. Ex-AUC powder with 4% percent of U_3O_8 and Zinc Distearate was prepressed to a green density of 3.8 g/cm^3 and then granulated with a mesh of 1600 µm to obtain UO_2 powder. After that, the percentage of Zinc Distearate was adjusted in the mixer and then the pressing and sintering stages were performed. Two sintering conditions were evaluated. In Test 1 the sintering temperature was 1,640 °C, which is the same temperature used for ex-ADU pellet. A temperature of 1750°C, which is used in the current industrial process, was used in Test 2. In both conditions the increase in density was achieved, but the grain size decreases.

Considering the improvement in density, a new set of tests is designed to quantify the variable of the process and to evaluate the possibility of increasing the grain size. These tests will include the addition of treated U_3O_8 powder in a pre-mixing step.

As a result of the literature survey and the first tests, with UO_2 ex-AUC powder prepressed and granulated, it is possible to conclude that a slight modification of the temperature to obtain U_3O_8 may have a positive benefit on obtaining pellets with large grain sizes. This benefit could be also extended to the density of the pellets if the ex-AUC powder for pellets fabrication is previously submitted to a pre-pressing and granulating process.

I-5. GENERAL CONCLUSIONS AND FINAL STATEMENTS

The operational experience in Atucha-1 reactor (vertical channel type PHWR) supported that SEU with 0.85% enrichment allows increasing the discharge burnup to about twice of the typical NU burnup without requiring any modification of reactor control mechanisms. Several fuel performance parameters are identified as life limiting factors to high burnup operation.

These life limiting factors could be controlled by reducing LER or with specific design measures or new fuel management schemes. Through a literature survey, the large grain sized pellet has been proposed as a viable design to reduce the fission gas release and associated internal gas pressure in the fuel element. Internal coating with poly-siloxane or zirconium liner on the inside surface of the cladding has been proposed to prevent PCI-induced fuel failures. The final selection of a coating material will require additional experimental evidences which will include the irradiation of experimental fuel rods and LTAs.

Computational codes are valuable tools to assist the verifications and the design process of the advanced high burnup fuels. The activities of this CRP also included validation exercises considering typical power histories of the PHWR with vertical channels, specific conditions that led to PCI-SCC failures in Atucha-1 and information from irradiation tests available in the literature. Based on the results obtained in this exercise it is possible to extend the validation of the codes used in this activities to the high burnup conditions associated with advanced fuels for the above-mentioned type of reactor.

ACKNOWLEDGEMENTS

This Research Contract was led by Chief Scientific Investigator, Luis Alvarez of CNEA, Argentina. Co-investigators included: Pablo Tripodi, Alejandro Bussolini, Alejo Minetti, Juan Pablo Medina, Maria Emilia Medina of CNEA, Argentina.

REFERENCES TO ANNEX I

[I-1] BUSSOLINI, A., TRIPODI, P., ALVAREZ, L., “Preliminary Design Studies to Evaluate the Utilization of SEU in Atucha-2 Fuel Rods”, paper presented at Technical Meeting on Advanced Fuel Cycles in Pressurized Heavy Water Reactors, Mumbai, India, 2013.

[I-2] INTERNATIONAL ATOMIC ENERGY AGENCY, Report of the Coordinated Research Project 2002-2007: Fuel Modelling at Extended Burnup (FUMEX-II), IAEA-TECDOC-1687, IAEA, Vienna (2012).

[I-3] RISO NATIONAL LABORATORY, The Third Risø Fission Gas Project: Bump test AN3 (CB8-2R), Risø-FGP3-AN3, RISO (1990).

[I-4] MARINO, A. SAVINO, E., HARRIGUE, S., BACO (Barra Combustible) Code Version 2.20: A Thermo-Mechanical Description of a Nuclear Fuel Rod, Journal of Nuclear Materials **229** (1996) 155.

[I-5] FERRERI, A., SIDELNIK, J., GRANT, C., Simulación del transitorio de potencia ocurrido en la CNA-1, el 14/6/85. Tomando en cuenta la dependencia espacial del Xenón, paper presented at AATN Annual Meeting (Argentine Nuclear Technology Association), 1986.

[I-6] COX, B., Pellet-Clad Interaction (PCI) Failures of Zirconium Alloy Fuel Cladding – A Review, Journal of Nuclear Materials **172** (1989) 249.

[I-7] CHAN, P.K., KADDATZ, K.J., “How does CANLUB work?”, Proceedings of the 15th Annual Conference of the Canadian Nuclear Society, Montreal, Canada, 5-8 Jun 1994.

[I-8] WOOD, J.C., HARDY, D.G., BAIN, A.S., “Improved CANDU Fuel Performance”, IWGFPT/5 (Proceedings of Specialists' Meting on Power Ramping and Power Cycling of Water Reactor Fuel and its Significance to Fuel Behavior, Arles, France, 1979), IAEA, Vienna (1979) 79-83

[I-9] FARAHANO, M., FERRIER, G.A., CHAN, P.K., CORCORAN, E.C., "Beyond CANLUB: An Improved Alternative Coating Development", Proceedings of 12th International Conference on CANDU Fuel, Kingston, Ontario, Canada (2013).

[I-10] KIM, H-G., PARK, J-Y., JEONG, Y-H., KOO, Y-H., YOO, J-S., MOK, Y-K., KIM, Y-H., SUH, J-M., In-Pile Performance of HANA Cladding Tested in Halden Reactor, Nuclear Engineering and Technology **46** (2014) 423.

[I-11] MASSIH, A., Effects of Additives on Uranium Dioxide Fuel Behavior, Report number 2014:21, Swedish Radiation Safety Authority (2014); ISSN: 2000-0456.

[I-12] ARBORELIUS, J., BACKMAN, K., HALLSTADIUS, L., LIMBACK, M., NILSSON, J., REBENSDORFF, B., ZHOU, G., KITANO, K., LOFSTROM, R., RONNBERG, G., Advanced Doped UO_2 Pellets in LWR Applications, Journal of Nuclear Science and Technology **9** (2006) 967.

[I-13] KASHIBE, S., UNE, K., Effect of Additives (Cr_2O_3, Al_2O_3, SiO_2, MgO) on Diffusional Release of ^{133}Xe from UO_2 Fuels, Journal of Nuclear Materials **254** (1998) 234.

[I-14] AREVA INC., Incorporation of Chromia-doped Fuel Properties in AREVA Approved Methods, Topical Report, ANP-10340NP Rev. 0, AREVA (2016).

[I-15] HARADA, Y., UO_2 Sintering in Controlled Oxygen Atmospheres of Three-Stage Process, Journal of Nuclear Materials **245** (1997) 217.

[I-16] JOUNG, C.Y., LEE, S.C., KIM, S.H., KIM, H.S., SOHN, D.S., Fabrication Method for UO2 Pellets with Large Grains or a Single Grain by Sintering in Air, Journal of Nuclear Materials **375** (2008) 209.

[I-17] PRAMANIK, D., RAVINDRAN, M., RAO, G.V.S.H., JAYARAJ, R.N., "Innovative Process Techniques to Optimize Quality and Microstructure of UO_2 Fuel for PHWRs in India", Advanced Fuel Pellet Materials and Fuel Rod Design for Water Cooled Reactors (Proceedings of a Technical Committee Meeting held in Villigen, 23-26 November 2009), IAEA-TECDOC-1654, IAEA, Vienna (2009) 13-34.

[I-18] SONG, K.W., KIM, K.S., KANG, K.W., JUNG, Y.H., Large-Grained UO_2 Pellets without Impurity Additives, Conference on Characterization and Quality Control of Nuclear Fuels, Allied Publishers (2002) 247-257.

[I-19] SONG, K.W., KIM, K.S., KANG, K.W., JUNG, Y.H., Grain Size Control of UO_2 Pellets by Adding Heat-Treated U_3O_8 Particles to UO_2 Powder, Journal of Nuclear Materials **317** (2003) 204.

[I-21] KANG, K.W., JANG, J.H., KIM, J.H., RHEE, Y.W., KIM, K.S. Kim, SONG, K.W., Improvement of UO_2 Pellet Properties by Controlling the Powder Morphology of Recycled U_3O_8 Powder, Journal of Nuclear Science and Technology **11** (2008) 1150.

[I-22] LEE, S.J., JUNG, D.H., SUH, J.M., KIM, J.I., JEON, K.L., LEE, J.R., KIM, K.S., SONG, K.W., Development of Commercial Manufacturing Technology for Large Grain UO_2 Pellets, Transactions of the Korean Nuclear Society Autumn Meeting (2010) 283-284.

[I-23] YANG, J.H., KANG, K.W., KIM, K.S., RHEE, Y.W. and SONG, K.W., Recycling Process for Sinter-Active U_3O_8 Powders, Journal of Nuclear Science and Technology **6** (2010) 538.

[I-23] MARAJOFSKY, A., PEREZ, L., CELORA, J., On the Dependence of Characteristics of Powders on the AUC Process Parameters, Journal of Nuclear Materials **178** (1991) 143.

ANNEX II.

ANNEX II: USE OF NEUTRON ABSORBERS TO IMPROVE CANDU OPERATING MARGINS FOR NATURAL URANIUM AND OTHER ADVANCED FUEL CYCLES

A Summary Report of Research Agreement with Royal Military Collage of Canada, Canada

II-1. BACKGROUND

On-power refueling is the primary means of maintaining a CANDU reactor critical. Replacing irradiated fuel with fresh fuel in a specific channel has immediate consequences on the local power distribution and reactivity. The ratio of the peak transient channel power relative to the steady state channel power can often be as high as several percentages. These power ripples (also known as refueling power ripples) often bring channel operating parameters very close to a neutron overpower protection trip setpoint and require immediate zone reactivity control system actions. With the added effects of heat transport system aging, where the trip margin is already tight, xenon-free effects and plutonium production in the natural uranium (NU) fuel could potentially lead to a temporary power derating following a CANDU reactor fueling operation. Therefore, a significant margin is needed to accommodate for these refueling power ripples during the operation of the reactor, which has a large impact on fuel and physics, and reactor operation.

Online-refueling is daily carried out, and refueling alone cannot achieve the fine control of the desired flux and power distributions. In practice, the latter is controlled using adjuster rods and liquid zone controllers (LZCs), in addition to strategic refueling schemes in CANDUs. The adjuster rods, normally inserted and fixed in position near the central region of the core (where the magnitude of the neutron flux is highest), provide flux and power flattening, as well as xenon override capability [II-1]. The LZCs provides fine reactivity control that compensates for minor perturbations in parameters such as temperature, reactivity and power due to daily refueling operations. The LZCs consist of six vertically oriented tubes running between the fuel channels from the top to the bottom of the core. There is a total of fourteen individual zone compartments in the CANDU reactor core: the two central tubes are divided into three compartments each and the four outer tubes into two compartments each. The reactor regulating system adjusts the amount of light water (H_2O) fills in the individual compartments according to the magnitude of the signals from in-core self-powered detectors.

When a given channel is refueled, the reactivity of the whole reactor core increases by a very modest amount, but the refueled channel and its neighbor will experience a significant increase of the local flux and power density values. This is due to the high reactivity of the fresh fuel bundles. Figure II-1 displays the power profile of a 37-element fresh fuel bundle subjected to a constant thermal neutron flux corresponding to 90% of the maximum licensed bundle power (90% of 935 kW) [II-2]. Eventually, the fuel bundle becomes a net neutron absorber and a refueling is required (at Region 5). Replacing this fuel bundle with a fresh unit will create a local power increase of almost 8.3% (from approximately 770 kW to 840 kW), the so-called power (fueling) ripple as shown in Fig.II-1.

As previously explained, the LZCs are separated into fourteen individual zone compartments strategically located within the CANDU reactor core. Taking into account the number of fuel channels found in a CANDU reactor core (380 or 480 channels), it is implied that the LZCs

derate power in many more channels than the ones affected by the fuel bundles experiencing transient powers. In other words, it is disadvantageous for the reactor's economy of neutron.

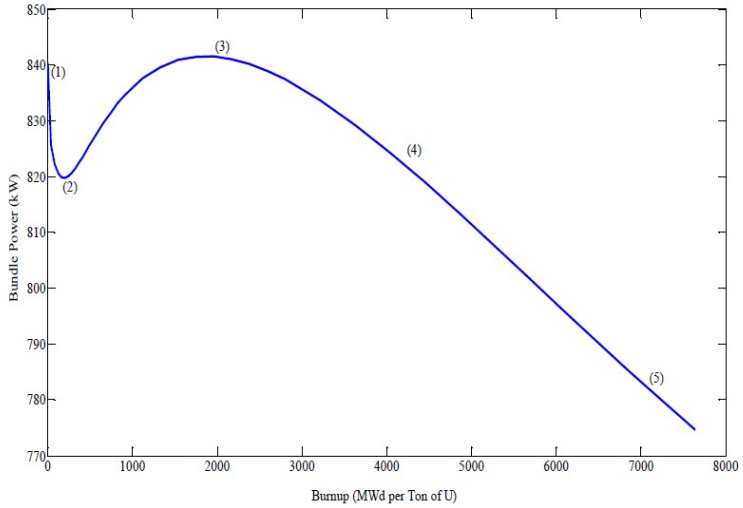

FIG.II-1. Bundle power versus burnup.

This work proposed a novel modification of the existing CANDU fuel element to improve reactor operating margins and to relax the constraints on fuel management posed by tight operating power limits.

The intent was to dope the existing CANDU fuel bundle with minute amounts of Burnable Neutron Absorbers (BNAs) to reduce the magnitude of the refueling power ripples. The design work was performed with WIMS-AECL 3.1 [II-3], MCNP 6 [II-4] and RFSP [II-5] codes. It was anticipated that adding small amounts of BNAs in the CANDU fuel elements could mitigate the fueling transient (also known as xenon free effects) and lower the reactivity/power peak due to the plutonium production in fresh fuels. The BNAs were added strategically to certain locations of a fuel bundle to further mitigate on end-flux peaking (EFP) and coolant void reactivity (CVR). Coupled with an improved fueling strategy, this concept might improve the fuel utilization and increase safety margins by lowering the maximum channel and bundle powers.

Fuel reliability and performance are always important topics to a nuclear utility. If this project is successful, benefits of improving operating margins (transient and steady states) could be realized for reasonably simple changes. Inputs from fuel manufacturers are being considered as part of this study to mitigate manufacturing risks. A high capacity factor is reliant upon the continued and safe operation of reactors and this in turn requires a sound fundamental understanding of fuel designs and a need to be able to maintain them.

This proposal advances further fuel design and management optimization that might potentially offer a more reliable and convincing solution to manage the adverse impact of aging on safety and performance of operating reactors.

II-2. APPROACH

II-2.1. Analysis approach

This CRP explored the use of BNAs to increase the operating margins of CANDU reactors while accommodating the concern for neutron efficiency, which was achieved by

incorporating trace quantities of BNAs (such as Gd_2O_3) that would be rapidly consumed during the initial period of excess reactivity within fresh fuels. In Chan et al. [II-6], lattice-burnup calculations using WIMS-AECL 3.1 was used to demonstrate that ~180 mg (~9 ppm) of Gd_2O_3 and ~1000 mg (~50 ppm) of Eu_2O_3 could be used to tailor the trend in the evolution of the reactivity of the CANDU NU fuel to a more optimal shape.

The fuel lattice-based investigation conducted by Chan et al. [II-6] had thus far provided insight on the impact of the BNAs at the fuel level. However, lattice-depletion calculations could not capture the effects of BNAs at the channel and core levels, and more importantly, the transient caused by refueling. Moreover, the actual reductions in the peak powers and the discharge burnup of fuels are highly dependent on the history of refueling, which also cannot be emulated using a lattice code. RFSP code developed by AECL was used to extend the study beyond the parameters of a single lattice cell and capture the effects of BNAs in 3 dimensions, at the core level. The simulations were based on a model of a commercial CANDU reactor that has been qualified by a utility operator. The objective of the study was to determine the reductions in the transient or 'rippled' channel powers during a sequence of individual refueling events, and to determine the reductions in the average LZC fill levels during extended core-following simulations. By determining these parameters as a function of BNA content, it was proposed that the ideal range of the quantity of BNAs could be determined with greater accuracy, along with their impact on the operation of reactors. The core-following analyses were also carried out for various Gd_2O_3-Eu_2O_3 and Gd_2O_3-B_2O_3 mixtures.

End flux peaking (EFP) is a phenomenon which affects the flux profile of a fuel bundle and occurs in the end regions that separate two individual bundles. The geometry of the end regions consists of a D_2O coolant, Zircaloy bundle endplate and endcaps, and uranium dioxide fuel pellets. MCNP 6.1 [II-4] was used to simulate the addition of a small amount of neutron absorbers strategically at the bundle ends. In the MCNP 6.1 model, as illustrated in Fig.II.2, 37 individual half elements were modelled for each half bundle. The fuel within each element was modelled as a solid rod, opposed to a fuel stack of individual pellets, with the exception to the last two pellets. The last two pellets were defined separately for the purpose of adding neutron absorbers to the fuel. The occurrence of EFP leads to higher fission rates, leading to more heat being produced and therefore higher overall temperatures within the pellets that exist adjacent to these end regions. Higher temperatures lead to an increased risk for sheath strain, corrosion and fuel centerline melting. All of which have significant impact on the integrity of the sheath and fuel pellets during a loss of coolant accident (LOCA), especially for a fresh core after refurbishment. An estimate on the impact of the added BNAs on CVR was also performed.

Using a conventional fueling pattern, refueling occurs four times per day, and serves to keep certain CANDU reactors functioning within a safe operating envelope. Attempts were made to minimize the use of the fueling machine in a multi-step approach. The conventional fueling scheme was altered in an iterative manner with the addition of 8 bundle shifts using an outside-in, an inside-out and a salt-and-pepper approach.

II-2.2. Design tools

The MCNP 6 code [II-4] is a general-purpose, continuous-energy, generalized-geometry, time-dependent, coupled neutron/photon/electron Monte Carlo transport code with the capability to calculate k_{eff} eigenvalues for fissile systems. The code simulates individual neutrons in a 3-D fissile environment based on transport data and records their average

behaviors. It follows the nuclear particles from the source throughout their entire life. The outcome at each step of their life is determined based on probabilistic events (based on random probability generators). The MCNP 6 code provides the effective multiplication factor of a system in the form of a statistical answer to the transport equation.

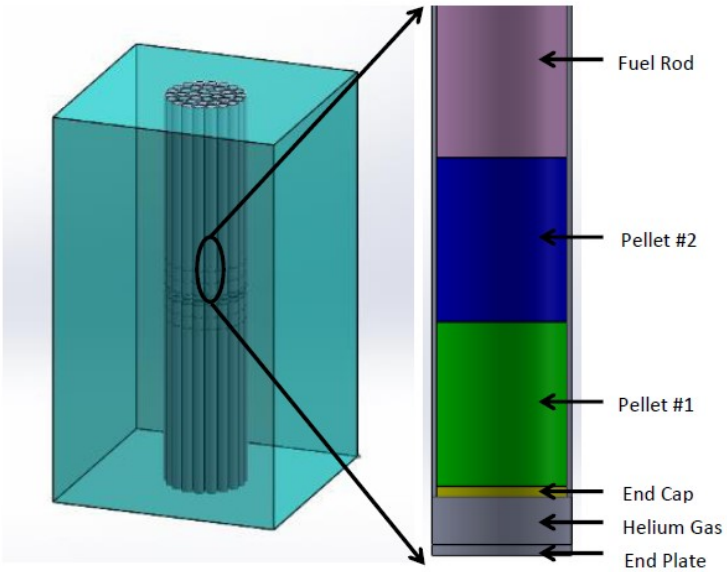

FIG.II-2. Two-half CANDU bundle model, including blown up cross-section of a fuel element.

For the EFP analysis, neutrons in the MCNP model were generated using the KCODE module. KCODE is a method used primarily to calculate reactivity and steady state neutron distributions. The code calculates an appropriate neutron source term by propagating an initial guess and refining the source term for an additional iteration. It makes use of a Watt's fission spectrum to generate neutrons. The added benefit of simulating the neutrons using KCODE is that the simulation iterates, improving each time it runs.

The computer code WIMS - AECL, Version 3.1, is a two-dimensional multi-group neutron transport code capable of applying leakage corrections and of performing fuel depletion routines for multi-cell lattices [II-3]. The code, which is an industry standard toolset (IST), is well suited for flux distribution calculations and determines the reactivity of a nuclear reactor by solving the integral form of the neutron transport equation. Therefore, WIMS - AECL is called a 'deterministic' code; whereas MCNP 6 is referred to as a probabilistic code since it uses a random probability generator.

The computer code RFSP [II-5] is a multi-modular industry standard toolset code used as the standard design and safety modelling tool by the CANDU industry. The RFSP code incorporates the fuel cell multi-group macroscopic cross-sections and diffusion coefficients generated by WIMS-AECL, and incremental cross-sections for reactivity devices generated by DRAGON-IST [II-7], to perform multitudes of neutron diffusion calculations for CANDU cores for specified geometries. RFSP is capable of simulating the effects of the local power transients caused by individual refueling events.

For the core following analysis, a standard CANDU lattice containing the 37-element NU fuel with varied quantities of BNAs was initially modelled using the WIMS-AECL code. The model was used to conduct lattice depletion calculations, and the results were used to generate

a set of 'fuel tables' containing lattice properties as functions of burnup for subsequent use by RFSP. A reference dataset of a 2650 MW_{th} (480 channels) CANDU reactor was used for the RFSP core model. The immediate impact of BNAs following refueling was determined by simulating individual fueling events designed to test the range of reductions in power ripples for every fuel channel in the core. The evolution of the impact of BNAs over extended periods of time was determined via core-following simulations designed to track a generic refueling history.

II-3. RESULTS AND DISCUSSION

The project is divided into four distinctive parts:

II-3.1. Part 1

The first step consisted of identifying viable BNAs capable of meeting the requirements of the current project. A literature review revealed that gadolinium, boron, europium and samarium are commonly used as BNAs in power reactors [II-8] – [II-11]. The current project has considered the stable oxide form for these BNAs (readily available off the shelf). A parametric study was conducted using WIMS - AECL 3.1 and MCNP 6 (See Table II-1). The intent was to observe the effects that various amounts of these common BNAs would have on a typical CANDU nuclear reactor core reactivity and burnup over time (See Fig.II-3).

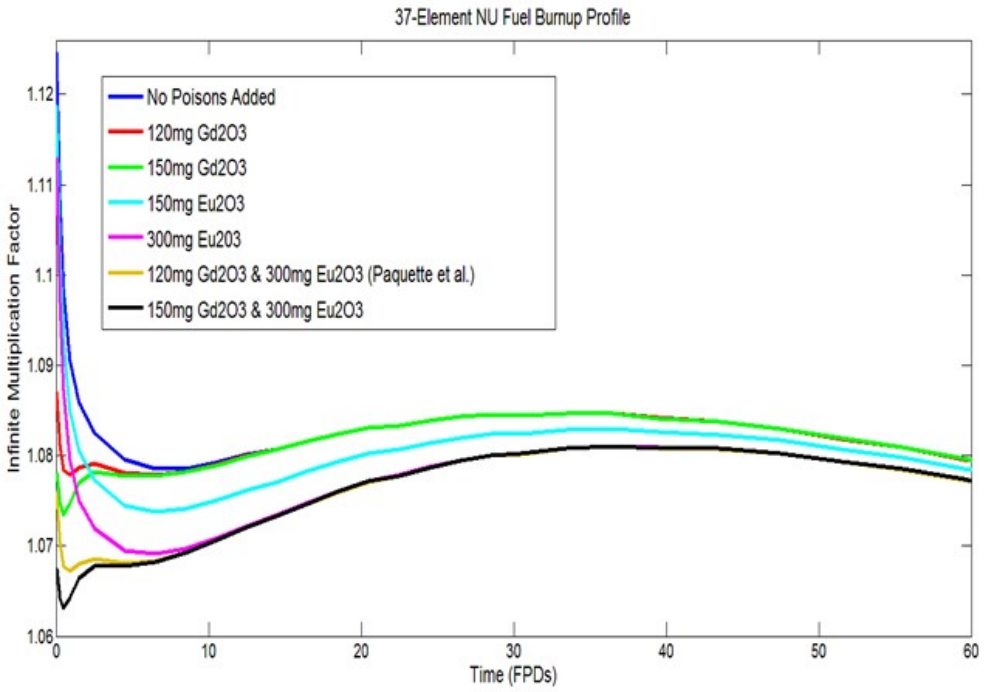

FIG.II-3. k_{inf} vs. time (0-60 FPD) for a CANDU reactor using varied quantities of Gd_2O_3 and Eu_2O_3 distributed in the CANLUB layer of a 37-elements fuel bundle.

Results revealed that samarium oxide (Sm_2O_3) and gadolinium oxide (Gd_2O_3) are short-lived BNAs and are capable of reducing the initial fueling transient. However, Gd_2O_3 was clearly more efficient and its impact on fuel burnup was negligible. Europium oxide (Eu_2O_3) and boron oxide (B_2O_3) are longer-lived BNAs. Boron was by far the most effective longer-lived BNA, regardless of its chemical form (both B_4C and B_2O_3 are commercially available).

Figure II-4 indicated that the optimal of amount of B_2O_3 and Eu_2O_3 was 35 mg 125 mg, respectively. This would bring the mean maximum channel power down by 20 kW with the LZC at ~20% and with no impact on discharged burnup.

TABLE II-1. CRITICALITY CALCULATION RESULTS (k_{inf}) USING Gd_2O_3 and Eu_2O_3

Gd_2O_3 added per fuel bundle (mg)	***MCNP (±0.003)***	***WIMS (±0.001)***
0	1.138	1.139
9	1.134	1.136
30	1.126	1.129
100	1.105	1.107
140	1.094	1.094
150	1.090	1.091
160	1.086	1.088
170	1.085	1.085
180	1.081	1.082
190	1.080	1.078
200	1.077	1.075
308	1.047	1.042

Eu_2O_3 added per fuel bundle (mg)	***MCNP (±0.003)***	***WIMS (±0.001)***
0	1.138	1.139
25	1.136	1.138
50	1.135	1.137
75	1.134	1.136
100	1.134	1.135
150	1.131	1.133
200	1.130	1.130
300	1.126	1.126
700	1.112	1.109
1000	1.105	1.102

II-3.2. Part 2

Core-following simulations were performed to demonstrate the design concept used in the current work, Gd_2O_3 was selected as the short-lived BNA and Eu_2O_3 as the longer-lived BNA, was feasible [II-12].

The core-following study for each respective BNA (different quantities of absorbers) was conducted using a generic set of refueling history. The generic refueling history was created based on an initial core-following study using the regular 37-element NU fuel. Every 0.25 FPD, the instantaneous core state was logged and its data was analyzed using a refueling algorithm written in MATLAB to decide if refueling was necessary. The algorithm was capable of deciding when refueling was necessary and which channel should be refueled, such that the desired (reference target) core state for normal operation was maintained at all times.

The core-following simulations demonstrated the effects of added neutron absorbers imparted over 400 FPDs of normal operation. Reductions in the maximum channel and fuel bundle powers, the average discharge burnup of fuels, the channel power peaking factor, the radial form factor, and the LZC fill levels were tracked in the duration of core-following to determine the impact of the added absorbers. Table II-2 summarized the results of core-following for the regular NU fuel and 6 BNAs, for a core refueled using a reference fueling

scheme. Parameters exhibiting significant changes as the result of transition from regular NU fuel to BNAs were indicated in brackets.

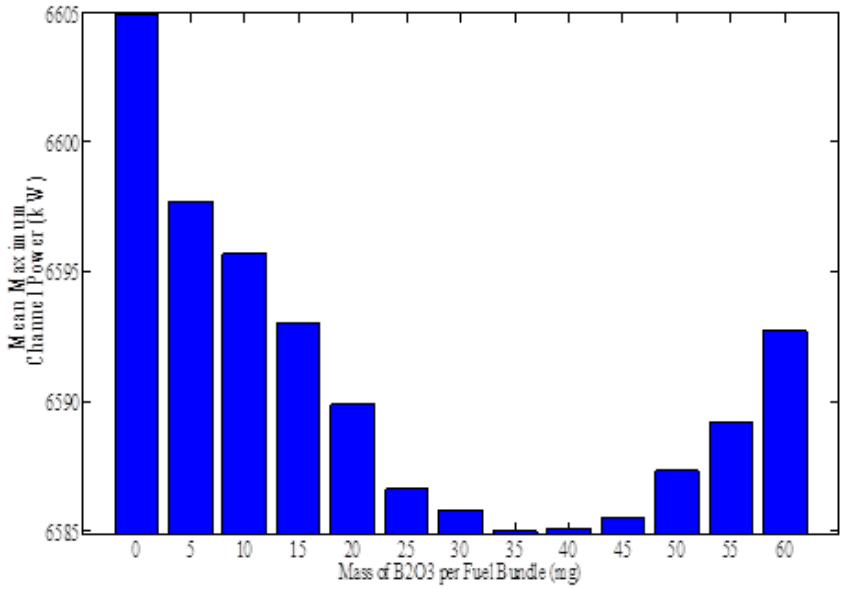

(a) B_2O_3

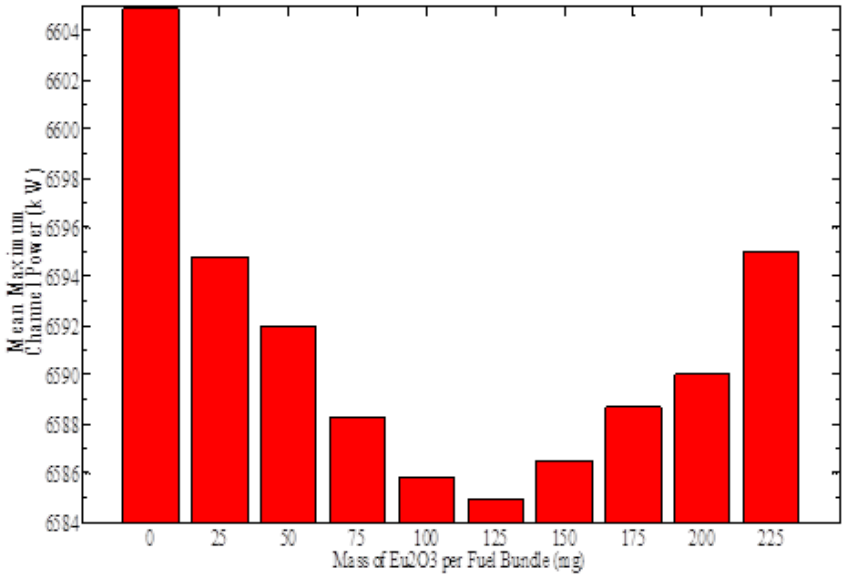

(b) Eu_2O_3

FIG.II-4. Mean maximum channel power (kW) at an equilibrium core for various amounts of (a) B_2O_3 and of (b) Eu_2O_3.

TABLE II-2. AVERAGED RESULTS FROM 400 FPDs OF CORE FOLLOWING USING 6 DIFFERENT BNAs

	Regular NU (control)	***120mg Gd_2O_3***	***150mg Gd_2O_3***	***150mg Eu_2O_3***	***300mg Eu_2O_3***	***120mg Gd_2O_3 & 300mg Eu_2O_3***	***150mg Gd_2O_3 & 300mg Eu_2O_3***
Mean exit burnup (MW-h/kgU)	169	169	169	169	169	169	169
Average peak channel power (kW)	6717	6707 (-10)	6704 (-13)	6673 (-44)	6632 (-85)	6624 (-93)	6623 (-94)
Mean CPPF	1.13	1.12	1.12	1.11	1.12	1.12	1.12
Average peak bundle power (kW)	821	820	819	814 (-7)	809 (-12)	809 (-12)	809 (-12)
Mean RFF	1.22	1.21	1.21	1.21	1.2	1.2	1.2
Mean average LZC fill level	45%	40%	40%	30%	19%	17%	17%
Mean maximum LZC fill level	92%	88%	88%	78%	53%	49%	49%

When sufficiently large quantities of BNAs were added (greater than 300mg of Eu_2O_3), the LZCs completely emptied out over a short amount of time and the excess reactivity of the core began to decline. These results provided an important consideration for the upper limit of the quantity of BNAs that could be added to the fuel, assuming that a higher rate of refueling than the reference rate was not, or could not, be utilized to compensate for the lower reactivity provided by the fuels. As the mechanical performance of refueling machines was a prime consideration for CANDU nuclear generating stations, it was understood that such increases in the rate of refueling were undesirable.

Using a reference fueling scheme, keeping the LZC level at approximately 20 to 25% and targeting the same average discharge burnup, a mixture of 150 mg Gd_2O_3/125 mg Eu_2O_3 or 150 mg Gd_2O_3/35mg B_2O_3 was recommended in this study to mitigate refueling ripples and low the Pu-peak. A feasibility study to minimize the use of the fueling machine by increasing the number of 8 bundle shifts, under various fueling schemes, could be found in part 4.

Studies performed so far were under normal operating conditions. The behavior of a 37-element fuel bundle undergoing a degraded coolant conditions during a loss-of-coolant accident was also simulated. It was determined that the industry used input density for coolant under normal operation was 0.8179 g/cc, while the voided condition commonly used for simulation was 0.05 g/cc. The AECL-WIMS code was used to conduct an analysis of the infinite multiplication factor for four cases. These cases include fresh fuel (zero full power days in core) with and without burnable neutron absorbers and burnt fuel (forty-five full power days in core) with and without burnable neutron absorbers. For these analyses, neutron absorbers were uniformly distributed within a bundle. These two cases represent a reactor starting up with a fresh core and, subsequently, going through a plutonium peak.

Preliminary results from Table II-3 indicated that the concentration of Gd_2O_3 added had a minimal effect on the plutonium peak at forty-five full power days. Similarly, the concentration of Eu_2O_3 added had a very minimal effect on the initial refueling transient peak. Table II-4 illustrated the reactivity decreased from Case 1 with NU to each of the other cases that contained various amounts of burnable neutron absorbers. For fuel containing 150 mg Gd_2O_3 and 125 mg Eu_2O_3, reductions in reactivity under a typical degraded coolant condition were 56.57 mk and 0.803 mk for fresh fuel and fuel after 45 FPD, respectively. This reduction in CVR implied that the positive void reactivity experienced in CANDU reactors during a LOCA could be mitigated through the use of a small amount of burnable neutron absorbers in fuel, without an impact on discharged burnup. This comparative study was conducted to provide an additional safety-related argument in favor of industry implementation of this design. A more detailed analysis for a fast transient using RFSP CERBERUS with the model coupled with CATHENA for thermalhydraulics conditions is being initiated as a separate study.

TABLE II-3. INFINITE MULTIPLICATION FACTOR CALCULATED FROM WIMS FOR COOLANT VOIDED CASES

Full power days in core	***Coolant void reactivity results***			
	Case 1: Natural Uranium K_∞	***Case 2: Natural Uranium with 120mg Gd_2O_3 and 300mg Eu_2O_3 K_∞***	***Case 3: Natural Uranium with 150mg Gd_2O_3 and 125mg Eu_2O_3 K_∞***	***Case 4: Natural Uranium with 90mg Gd_2O_3 and 425mg Eu_2O_3 K_∞***
0	1.146612	1.090901	1.090038	1.09482
45	1.109875	1.107443	1.109072	1.10619

TABLE II-4. DIFFERENCE IN INFINITE MULTIPLICATION FACTOR BETWEEN THE BASE CASE (NU FUEL) AND CASES CONTAINING VARIOUS AMOUNTS OF BURNABLE NEUTRON ABSORBERS

Full power days in core	***Coolant void reactivity improvements***			
	Case 1: Δk_∞	***Case 2: Δk_∞***	***Case 3: Δk_∞***	***Case 4: Δk_∞***
0	0	0.055711 (-56mk)	0.056574 (-57mk)	0.051792 (-52mk)
45	0	0.002432 (-2.4 mk)	0.000803 (-0.8mk)	0.003685 (-3.7mk)

II-3.3. Part 3

An EFP model using MCNP 6 was developed. To ensure that the model was predicting the correct values for the peaking factors, comparisons were done to both experiments performed at the ZED-2 reactor at Chalk River Nuclear Laboratories, and to a similar model performed with DRAGON 3.03a using the 89-group ENDF/B-V library [II-7]. While the MCNP 6.1 model used the more up to date ENDF/B-VII.1 library. Table II-5 summarized the results.

From Table II-5, one could see that the model done in MCNP was able to accurately predict the peaking factors of each fuel ring. Trials were performed to determine the amount of Eu_2O_3 to be placed within the last two pellets. Another relevant conclusion taken from Table 5 was

that the peaking factors for each ring have different values. This means that the amount of Eu_2O_3 placed into each element would vary for each ring.

TABLE II-5. MCNP 6.1 MODEL COMPARISON

Fuel ring	*End flux peaking factors in NU-37*		
	Experimental	*DRAGON*	*MCNP 6.1*
Centre	1.268	1.257 (-0.9)	1.265 (-0.2)
Inner	1.246	1.236 (-0.8)	1.248 (0.2)
Intermediate	1.205	1.194 (-0.9)	1.212 (0.6)
Outer	1.142	1.127 (-1.3)	1.142 (0.0)

Figure II-5 illustrated the effect of europium within an end pellet and its adjacent pellet on EFP. Comparing with the no absorber case, EFP was mitigated significantly. Once could notice that EFP still occurred within the second-half of the end pellet. This was deal to the exponential nature of the EFP within the fuel elements. A simple mitigation solution using end-pellets to address a phenomenon like EFP did not seem to be easy. Using an optimization routine, the amounts of Eu_2O_3 added to the inner and outer rings were presented in Table II-6, with EFP results illustrated in Fig.II-6. Figure II-6 compared the flux curves for the ring-optimized case, having the cross-ring effects being considered from each ring, with the no-absorber case.

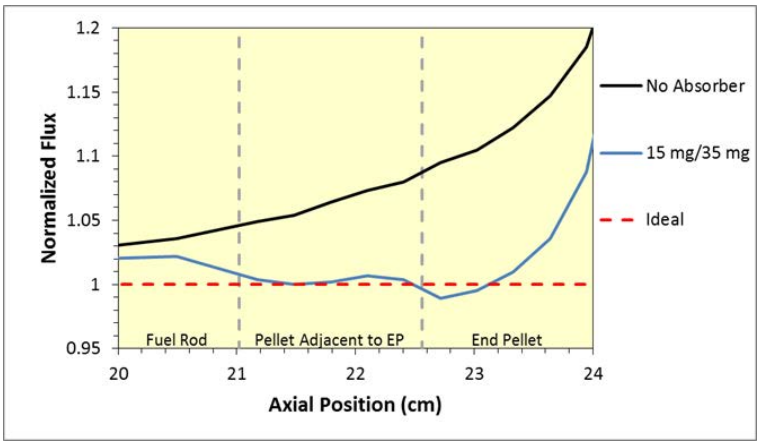

FIG.II-5. Comparing the europium trials with the case of having no absorber (15 mg and 35 mg of Eu_2O_3 were located at the pellet adjacent to the EP and at the EP, respectively).

TABLE II-6. BUNDLE-OPTIMIZED AMOUNT OF Eu_2O_3 IN THE INNER AND OUTER FUEL ELEMENTS

Fuel ring	*Eu_2O_3 in Adjacent Pellet (mg)*	*Eu_2O_3 in End Pellet (mg)*
Inner (6 elements)	4	12
Outer (18 elements)	2	6

The MCNP 6.1 code [II-4] was developed as a three-dimensional tool to simulate the addition of a small amount of neutron absorbers strategically at the bundle ends. The model improved

upon results from two-dimensional models in literature by being fully three dimensional while maintaining the ability to predict accurate EFP results.

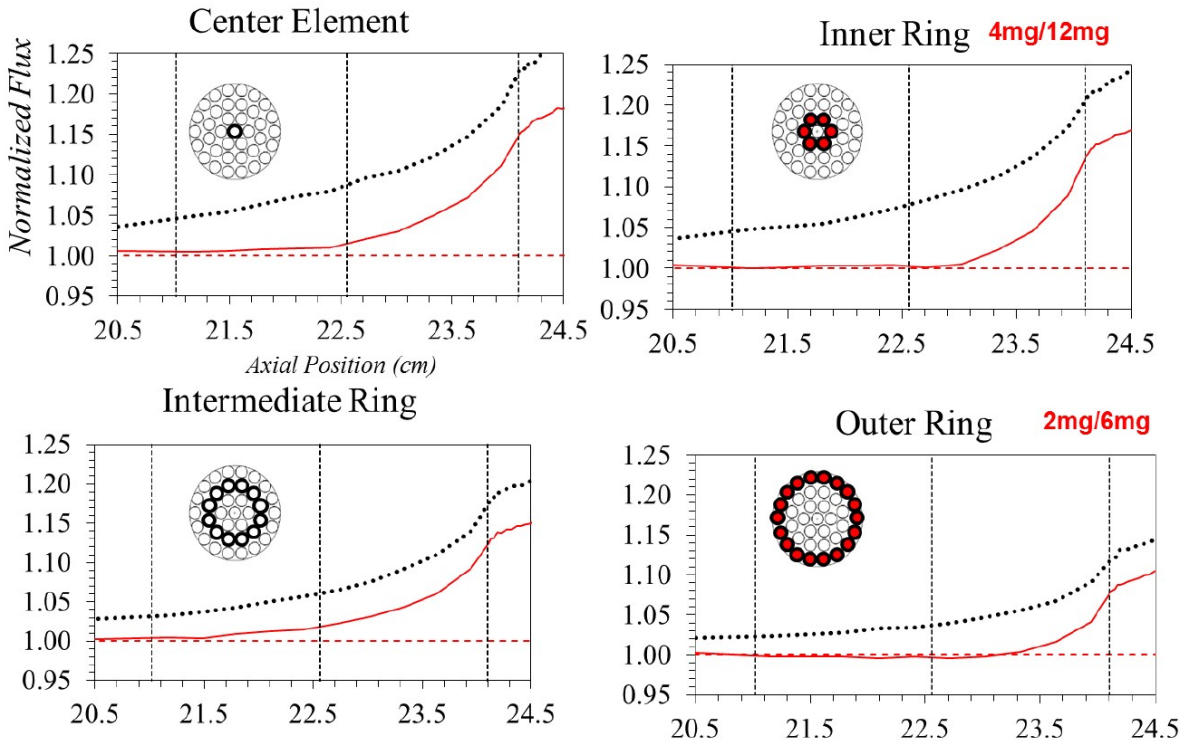

FIG.II-6. Mitigation of EFP for a Bundle Containing Eu_2O_3 as Shown in TABLE II-6.

II-3.4. Part 4

An attempt to modify the existing fueling scheme had proven to be difficult. Results indicated that the reference fueling scheme that is currently used with this CANDU model is quite robust. Though the reference fueling scheme was altered in various fashions, these changes could not out-perform the conventional pattern. Average maximum channel power and bundle power increased for all trials executed in this study, although some trials are still within the current licensing limits, as more 8 bundle-shifts were utilized. Moreover, it was determined that reducing the fueling frequency to three times per day for this CANDU model is not viable simply by increasing the number of eight bundle shifts. However, this project did reaffirm that the absolute maximum channel power, bundle power, and LZC fill fractions were reduced when BNAs were added to NU fuel; these findings were unanimous for the various fueling schemes considered, with a fixed fueling frequency of four times per day. The average discharge burnup of irradiated fuel containing the BNAs also increased slightly for most core following studies. This provides reassurance that BNAs reduced both channel power and LZC levels regardless of the chosen fueling scheme.

The salt-and-pepper approach (Fig.II-7) was promising as the number of channels, require for 8-bundle shifts, is only increased by 24 (16+8). As observed from Table II-7, the LZC level was increased by 12%, instead of a decrease by 25%, even with the present of 150 mg Gd_2O_3 and 125 mg Eu_2O_3. This would address the utilities' concern on the low LZC level at 20%. The salt-and-pepper approach has demonstrated that the fueling frequency, and thus the demand on temperamental fueling machines could be potentially reduced. With further

attempts that are to be completed, the observed limiting channels (D13, J21 and Q20) will be kept far from channels that are to be fueled with eight-bundle-shifts. Hence the maximum bundle and channel powers should be further reduced.

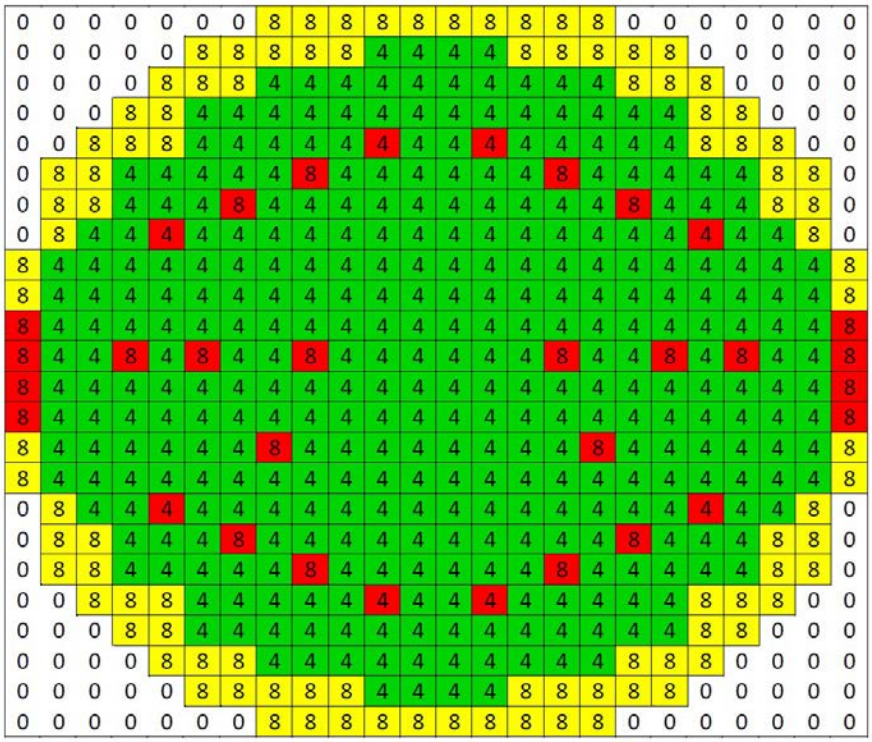

FIG.II-7. Reference fueling scheme modified in salt-and-pepper fashion (with 24 Additional 8-bundle Shifts).

TABLE II-7. CORE FOLLOWING STUDY FOR 500 FPD USING SALT-AND-PEPPER FUELLING SCHEME

	NU	***NU with 150 mg Gd_2O_3 and 125 mg Eu_2O_3***
Mean exit burnup [MW-h/KgU]	191.5	191.7 **(+0.2)**
Maximum highest bundle power [kW]	900.0	896.5 **(-3.5)**
Average maximum bundle power [kW]	823.0	820.4 **(-2.6)**
Maximum highest channel power [kW]	7174.7	7149.7 **(-25)**
Average maximum channel power [kW]	6710.4	6709.0 **(-1.4)**
Average LZC fill [%]	63.2	57.1 **(-6.1)**
Max LZC fill [%]	95.7	95.7 **(+0.0)**

II-4. CONCLUSIONS

A three-dimensional CANDU fuel bundle model using MCNP 6.1 has been developed to accurately simulate EFP. This research concludes that ~150 mg of Gd_2O_3 and ~125 mg of Eu_2O_3 within a fuel bundle could suppress both the refueling transient and lower the axial plutonium peak, with the LZC kept at ~20%, without a burnup penalty.

The proposed fuel design for the current CANDU fuel bundle is to distribute Gd_2O_3 within the CANLUB coating and Eu_2O_3 within the 24 end-pellets (2 mg/8 mg), or within the 12 end-pellets (10 mg), from the inner 6-elements. Fuel reliability and performance are topics of great interest for the nuclear industry. Use of BNAs is a relatively simple modification to the existing fuel design and it offers the potential of improving operating margins and fuel performance. It has been demonstrated that the initial fueling transient could be reduced by ~45 mk with no impact on discharged burnup. With further development, and depend on design requirements, adding burnable neutron absorbers (< 0.001 wt.%) to CANDU fuel could, potentially:

- help to meet power compliances;
- gain on NOP/ROP margin;
- mitigate coolant void reactivity and end-flux peaking;
- reduce involvement of LZCs and adjuster rods during operation;
- offer flexibility on fuel management;
- facilitate reactor startup after a long outage and the in-core LOCA analysis for fresh core (after units' refurbishment);
- facilitate the use of very slightly SEU fuel to minimize the burden on fueling machine usage.

If a design is to incorporate BNAs into an NU fuel type with more 8 bundle-shifts to keep the LCZ level closer to current operating experience, its fueling pattern should be revisited to minimize the burden of the fueling machine using the salt-and-pepper approach. Overall, it is expected that the application of BNA fuel would lead to improved core-flattening, better fuel utilization, increased practicality of refueling decisions, and, of upmost importance, enhanced operational safety of the reactor.

ACKNOWLEDGEMENTS

This Research Agreement was led by Chief Scientific Investigator, Paul. K. Chan of Royal Military College of Canada. Co-investigators included: Hugues Bonin, Jason J Song, Stephane Paquette, Dylan Pierce and Christy Bruce from Royal Military College of Canada.

REFERENCES TO ANNEX II

[II-1] GLASSTONE, S., SESONSKE, A., Nuclear Reactor Engineering, 3rd ed., Van Nostrand Reinhold Company, New York, N.Y. (1981) p788.

[II-2] ROUBEN, B., CANDU Fuel Management Course, Atomic Energy of Canada Limited (AECL), Mississauga, Ontario (1997).

[II-3] JONKMANS, G., WIMS-AECL User's Manual (Version 3.1), AECL, Chalk River, Ontario (2006).

[II-4] BROWN, F.B., MCNP - A General Monte Carlo N-Particle Transport Code: Overview and Theory, Version 5 Volume 1, Los Alamos National Laboratory (2003).

[II-5] SHEN, W., RFSP-IST Version REL_3-04: Theory Manual, SQAD-06-5058, CANDU Owners Group (2006).
[II-6] CHAN, P.K., PAQUETTE, S., BONIN, H.W., Variation of Burnable Neutron Absorbers in Heavy Water-Moderated Fuel Lattice: A Potential to Improve CANDU Reactor Operating Margins, Nuclear Technology **1** (2015) 191.
[II-7] SHEN, W., CANDU Three-Dimensional Neutron Transport Calculations with DRAGON, AECL, Mississauga, Ontario (2014); http://pbadupws.nrc.gov/docs/ML0236/ML023600301.pdf.
[II-8] WAGNER, J.C., PARK C.V., Impact of Burnable Poison Rods on PWR Burnup Credit Criticality Safety Analyses, Oak Ridge National Labaratory (2000).
[II-9] GLASSTONE, S., SESONSKE, A., Nuclear Reactor Engineering, 3rd ed., Van Nostrand Reinhold Company, New York, N.Y. (1981) p300.
[II-10] LOVECKY, M., SKODA, R., HUSSEIN, M., SONG, J., CHAN, P.K., The Application of UWB1 Nuclear Fuel Depletion Code on a CANDU Fuel Bundle, Progress in Nuclear Energy **90** (2016) 127.
[II-11] KLOOSTERMAN, J.L., Application of Boron and Gadolinium Burnable Poison Particle in UO_2 and PuO_2 Fuels in HTRs, Delft University of Technology, Netherlands (2003).
[II-12] SONG, J.J., CHAN, P.K., BONIN, H.W., PAQUETTE, S., Fuelling Study of a CANDU Reactor Using Fuels Containing Burnable Neutron, Nuclear Technology **195** (2016) 310.

ANNEX III.

ANNEX III: PERFORMANCE OF EXTENDED BURNUP PHWR FUEL

A Summary Report of Research Agreement Bhabha Atomic Research Centre (BARC), India

III-1. BACKGROUND

The focus on high burnup fuel and its reliability is of primary importance in nuclear plant operation. High burnup has led to increased fuel duty and residence time pushing fuel operation into new regimes. This makes it necessary to pursue research and development in high burnup fuel more aggressively. Most of the extended burnup studies have been reported for light water reactor (LWR) fuels [III-1], [III-2]. The average discharge burnup of a Pressurized Heavy Water Reactor (PHWR) fuel is about 7000 MWd/tU [III-3]. India plans to extend the discharge burnup of Indian PHWR fuels for improving the fuel economy using advanced fuel cycles. However, the design features of a PHWR fuel element, like thin walled cladding, high density of the fuel pellets, absence of fission gas plenum and higher linear heat rating during operation pose limitations on fuel performance during extended burnup [III-4], [III-5]. High burnup issues related to PHWR fuels are fission gas release, clad corrosion and hydriding, fuel swelling and higher fuel temperatures.

To accumulate high burnup experience with PHWR fuel, few natural UO_2 fuel bundles were irradiated for extended periods. Irradiation experience and post irradiation examination (PIE) of few bundles up to a burnup of ~15 000 MWd/tU has shown satisfactory performance under normal operating conditions [III-6] – [III-8]. Trial irradiation of few fuel bundles has been carried out up to the burnup of ~25 000 MWd/tU to evaluate the performance at extended burnups. Detailed post irradiation examination (PIE) of one of these fuel bundles (Bundle No. 145530) was carried out to generate data on their performance at extended burnup, with respect to fuel restructuring, fuel swelling, fission gas release, cladding corrosion, cladding strain and ductility etc. Similar hot cell examinations to evaluate the performance of high burnup CANDU fuel has been reported by other investigators [III-9], [III-10]. The details of PIE carried out on the extended burnup PHWR fuel bundle and results are presented in this Annex.

III-2. EXPERIMENTS

III-2.1. Design data of the fuel element

The design of the fuel elements as per specification data are given in Table III-1 [III-11].

III-2.2. Irradiation history

Fuel bundle No. 145530 was irradiated in the channel O-8 at the 6th string location of Kakrapara Atomic Power Station Unit 2. The fuel bundle accumulated a burnup of 22 263 MWd/tU during the residence period of ~1000 days. Peak linear element rating (LER) and peak power of the fuel bundle was 53.6 kW/m and 448 kW, respectively. Average LER of the outer fuel pin was 42.3 kW/m. Figure III-1 shows the irradiation history of the fuel bundle.

TABLE III-1. DESIGN DETAILS OF A PHWR FUEL ELEMENT

Pellet design	***Description***
Material	Natural UO_2
Density	96.3% TD (10.55 g/cm3)
Pellet outside diameter	14.32 mm
Length/diameter ratio	1.2
Grain size (average)	10 micrometers

Cladding design	***Description***
Material	Zircaloy-4
Cladding outside diameter	15.20 mm
Wall thickness	0.4 mm
Metallurgical condition	Stress relieved

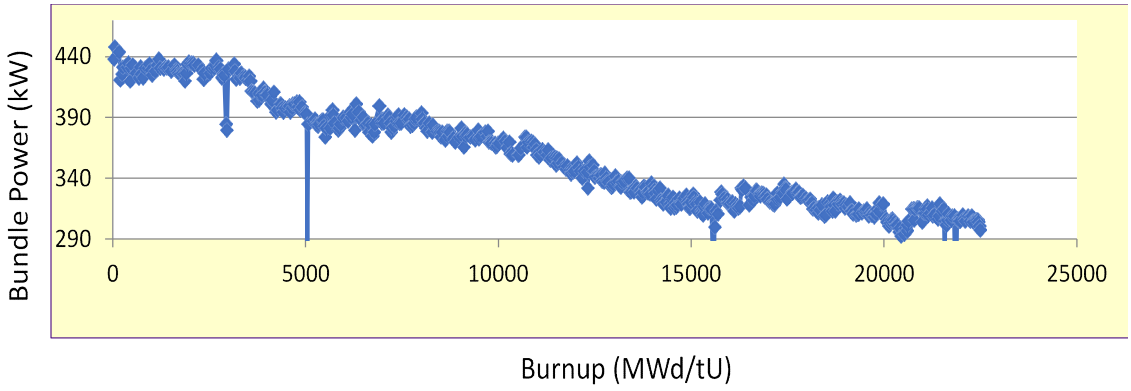

Fig. III-1. Irradiation history of fuel Bundle No. 145530.

III-2.3. Post irradiation examination

The fuel bundle after receipt in the hot cells was dismantled to carry out PIE on individual fuel elements. Various non-destructive and destructive techniques like, visual examination, leak testing, profilometry, ultrasonic testing, gamma scanning, fuel element puncturing and fission gas release measurement, microscopic examination and mechanical testing of cladding were carried out during PIE inside the hot cells.

Visual examination of the fuel pins of the fuel bundle was carried out using an in-cell camera with pan-tilt-zoom facility. Leak testing of all the fuel elements was carried out using liquid nitrogen-alcohol leak test method to check the integrity of the fuel elements. A laser based profilometer was used to measure the diameter of the fuel elements at different axial locations. Ultrasonic testing was carried out to check the soundness of the cladding and the end plug weld. Gamma scanning was carried out to evaluate the axial distribution of fission products in the fuel elements. Fuel elements from the outer ring, intermediate ring and the central fuel element were subjected to puncture tests to carry out fission gas extraction and

analysis. The percentage of fission gas release and internal pressure in the fuel elements were calculated. Metallographic examination was carried out on transverse and longitudinal fuel sections taken from one outer, intermediate and the central fuel pin. The fuel samples were examined under a shielded optical microscope remotely. Transverse tensile properties of the cladding were evaluated using the ring tension test method. The ring tension test was carried out at 25°C and 300°C on cladding specimens extracted from outer elements of the fuel bundle.

III-3. RESULTS AND DISCUSSION

Leak was not detected in any of the fuel elements, confirming absence of any fuel failure at the extended burnup. Circumferential parallel lines at regular intervals were noticed during visual examination along the length of the outer fuel elements. The distance between these lines was measured to be ~17 mm, which corresponds to the length of the pellet of PHWR fuel pins. Figure III-2 shows a comparison of the visual appearance of a typical outer, intermediate and the central fuel pin.

FIG. III-2. Appearance of the outer (bottom), intermediate (middle) and central (top) fuel elements.

Higher diameter at regular axial locations corresponding to the pellet interfaces was noticed in the outer fuel pins of the bundle during profilometry. Figure III-3 shows the diameter profile of two outer fuel pins of the fuel bundle. Higher diameter and circumferential parallel lines at regular axial locations of the outer fuel pins indicates ridge formation. Maximum ridge height up to 40 μm was observed in the outer fuel elements. Ridges commonly observed in high burnup fuel elements are formed because of tendency of the pellet to acquire the hour glass shape due to the temperature gradient. In addition, under the coolant pressure, the cladding deforms and eventually takes the shape of the pellet [III-12], [III-13].

Figure III-3 shows the fuel element diameter along the length of two typical outer fuel elements. It is evident from the profiles that some outer fuel elements have shown higher diameter all along the fuel element length. Diametral deformation of the cladding occurs due to thermal expansion and swelling of the fuel pellets; swelling of UO_2 may cause considerable strain at burnups over 20 000 MWd/tU [III-12], [III-14]. Mid-pellet cladding strain in the range of 0.06% to 0.6% was observed in the outer fuel elements. Maximum observed cladding strain of 0.6% is lower than the limiting uniform plastic clad strain value of 1% as per the fuel design criteria for burnup up to 15 000 MWd/tU. Higher cladding strain indicates swelling in the fuel and the variation in strain in outer fuel pins may be possibly due to different void volume in the fuel elements. Compressive strain was observed in the intermediate and central fuel element. Higher cladding strains are exhibited in fuel elements that operate at high

powers, as reported by Floyd [III-9] in fuel irradiated to extended burnup of ~32 000 MWd/tU; the average mid-pellet strain in the outer fuel element was about 0.9%. Lower cladding strain was reported in fuel elements with burnup of ~37 600 MWd/tU but at lower linear power [III-10].

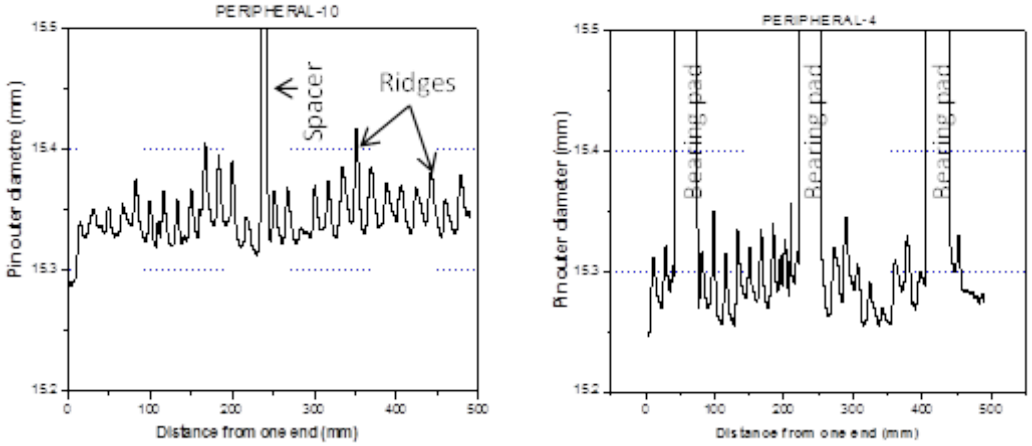

FIG.III-3. Diameter profile of the outer fuel elements.

Figure III-4 shows a typical gamma spectrum of an outer fuel element of the bundle. Gamma spectrometry is a non-destructive technique for determination of fuel burnup and power by measuring the concentration of long lived fission products [III-15]. The gamma energy spectrum showed distinct peaks of Cs-137 (662 keV) and Cs-134 (604 and 796 keV). The axial profile of Cesium reveals the distribution volatile fission products along the length of the fuel pin [III-16]. Figure III-5 shows the axial distribution of Cs-137 in the outer, intermediate and the central fuel element. Results show uniform axial burnup distribution in the fuel elements.

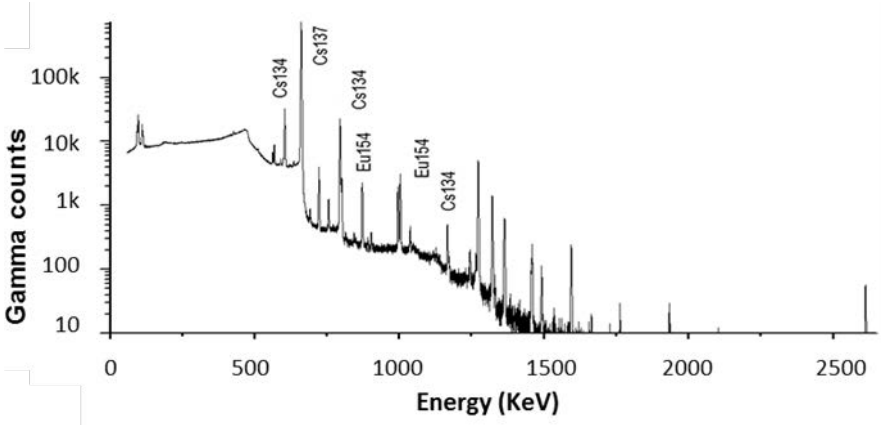

FIG.III-4. Typical gamma spectrum of an outer fuel element.

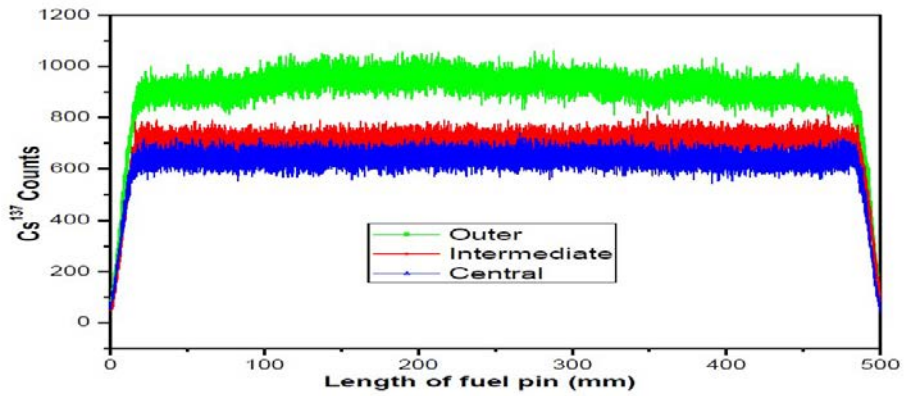

FIG.III-5. Axial gamma scanning of the outer, intermediate and central fuel elements.

Fission gas release measurements showed that percentage gas release and internal gas pressure in the outer fuel pins were up to 13.66 % and 34.39 atm., respectively at ambient temperature. The results obtained from fission gas analysis of the outer, intermediate and central elements are presented in Table III-2. Low void volume observed in the central fuel pin is due to reduction in the fuel pin diameter under to the coolant pressure. Low void volume observed in the central fuel element is due to reduction in the fuel element diameter under the coolant pressure.

TABLE III-2. RESULTS OF THE FISSION GAS ANALYSIS

Details	***Outer fuel element***	***Intermediate fuel element***	***Central fuel element***
Void volume (cc)	3.31	2.10	1.09
% Release	13.66	3.89	0.21
Pressure inside element (atm.)	34.39	14.75	2.45

Percent fission gas release in fuel elements shows an exponential dependence on power and plays an important role in fuel performance and fuel pin integrity at high burnup [III-9], [III-10].

Figure III-6 (a) and (b) show the photo-macrograph and β-γ autoradiograph of a fuel section from the outer fuel element. The radial extent of intergranular porosity region in the fuel and extent of fission product (cesium) migration in the autoradiograph are measured and used to estimate the fuel centre temperatures [III-7]. The average fuel centre temperature estimated for the outer, intermediate and central fuel elements are found to be 1738°C, 1223°C, and 1157°C respectively with an error band of ±5%. The average grain size measured at the centre of the fuel section of outer fuel pin was 35 µm as shown in Fig.III.6 (c).

Fuel density and porosity changes are examined by different techniques; porosity measurements by image analysis of metallographic samples, immersion density measurements and clad outer diameter measurements [III-17]. The porosity was examined by image analysis at different radial locations of the fuel section to obtain the radial porosity profile. Pellet average fuel swelling was estimated from the radial distribution of porosity in the pellet. Swelling was taken as the difference between total porosity in irradiated fuel (by image analysis) and initial porosity. Initial fuel porosity was assumed to be 3.7% [III-11].

The Estimated % swelling in the fuel pins are given in Table III-3. Intermediate and central fuel elements indicated compressive strain in the cladding. Swelling observed in the fuel elements is possibly getting accommodated in the dish volume.

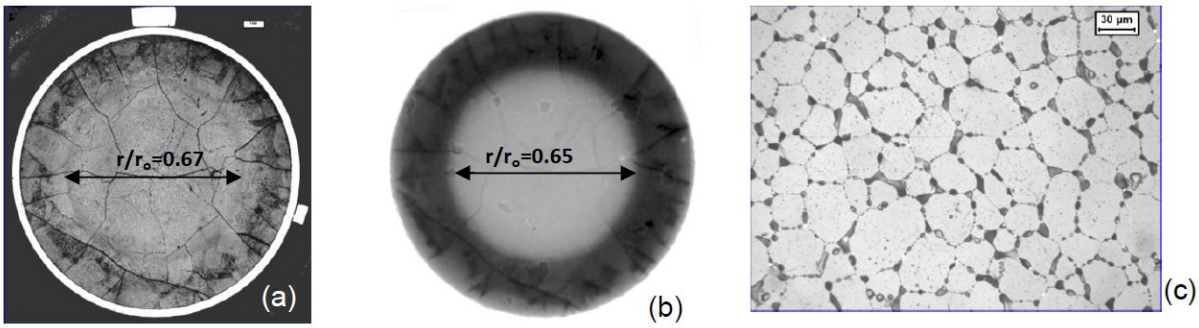

FIG.III-6. (a) Photo-macrograph and (b) β-γ autoradiograph of a fuel section from the outer fuel element, and (c) grains revealed at the centre of the fuel section.

Examination of the longitudinal fuel sections revealed filling up of the pellet dish in the central region as shown in Fig.III-7. Dish filling is generally observed due to swelling in the fuel [III-18].

TABLE III-3. FUEL SWELLING ESTIMATION

Pin	***Total porosity, % (P)***	***Initial porosity, %(p)***	***Swelling, % (P-p)***
Outer	8.5	3.7	4.8
Intermediate	4.8	3.7	1.1
Central	4.3	3.7	0.6

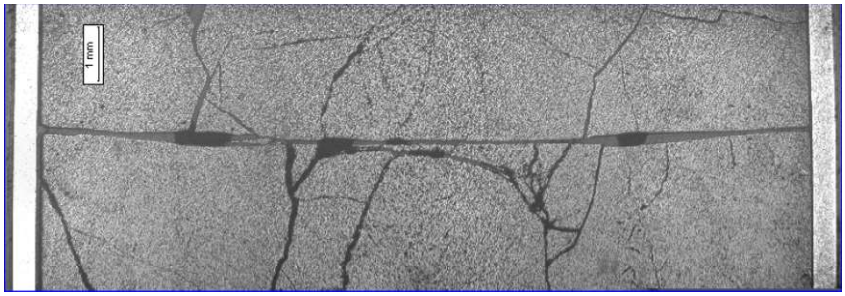

FIG.III-7. Dish filling in a longitudinal section of the outer fuel element.

Dark regions were observed in the periphery of the fuel section of outer fuel element due to grain pull-out as shown in Fig.III-6 (a). Similar observation in high burnup PHWR fuels have been reported and has been linked to preferential etching of the grain boundaries leading to grains 'pull-out' during polishing. This is a typical observation in a fuel that has experienced oxidation at the grain boundaries [III-9]. Such evidences indicate possibility of increase in the O/M ratio at the periphery of the fuel at extended burnup.

Localized oxide patches on the inner surface of the cladding of the outer fuel element was observed with the average oxide layer thickness of 6.2 µm. Oxide layer on the outer surface of

the cladding of the fuel pins was found to be uniform with the average thickness of 5 μm. Fuel-cladding interaction was not observed.

Figure III-8 shows a grain of UO_2 taken from the central region of the fuel section of the outer fuel element. It revealed larger bubbles and wider channels on the grain faces as compared to small bubbles observed in low burnup fuels. Large numbers of white precipitates were observed on the grain faces. Energy dispersive spectroscopy was carried out on the white precipitates. The energy dispersive spectroscopy analysis confirmed the precipitates to be metallic fission products containing Mo, Ru, Tc, Rh, Pd. Such precipitates of metallic fission products are reported to form at the high temperature location in high burnup oxide fuels [III-19], [III-20].

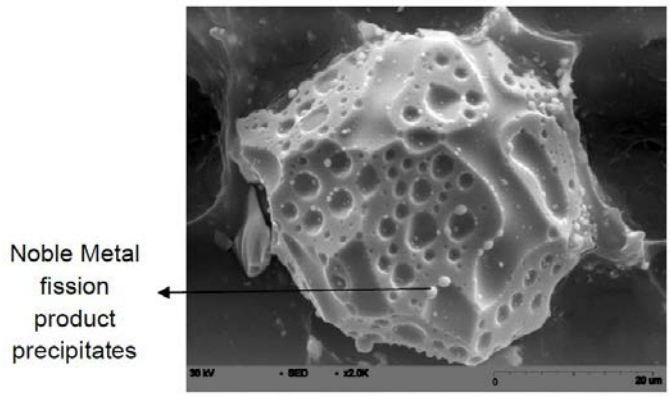

FIG.III-8. Grain from the centre of the fuel section of outer fuel element showing fission gas bubbles, channels and metallic fission products on the surface.

Few hydride platelets were observed in the cladding from the outer fuel element; most of the platelets were present towards the outer surface of the cladding as shown in Fig.III-9 (a). The platelets were oriented in the circumferential direction. The density of the hydride platelets in the bearing pad and spacer pad was higher than that in the cladding. Higher density of hydrides towards the outer surface of the cladding and in the appendages (spacer and bearing pad) is due to migration of hydrogen to the cooler locations. The average hydrogen content in the cladding from outer fuel element was 38 ppm.

Figure III-9 (b) and (c) show typical tested, ring specimens from the outer fuel element. The load and crosshead displacement record obtained from the tests were analyzed to get the stress-strain data and plot. Typical engineering stress-strain diagrams at ambient temperature for the unirradiated and irradiated specimens are shown in Fig.III-10.

Transverse tensile properties of the cladding estimated from ring tension tests showed a total elongation of around 5-7% at 25ºC. The total elongation increased up to 22% at 300ºC. It is evident from the plots that there is increase in strength and decrease in ductility of the cladding due to reactor operation. At the ambient temperature, the minimum strength increase and maximum ductility decrease has been found to be about 30% and 85% respectively.

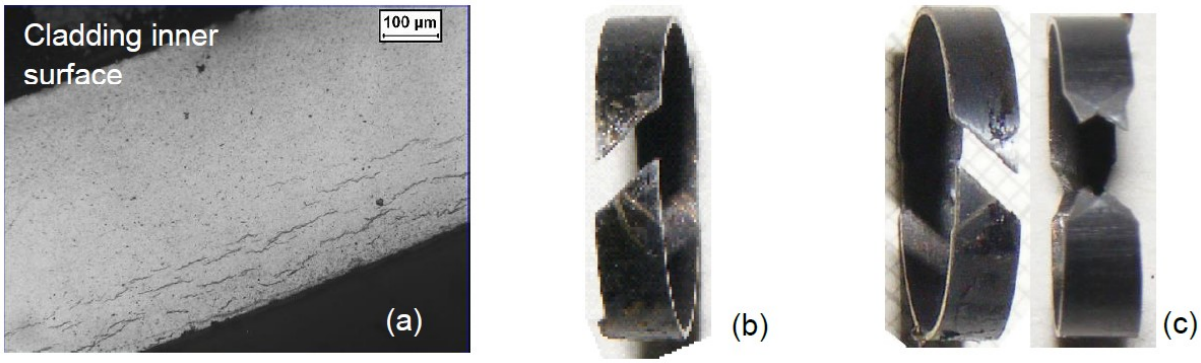

FIG.III-9. (a) Hydride plate distribution in the cladding from the outer fuel element. Typical irradiated cladding specimens tested at (b) 25°C and (c) 300°C.

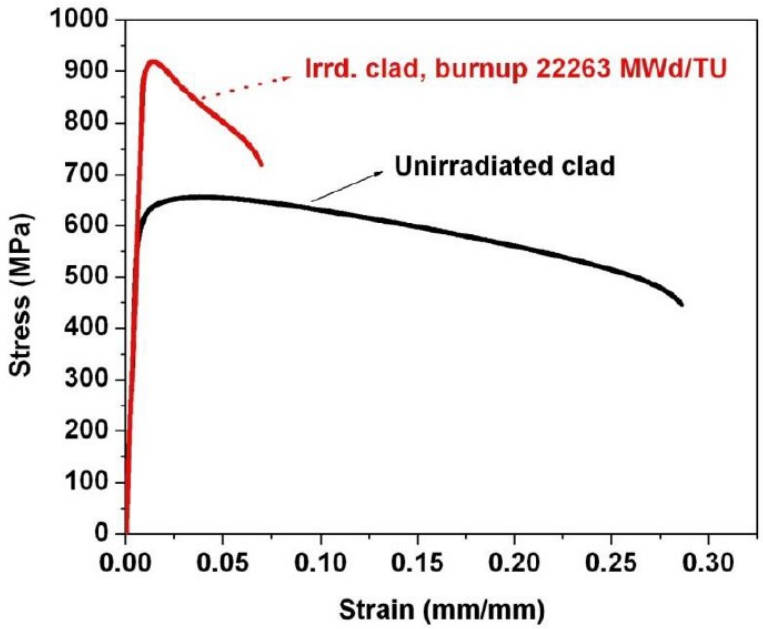

FIG.III-10. Typical engineering stress-strain diagrams for the unirradiated and irradiated cladding specimens at the ambient temperature.

III-4. SUMMARY

- Post irradiation examination of a PHWR fuel bundle with natural UO_2 fuel irradiated to a burnup of ~22 000 MWd/tU has shown that the bundle has successfully achieved this burnup without failure.

- Circumferential ridges were observed on all the outer fuel elements of the bundle. Maximum ridge height observed in the fuel elements was 40 µm. Increase in the diameter throughout the length of the fuel pin, indicated fuel swelling in the outer fuel elements. Permanent mid-pellet strain in the cladding of the outer fuel pins was up to 0.6%.

- Uniform axial burnup distribution was observed in the fuel elements.

- The maximum internal gas pressure measured in the outer fuel pins was 34.39 atm at standard temperature and pressure.

- The average estimated fuel centre temperature in the outer fuel element during operation was 1738ºC. The maximum volumetric swelling of fuel estimated by image analysis was 4.8% in this element.

- No excess pellet-cladding interaction has been observed in the fuel at this burnup under declined power operation.

- Localised oxide patches with average oxide layer thickness of 6.2 μm were observed on the inner surface of the cladding of outer fuel elements. Higher hydride platelet density was observed in the bearing pads and the spacer pads of the fuel pins than that in the cladding.

- Average hydrogen concentration in the cladding of the outer fuel element was found to be 38 ppm.

- Large fission gas bubbles and channels were observed on the grain faces. White precipitates observed in the fission gas bubbles were found to be metallic fission products.

- Transverse tensile properties of the cladding estimated from ring tension tests showed a total elongation of around 5-7% at 25ºC. Whereas, the total elongation increased up to 22% at 300ºC.

III-5. CONCLUSIONS

Post irradiation examination of PHWR fuel bundle irradiated to an extended burnup of ~22 000 MWd/tU has shown satisfactory performance, fulfilling the fuel design criteria applicable for fuel irradiated up to 15 000 MWd/tU. However, irradiation to still higher burnups requires modifications in the fuel design parameters to improve fuel performance. Increase in the dish depth of the pellet and use of fuel pellets with lower density will limit the extent of fuel swelling; hence the permanent strain in the cladding. Use of large grain size pellets shall control the fission gas release at extended burnup.

ACKNOWLEDGEMENTS

This Research Agreement was led by Chief Scientific Investigator, J.L. Singh of BARC, India. Co-investigators included: Prerna Mishra, B.N. Rath, Ashwini Kumar, V.P. Jathar, H.N. Singh and P. K. Shah, R.S. Sriwastaw, J.S. Dubey, G.K. Mallik from BARC.

REFERENCES TO ANNEX III

[III-1] RESTANI, R., HORVATH, M., GOLL, W., BERTSCH, J., GAVILLET, D., HERMANN, A., MARTIN, M., WALKER, C.T., Journal of Nuclear Materials **481**, (2016) 88.

[III-2] ROMANO, MATTHIAS, A., HORVATH, I., RESTANI, R., Journal of Nuclear Materials **361** (2007) 62.

[III-3] BHARDWAJ, S.A., DAS, M., "Fuel Design Evolution in Indian PHWRs", Proceedings of symposium on Improvements in water reactor technology and utilization" Stockholm, 15-19 September 1986.

[III-4] PRASAD, P.N., TRIPATHI, R.M., KUMAR, A.N., RAY, S., DWIVEDI, K.P., "Fuel Element Design for Achieving High Burnups in 220 MW(e) Indian PHWRs", Advanced Fuel Pellet Materials and Fuel Rod Design for Water Cooled Reactors pages, IAEA-TECDOC-1654, IAEA, Vienna (2010) 75-81.

[III-5] PRASAD, P.N., SONI, R., TRIPATHI, R.M., PANDARINATHAN, P.R., NEEMA, L.K., Derivation of Fuel Bundle Power Limits Using Fuel Element Modelling Code FUDA, Journal of Nuclear Materials **383** (2008) 150.

[III-6] SAH, D.N., VISHWANATHAN, U.K., UNNIKRISHNAN, K., MISHRA, P., SHRIWASTAW, R.S., ANANTHARAMAN, S., Post-Irradiation Examination of High Burnup PHWR Fuel Bundle 56504 from KAPS-1, Report BARC-2007/E/002, Bhabha Atomic Research Centre (BARC) (2007).

[III-7] SAH, D.N., VISHWANATHAN, U.K., RAMADASAN, E., UNNIKRISHNAN, K., ANANTHARAMAN, S., Post Irradiation Examination of Thermal Reactor Fuels, Journal of Nuclear Materials **383** (2008) 45.

[III-8] SAH, D.N., VISHWANATHAN, U.K., VISWANADHAM, C.S., UNNIKRISHNAN , K., RATH, B.N., Blind Prediction Exercise on Modeling of PHWR Fuel at Extended Burnup, Journal of Nuclear Materials **383** (2008) 144.

[III-9] FLOYD, M.R., NOVAK, J., TRUANT, P.T., "Fission Gas Release in Fuel Performing to Extended Burnups in Ontario Hydro Nuclear Generating Stations", Fission Gas Release and Fuel Chemistry Related to Extended Burnup, IAEA TECDOC-697, IAEA, Vienna (1993).

[III-10] ZHOU, Y.N., FLOYD, M.R., RYZ, M.A., "Performance of BRUCE natural UO_2 fuel irradiated to extended burnups", Proceeding of the 4th International Conference on CANDU Fuel, Pembroke, Ontario, Canada, 1-4 October, 1995.

[III-11] MISHRA, P., JATHAR, V.P., SINGH, J.L., SAH, D.N., SHAH, P.K., ANANTHARAMAN, S., Journal of Nuclear Materials **439** (2013) 217.

[III-12] AAS, S., Mechanical Interaction between Fuel and Cladding, Nuclear Engineering and Design **21** (1972) 237.

[III-13] VAN BRUTZEL, L., DINGREVILLE, R., BARTEL, T.J., Nuclear Fuel Deformation Phenomena, Report NEA-NSC-R--2015-5, OECD/NEA (2015).

[III-14] ASSMANN, H. and STEHLE, H., The Behaviour of Uranium Oxide Fuels in Nuclear Reactors, Volume A4, Gmelin Handbook of Inorganic chemistry.

[III-15] SANNEN, L., BORMS, L., DE RAEDT, Ch., GYS, A., "Gamma Spectrometric Determination of the Fission Power of Fuel Rods", Advanced Post-Irradiation Examination Techniques for Water Reactor Fuel, TECDOC-1277, IAEA, Vienna (2002).

[III-16] VENKITESWARAN, C.N. et al, Irradiation Performance of PFBR MOX Fuel after 112 GWd/t Burnup, Journal of Nuclear Materials **449** (2014) 31.

[III-17] LYSELL, G., "Fuel Behaviour at Different Power and Burnup Levels", Proceedings of TopFuel 97, Volume Two, Manchester, 9-11 June 1997.

[III-18] NONON, C., MENARD, J.C, LANSIART, S., NOIROT, J., MARTIN, S., DECROIX, G.M., RABOUILLE, O., DELAFOY, C., PETITPREZ, B., "PCI Behaviour of Chromium Oxide Doped Fuel", Proceeding of Pellet-Clad Interaction in Water Reactor Fuels, France, 9-11 March 2004.

[III-19] BRAMMAN, J.I., SHARPE, R.M., THOM, D., YATES, G., Metallic Fission Product Inclusions in Irradiated Oxide Fuel, Journal of nuclear materials **25** (1968) 201.
[III-20] KLEYKAMP, H., The Chemical State of the Fission Products in Oxide Fuels, Journal of Nuclear Materials **131** (1985) 221.

ANNEX IV.

ANNEX IV: DEVELOPMENT OF PHWR FUEL BUNDLE TO ENHANCE CRITICAL HEAT FLUX

A Summary Report of Research Agreement with Korea Atomic Energy Research Institute (KAERI), Korea

IV-1. BACKGROUND

The design of a reference CANDU fuel bundle comprises of 37 elements, concentrically arranged with: 1 central element, 6 inner ring elements, 12 intermediate ring elements and 18 outer ring elements. These 37 elements are welded at both ends of each fuel element with the endplates to maintain a circular type bundle structure (Fig.IV-1). For a C6 reactor, 12 fuel bundles are loaded into a horizontal fuel channel. Because the fuel bundles sit on the bottom inside of the horizontal pressure tube installed in the fuel channel, an open gap in the upper part of the fuel channel exists from the beginning of the reactor operation. The coolant tends to flow through this open gap rather than through the subchannels inside of the fuel bundle due to low flow resistance in the open gap region.

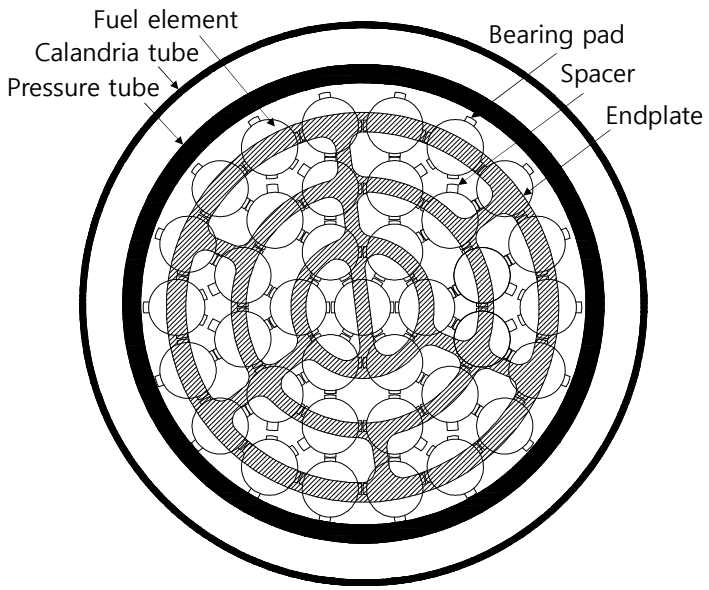

FIG.IV-1. Cross-sectional view of a reference -37-element bundle in the pressure tube.

As the reactor becomes aged, the open gap gradually increases due to the diametral increase of the pressure tube by creep. It allows a by-pass flow outside of the bundle in the pressure tube. The crept pressure tube deteriorates the critical heat flux (CHF) of the fuel bundle and decreases the reactor operating margins, leading to derating of the reactor power.

A reference 37 element fuel bundle (37R bundle) has a parabolic power profile across the radius of the bundle, which makes the linear element ratings (LERs) of the outer ring elements higher (i.e., hotter as shown in Fig.IV.2). Therefore, thermal margin to fuel melting is limited by the outer ring elements. Thermal margin to dryout is controlled by the flow areas between the central element and the inner ring elements (hereafter called central flow area), which remains unchanged in the crept pressure tubes due to aging [IV-1].

As the central flow area increases, the CHF of the 37R bundle increases. Two approaches are considered to increase the central flow area (i.e. centre subchannels in Fig.IV-3): a reduction of the radius of the centre element, or an increase of the inner ring radius. The former can increase the total flow area and CHF of a fuel bundle. (This approach has been implemented in the development of the modified 37-element bundle by the Canadian industry.) In addition, it contributes to a redistribution of the power density of all fuel elements. The latter can reduce the flow area between inner ring elements and the intermediate ring elements, while increasing the central flow area due to the outward movement of the 6 inner ring elements in the radial direction. This can also affect the enthalpy redistribution and the CHF of the fuel bundle. The CHF can also be enhanced by means of adjusting geometric configuration of the fuel bundle, for example, modification of the ring radii or bearing pad height [IV-1], [IV-2].

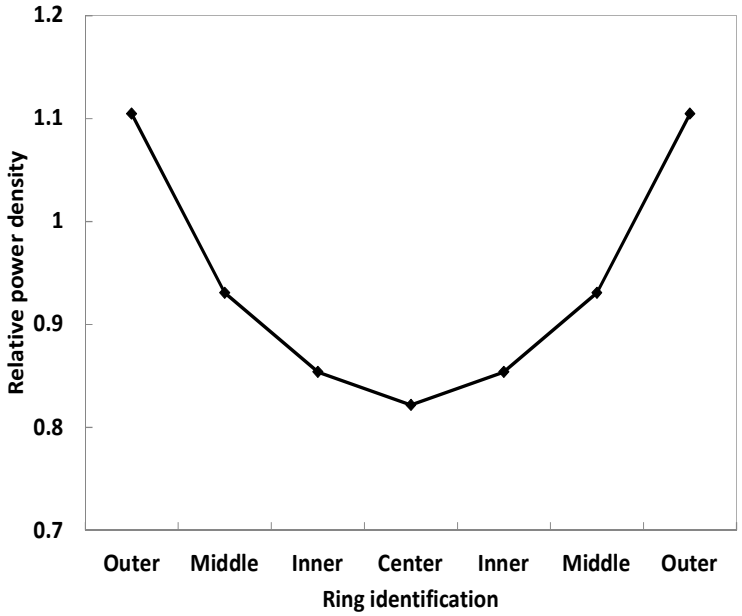

FIG. IV-2. Relative ring power profile of a 37R bundle.

In this research project, an increase of the central flow area by increasing the inner ring radius was selected, under the consideration that reactor safety, fuel performance and fuel fabrication are not much affected by such geometry modifications in comparison with those for the 37R bundle. In addition, modifications of the pitch circle radii of the intermediate ring and outer ring were also investigated to examine whether a further CHF enhancement could be achieved. The CHF evaluation of the modifications of the 37R bundle geometry were performed by applying a subchannel analysis method.

IV-2. APPROACHES

Sensitivity studies are performed to investigate the effects of the pitch circle radii on the dryout power of a fuel bundle. As the first approach, the variation of the inner ring radius is examined in terms of the dryout power enhancement. Once the inner ring radius is optimized in terms of dryout power, the intermediate ring radius is considered as the next step. And then, the outer ring radius is examined in terms of the dryout power enhancement of a fuel bundle. These sensitivities will be achieved using a subchannel methodology.

IV-2.1. Subchannel analysis

IV-2.1.1. Subchannel analysis code

Sensitivity studies to investigate the effect of the ring radii on the CHF (or dryout power) of a fuel bundle have been performed using the subchannel analysis ASSERT code [IV-3].

IV-2.1.2. Boundary Conditions

For a CANDU 6 reactor, the design values of coolant temperature at the reactor inlet header and coolant pressure at reactor outlet header are 262℃ and 10.0 MPa, respectively. The reference flow rate in the fuel channel of C6 reactors is 24 kg/s, and the maximum flow rate is estimated to be about 28 kg/s [IV-4]. For the subchannel analysis, the following boundary conditions are considered: one coolant inlet temperatures (262℃), 6 flow fates (2 kg/s step increase from 20 kg/s to 30 kg/s), and the coolant outlet pressure of 10.0 MPa. The coolant is heavy water.

IV-2.2. Modification of the 37R Bundle

A 37R bundle comprises of 37 fuel elements on the centre, inner ring, intermediate ring and outer ring of the bundle (Fig.IV-3). Each ring radius is summarized in Table IV-1.

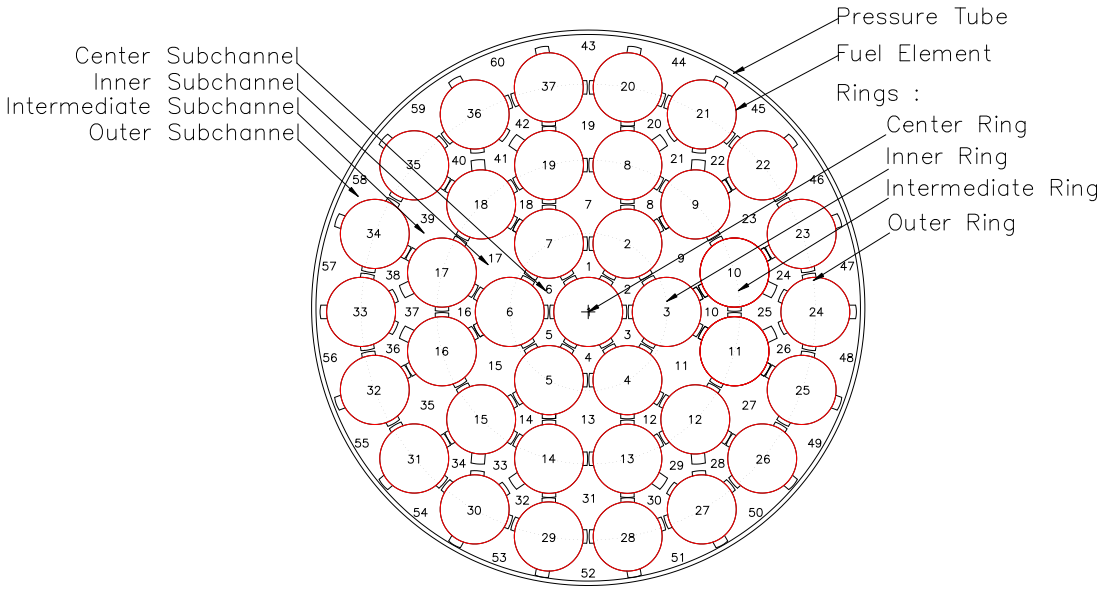

FIG.IV-3. Ring identification and subchannel configuration of a 37R fuel.

Conceptually, the subchannel is established by a hypothetical line connected from the centre of a fuel element to the centre of an adjacent fuel element. Hence, the subchannels of a 37R bundle are presented with three types, i.e., triangular, square and wall subchannels, as shown in Fig.IV-3. The total number of fuel elements and subchannels are 37 and 60, respectively. A subchannel analysis was performed for a 37R bundle as a reference case. Then, subchannel analyses on the modifications of a 37R bundle continued to be performed with use of the same channel boundary conditions as the 37R bundle.

TABLE IV-1. RING (PITCH CIRCLE) RADII OF THE 37R BUNDLE

Ring identification	*Ring radius, mm*	*No. of elements*
Centre	0.0	1
Inner	14.88	6
Intermediate	28.75	12
Outer	43.33	18

IV-2.2.1. Minimum gap between fuel elements

The increase of a ring radius can be allowed if a minimum gap size between fuel elements is maintained so that the fuel elements do not interfere each other. In the fuel design manual of the 37R bundle [IV-4], it is stated that "the average height reduction on the mating spacer pairs, measured for each bundle, ranged from 0.015 mm to 0.035 mm after 6,178 hours of testing. The maximum height reduction measured was 0.16 mm or about 25 percent of the specified minimum height of one inter-element spacer. The minimum height of one inter-element spacer is acceptable since spacer-to-sheath contact is not likely to occur until about 50 percent of the combined spacer thickness is removed". The minimum gap size of the 37R bundle was designed to be 1.8 mm in the bundle design. Based on this information, the allowable maximum inner ring radius can be found as follows:

- minimum height of one spacer: 0.64 mm (minimum allowable gap: 1.28 mm);
- excess gap height: 0.52 mm;
- allowable maximum inner ring radius: 15.4 mm (14.88 mm + 0.52 mm).

IV-2.2.2. Modification of the inner ring radius

A slight increase of the inner ring radius has been considered: from 14.88 mm to 15.38 mm with 0.1 mm incremental step. Other ring radii remained unchanged.

IV-2.2.3. Modification of the intermediate ring radius

A slight increase of the intermediate ring radius has been considered: from 28.75 to 29.25 mm with 0.1 mm incremental step. Inner ring radius is fixed to be 15.28 mm and outer ring radii remained unchanged.

IV-2.2.4. Modification of the outer ring radius

A slight increase of the outer ring radius has been considered: from 43.33 mm to 43.83 mm with 0.1 mm incremental step. Other ring radii remained unchanged. Inner and intermediate ring radii are fixed to be 15.28 mm and 29.25 mm, respectively.

IV-2.3. Results and discussion

IV-2.3.1. Definition of dryout power ratio

To evaluate dryout power enhancement of a 37R bundle with ring radius modification, the enhancement is defined as dryout power of 37R bundle with ring modifications divided by dryout power of 37R bundle.

IV-2.3.2. Modification of the inner ring radius

The first CHF occurrence locations in the 37R bundle are summarized in Table IV-2 – Table IV-4. For all conditions of mass flow and crept pressure tubes (0%, 3.3% and 5.1%) considered, CHF took place at the central subchannel #1 of the 37R bundle in Fig.IV-3. These analysis results by ASSERT code are consistent with experimental observations with the 37R bundle at a high flow [IV-5]. With the increase of the inner ring radius beyond 15.18 mm, most of the first occurrences of CHF were located at the inner subchannel #10, mainly due to a reduced flow area of the inner subchannels # 7 to #18 in Fig.IV-3. The locations of the first CHF occurrence under the 3.3% crept pressure tube condition were located at the subchannel #10 or #33 as inner ring radius increases. On the other hand, the first CHF occurrence locations under the 5.1% crept pressure tube condition were not much affected by the variation of the inner ring radius; however, most CHF locations for rather large radius of inner ring moved to subchannel #33 at high flows.

TABLE IV-2. FIRST CHF OCCURRENCE SUBCHANNEL LOCATION IN THE 37R BUNDLE WITH VARIOUS INNER RING RADII (0% CREPT PRESSURE TUBE)

Inner ring radius (mm)	Flow rate (kg/s)					
	20	22	24	26	28	30
14.88†	1	1	1	1	1	1
14.98	1	1	1	1	1	1
15.08	1	10	1	1	1	1
15.18	32	10	10	10	1	1
15.28	32	10	10	10	10	10
15.38	10	10	10	10	10	10

† the inner ring radius of the reference 37-element bundle.

TABLE IV-3. FIRST CHF OCCURRENCE SUBCHANNEL LOCATION IN THE 37R BUNDLE WITH VARIOUS INNER RING RADII (3.3% CREPT PRESSURE TUBE)

Inner ring radius (mm)	Flow rate (kg/s)					
	20	22	24	26	28	30
14.88†	7	1	1	1	1	1
14.98	7	1	1	1	1	1
15.08	7	1	1	1	1	1
15.18	7	1	1	32	10	10
15.28	7	1	33	33	10	10
15.38	7	10	33	33	10	10

† the inner ring radius of the reference 37-element bundle.

TABLE IV-4. FIRST CHF OCCURRENCE SUBCHANNEL LOCATION IN THE 37R BUNDLE WITH VARIOUS INNER RING RADII (5.1% CREPT PRESSURE TUBE)

Inner ring radius (mm)	Flow rate (kg/s)					
	20	22	24	26	28	30
14.88†	7	7	7	1	1	1
14.98	7	7	7	1	1	1
15.08	7	7	7	1	1	1
15.18	7	7	7	1	1	33
15.28	7	7	7	1	33	33
15.38	7	7	7	10	10	33

† the inner ring radius of the reference 37-element bundle.

The dryout powers of the 37R bundle and of 37R bundle with modified values of the inner ring radius were calculated for the various mass flow conditions (20–30 kg/s) and various crept pressure tubes (0%, 3.3% and 5.1%).

Figure IV-4 shows the results for dryout power ratios of the inner ring modification under uncrept PT condition. The dryout power ratio increases with the increase of the inner ring radius. The maximum ratios of the dryout powers were appeared when the inner ring radius was 15.18 mm. Figure IV-5 shows the results for 3.3% crept PT condition. The dryout power ratios increase with the increase of the inner ring radius. The maximum ratios of the dryout powers were the highest for the large inner ring radius. Figure IV-6 shows the results for 5.1% crept PT condition. The dryout power ratios increases with the increase of the inner ring radius. The maximum ratios of the dryout power were the highest for the large inner ring radius.

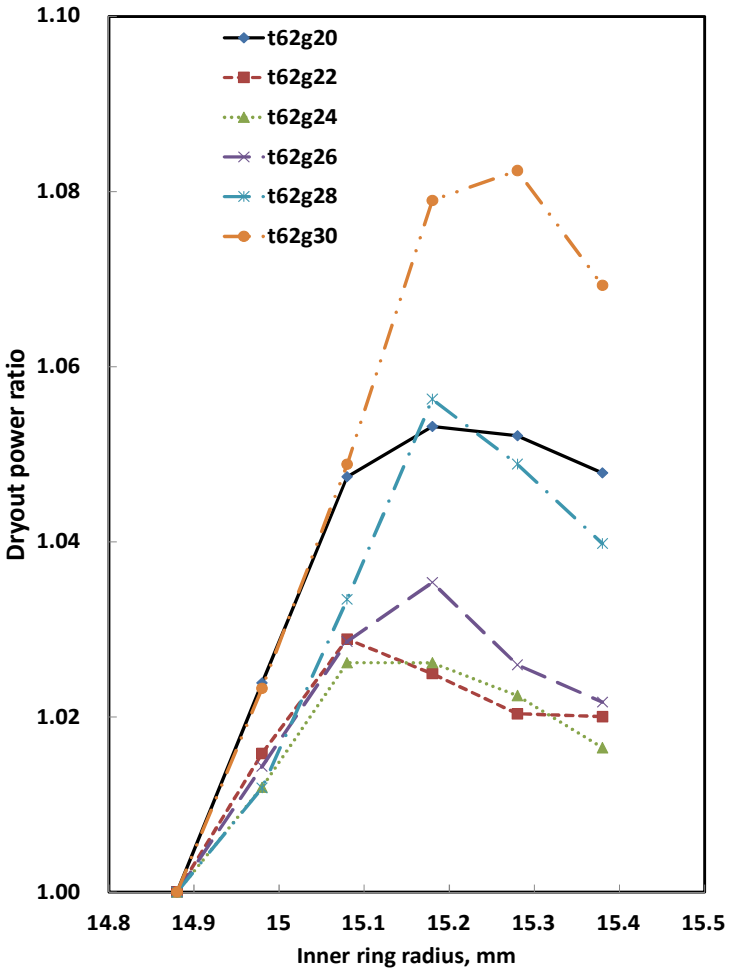

FIG. IV-4. Enhancement of dryout power vs. the inner ring radius for un-crept pressure tube.

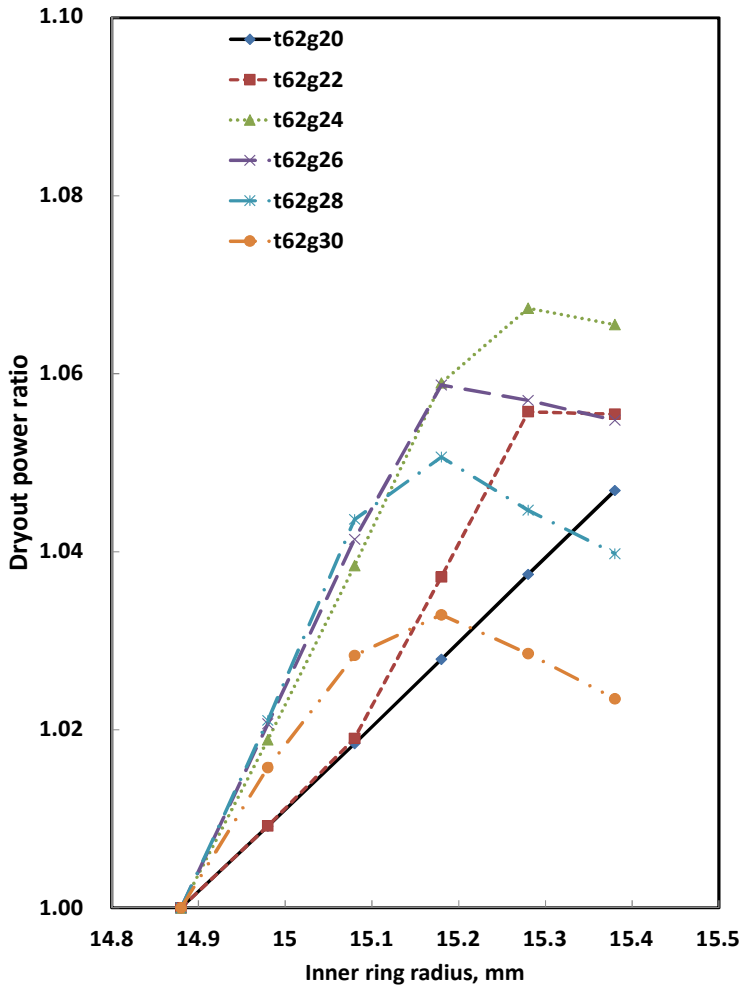

FIG. IV-5. Enhancement of dryout power vs. the inner ring radius for 3.3% crept pressure tube.

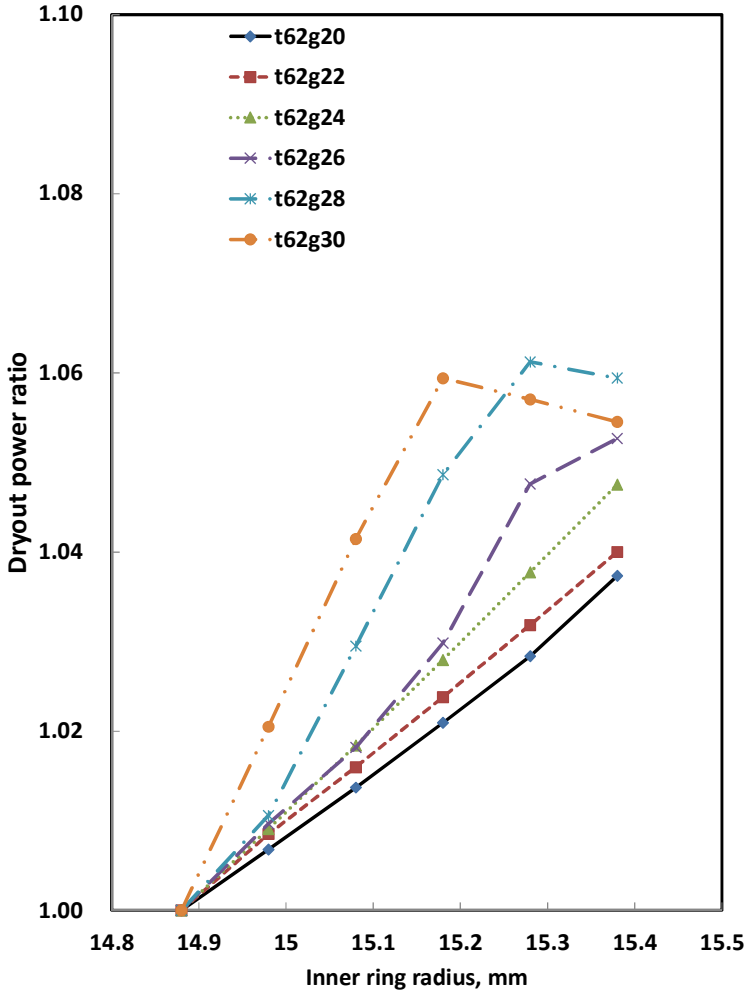

FIG.IV-6. Enhancement of dryout power vs. the inner ring radius for 5.1% crept pressure tube.

IV-2.3.3. Modification of the intermediate ring radius

Subchannel analyses for the 37R bundle with various intermediate ring radii were performed for the 0%, 3.3% and 5.1% crept pressure tubes. The intermediate ring radius can be increased from 28.75 mm to 29.25 mm, under the constraint for the minimum gap size [IV-4].

The first occurrence of CHF of the 37R bundle with various intermediate ring radius are summarized in Table IV-5 – Table IV-7. Most of the first CHF occurrences are located at the intermediate subchannel #32 or #33 for the large intermediate ring radii. This result is different from that for the case on the inner ring radius modification (in Table IV-2 – Table IV-4) because of the enlarged flow area of the inner subchannels with increased intermediate ring radius.

TABLE IV-5. FIRST OCCURRENCE LOCATIONS OF CHF IN THE 37R BUNDLE WITH DIFFERENT INTERMEDIATE RING RADII (0% CREPT PRESSURE TUBE)

Intermediate ring radius	Flow rate (kg/s)					
(mm)	20	22	24	26	28	30
28.75†	1	1	1	1	1	1
28.85	1	1	1	1	1	1
28.95	1	1	1	1	1	1
29.05	32	1	1	1	1	1
29.15	32	32	1	1	1	1
29.25	32	32	32	1	1	1

† the intermediate ring radius of the reference 37-element bundle.

TABLE IV-6. FIRST OCCURRENCE LOCATIONS OF CHF IN THE 37R BUNDLE WITH DIFFERENT INTERMEDIATE RING RADII (3.3% CREPT PRESSURE TUBE)

Intermediate ring radius	Flow rate (kg/s)					
(mm)	20	22	24	26	28	30
28.75†	7	1	1	1	1	1
28.85	7	1	1	1	1	1
28.95	1	1	1	1	1	1
29.05	1	1	1	1	32	32
29.15	1	1	1	33	32	32
29.25	1	1	33	33	32	32

† the intermediate ring radius of the reference 37-element bundle.

TABLE IV-7. FIRST OCCURRENCE LOCATIONS OF CHF IN THE 37R BUNDLE WITH DIFFERENT INTERMEDIATE RING RADII (5.1% CREPT PRESSURE TUBE)

Intermediate ring radius	Flow rate (kg/s)					
(mm)	20	22	24	26	28	30
28.75†	7	7	7	1	1	1
28.85	7	7	1	1	1	1
28.95	7	7	1	1	1	1
29.05	7	7	1	1	1	1
29.15	7	1	1	1	1	33
29.25	7	1	1	1	1	33

† the intermediate ring radius of the reference 37-element bundle.

The calculated dryout power ratio under the various PT conditions are shown in Fig. IV-7 through Fig. IV-9.

At low flow rates such as 20 kg/s and 22 kg/s, the dryout power ratio showed the maximum values with the middle ring radius of 29.05 mm under the uncrept pressure tube condition as shown in Fig.IV-7, while at high flow rates the dryout power ratio increased monotonically with increased radius of the intermediate ring. It should be noted that the maximum dryout power ratio was found to be the highest with a large intermediate ring radius for 3.3% and 5.1% crept pressure tube conditions. The influences of the open top section of 5.1% crept pressure tube on the dryout power ratio may be different from those of 0% or 3.3% crept pressure tube. Most of the dryout power ratios for the 5.1% crept pressure tube are monotonically increased when increasing the intermediate ring radius as shown in Fig.IV-9.

IV-2.3.4. Modification of the outer ring radius

The outer ring radius gradually increased from 43.43 mm to 43.83 mm with a fixed inner ring radius (15.28 mm) and an intermediate ring radius (29.25 mm).

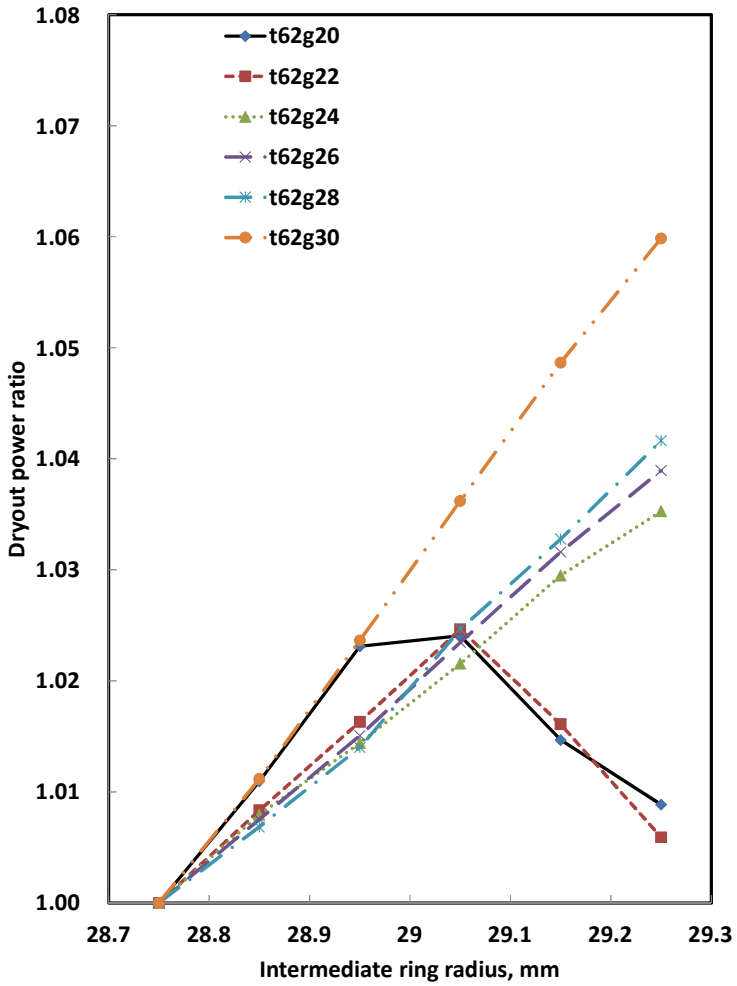

FIG. IV-7. Dryout power ratio vs. the inner ring radius for uncrept pressure tube.

The first CHF occurrence locations in the 37R bundle with various outer ring radii are summarized in Table IV-8 – Table IV-10. For low mass flow conditions and uncrept pressure tube, most CHF took place at the intermediate subchannel #34 while for high mass flow conditions of 28 kg/s and 30 kg/s, the CHF location, at subchannel #1, were not changed. For 3.3% crept pressure tube case, most CHF occurrences under all mass flow conditions were located at intermediate subchannel #32 or #33. This trend of the first CHF occurrence locations is similar to that of 5.1% crept pressure tube case except under low flow conditions of 20 kg/s or 22 kg/s.

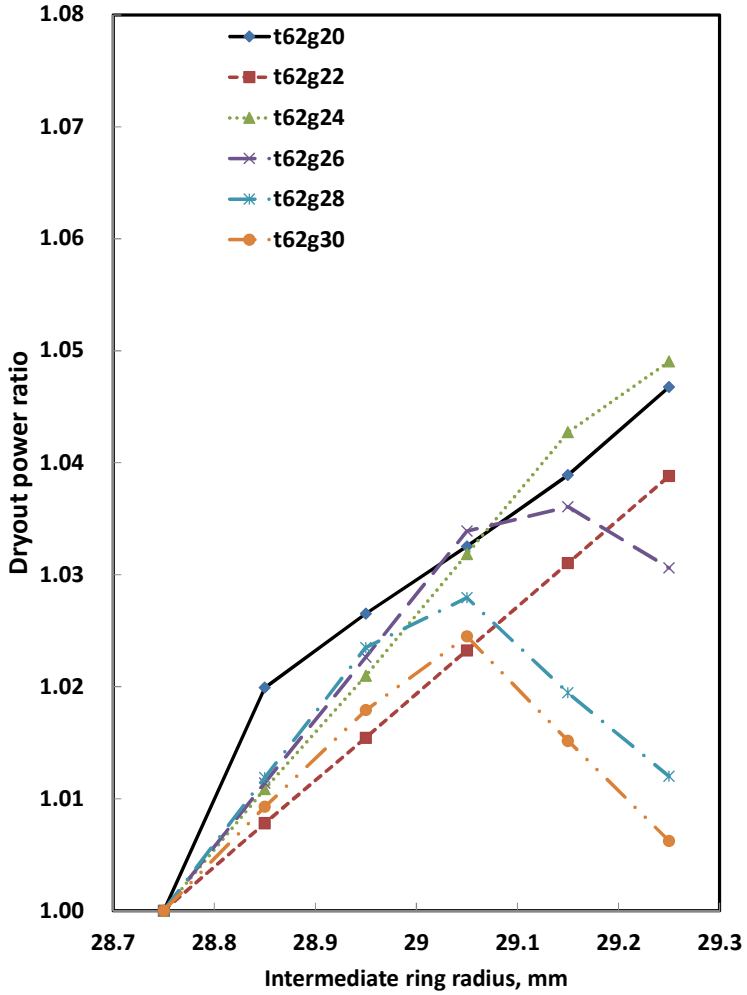

FIG. IV-8. Dryout power ratio vs. the inner ring radius for 3.3% crept pressure tube.

TABLE IV-8. FIRST OCCURRENCE LOCATIONS OF CHF IN THE 37R BUNDLE WITH DIFFERENT OUTER RING RADII (0% CREPT PRESSURE TUBE)

Outer ring radius (mm)	Flow rate (kg/s)					
	20	22	24	26	28	30
43.33†	1	1	1	1	1	1
43.43	34	34	34	34	1	1
43.53	34	34	34	1	1	1
43.63	24	34	1	1	1	1
43.73	42	18	1	1	1	1
43.83	42	1	1	1	1	1

† the outer ring radius of the reference 37-element bundle.

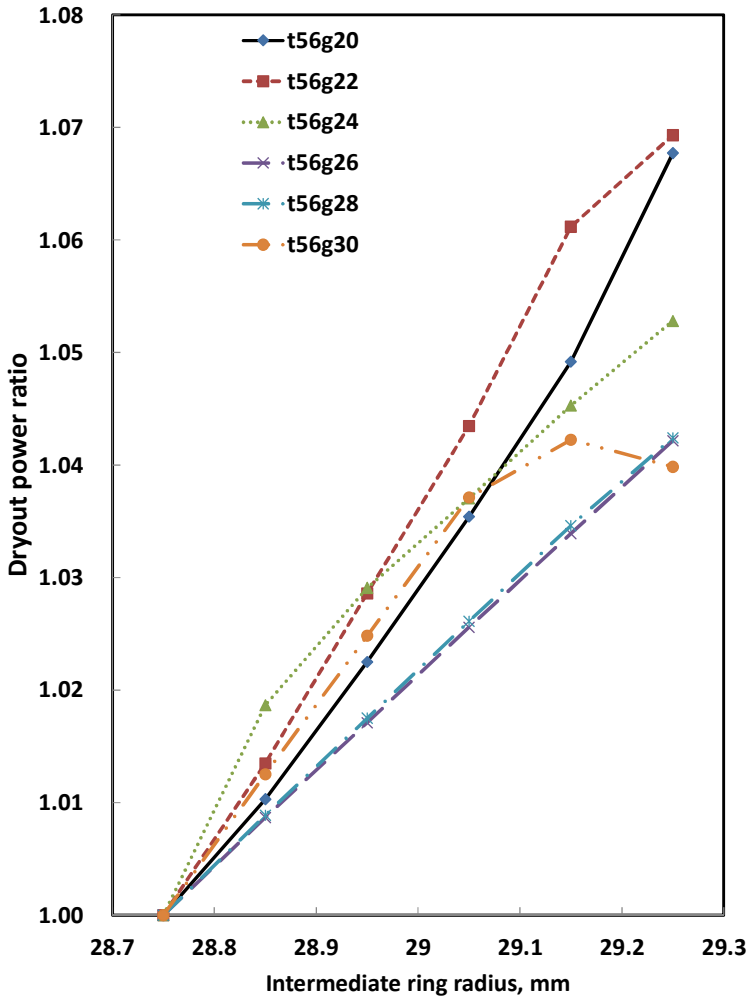

FIG. IV-9. Dryout power ratio vs. the inner ring radius for 5.1% crept pressure tube.

TABLE IV-9. FIRST OCCURRENCE LOCATIONS OF CHF IN THE 37R BUNDLE WITH DIFFERENT OUTER RING RADII (3.3% CREPT PRESSURE TUBE)

Outer ring radius (mm)	Flow rate (kg/s)					
	20	22	24	26	28	30
43.33†	7	1	7	1	1	1
43.43	33	33	33	33	32	32
43.53	33	33	33	32	32	32
43.63	33	33	33	32	32	10
43.73	33	33	32	32	10	1
43.83	33	33	32	10	10	1

† the outer ring radius of the reference 37-element bundle.

TABLE IV-10. FIRST OCCURRENCE LOCATIONS OF CHF IN THE 37R BUNDLE WITH DIFFERENT OUTER RING RADII (5.1% CREPT PRESSURE TUBE)

Outer ring radius (mm)	Flow rate (kg/s)					
	20	22	24	26	28	30
43.33†	7	7	7	1	1	1
43.43	1	1	33	33	33	33
43.53	1	1	33	33	33	32
43.63	1	33	33	33	33	32
43.73	1	33	33	33	32	32
43.83	1	33	33	33	32	32

† the outer ring radius of the reference 37-element bundle.

The calculated dryout power ratio for outer ring modification are shown in Fig.IV-10.

As shown in Fig.IV-10 for the uncrept pressure tube, the dryout power ratios at high flows quickly increased and then slowly increased with the increased radius of the out ring to 43.83 mm. At low flows (e.g. flows below 24 kg/s), the dryout power ratios increased with the increase of the outer ring radius.

Figure IV-11 shows the results for 3.3% crept pressure tube condition and the dryout power ratio monotonically increased with the increase of the outer ring radius at all flow conditions. This trend is similar to that for 5.1% crept pressure tube case as shown in Fig.IV-12. The maximum value was obtained when the maximum radius of the outer ring was 43.83 mm.

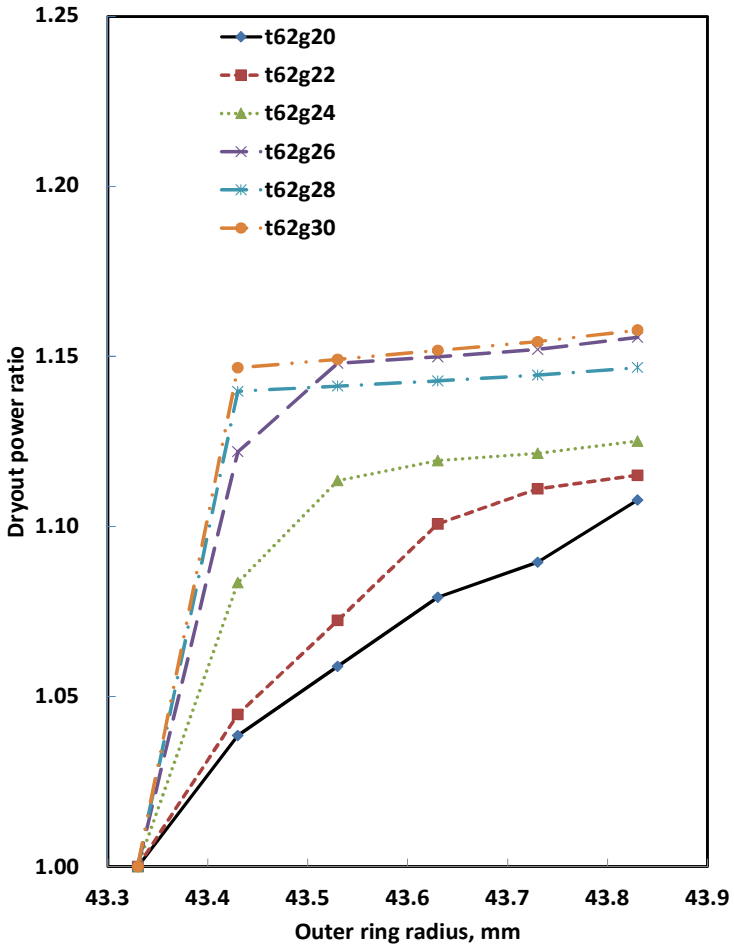

FIG. IV-10. Enhancement of dryout power vs. the outer ring radius for un-crept pressure tube.

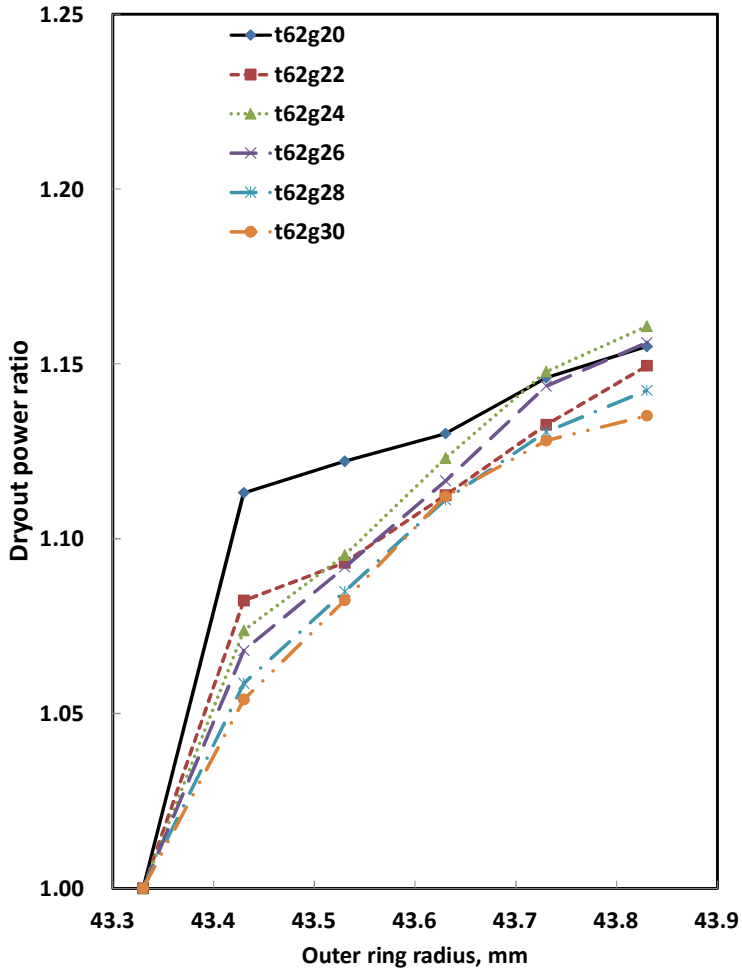

FIG. IV-11. Enhancement of dryout power vs. the outer ring radius for 3.3% crept pressure tube.

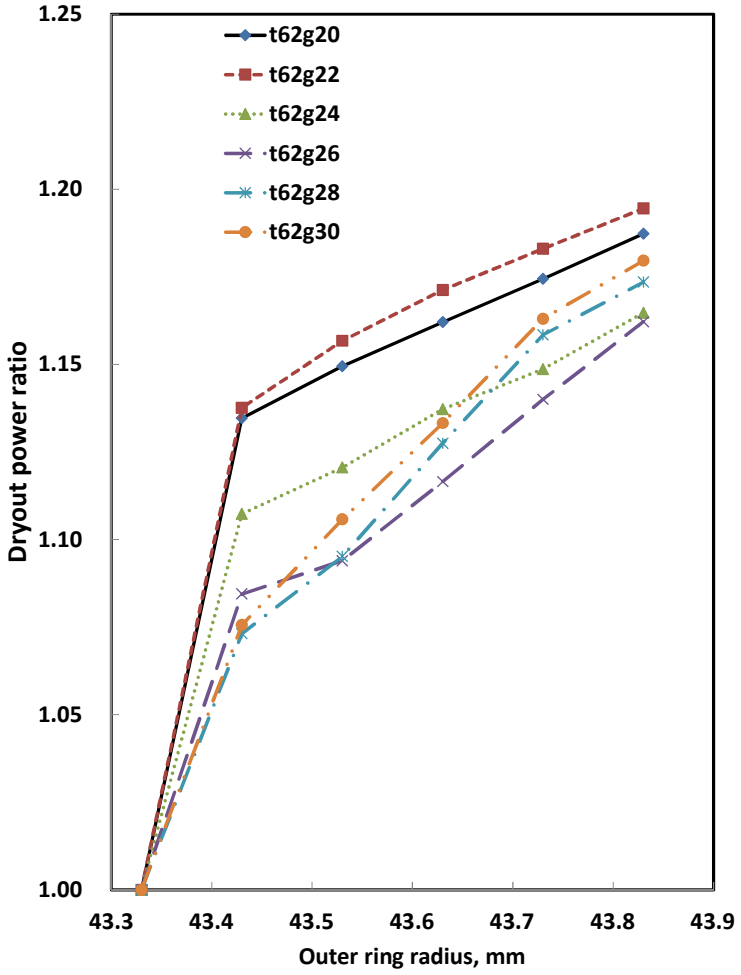

FIG. IV-12. Enhancement of dryout power vs. the outer ring radius for 5.1% crept pressure tube.

IV-3. SUMMARY AND CONCLUSIONS

Subchannel analyses using the ASSERT code were performed for the 37R bundle and for the 37R bundle with several pitch circle radii under uncrept and various pressure tube creep conditions to investigate associated changes in the dryout power.

The flowing conclusions were reached:

- Overall, any increase of the pitch circle radii of the 37R bundle enhances the dryout power. Especially, an increase of the outer ring radius together with an increase of the inner ring radius seems a viable option for the enhancement of the dryout power.

- Such enhancement of the dryout power is more dominant for the largest crept pressure tube.

- With an increased radius of the outer ring, the first CHF occurrence is expected to take place in an intermediate subchannel (e.g. #32 or #33), while it actually occurs in

a central subchannel (e.g. #1). This observation is likely due to flow mixing across subchannels owing to the changes in the outer ring radius.

ACKNOWLEDGEMENTS

This Research Agreement was led by Chief Scientific Investigator, J-H. Park of KAERI, Korea.

REFERENCES

[IV-1] PARK, J.H., SONG, Y.M., The Effect of Inner Ring Modification of Standard 37-Element Fuel on CHF Enhancement, Annals of Nuclear Energy **70** (2014) 135.

[IV-2] LEUNG, L.K.H., JUN, J.S., DIMMICK, G.R., BULLOCK, D.E., INCH, W.W.R., SUK, H.C. Suk, "Dryout Power of a CANFLEX Bundle String with Raised Bearing Pads", Proceeding of the 7th International Conference on CANDU Fuel, Kingston, Ontario, 2001.

[IV-3] CARVER, M.B., KITELEY, J.C., ZOU, R.Q.N., JUNOP, S.V., ROWE, D.S., Validation of the ASSERT Subchannel Code: Prediction of Critical Heat Flux in Standard and Nonstandard CANDU Bundle Geometries, Nuclear Technology **112** (1995) 299.

[IV-4] Atomic Energy of Canada Limited (AECL), Fuel Design Manual for CANDU-6 Reactors, Report DM-XX-37000-001, AECL, Mississauga, Ontario (1989).

[IV-5] LEUNG, L.K.H., DIAMAYUGA, F.C., Measurements of Critical Heat Flux in CANDU 37-Element Bundle with a Steep Variation in Radial Power Profile, Nuclear Engineering and Design **240** (2010) 290.

ANNEX V: DEVELOPMENT OF A FUEL BUNDLE WITH 43 ELEMENTS CONTAINING MIXED OXIDE OF THORIUM AND URANIUM (T43) IN ICN

A Summary Report of Research Contract with Institute for Nuclear Reactor (INR), Romania

V-1. BACKGROUND

Thorium represents a valuable fuel alternative to uranium, but since it has no fissile isotopes, it is necessary to foresee using a small amount of fissile material to initiate the chain reaction. Many studies (related to reactor physics and fuel performance) have been performed worldwide for Th+U, Th+Pu and even Th+Minor Actinides. In Romania, given the safeguard limitations, the only considered fissile material is U-235.

The thorium fuel cycles in CANDU nuclear reactors maintain their strategic interest as they ensure a long-term resources availability, especially for those countries possessing large thorium reserves but limited uranium resources. Again, driven by safeguard limitations, the 'once-through' thorium cycle without reprocessing was taken into account.

This report reviews the analytical and experimental work performed at Institute of Nuclear Reactor (INR) concerning the nuclear fuel containing mixed oxide of thorium and uranium to be used in existing CANDU reactors. A major request was that the CANDU power plant design, especially the reactor core design, should not be modified in order to comply with using the advanced fuel bundles, excepting for the fuel bundle itself. Based on previous studies performed in Canada, China, India and Korea, the fuel bundle considered for hosting mixed oxide of thorium and uranium would be T43, a 43 elements bundle.

V-2. T43 NUCLEAR FUEL BUNDLE

V-2.1. Fuel bundle design

In order to achieve a high burnup in a CANDU reactor, the fuel bundle design needs to be modified to lower the maximum linear heat generation rating (LHGR). The T43 fuel bundle is a result of a long process of analyses and improvements in which successive preliminary design version have been evaluated [V-1] through a step-by-step strategy.

The main feature of T43 fuel bundle is the increased number of fuel elements from 37 (in the reference CANDU-6 bundle) to 43. The T43 fuel bundle contains fuel elements with two different sizes: 11.50 mm small-diameter elements for the outer and intermediate rings and 13.50 mm large-diameter elements for the inner ring and centre (Fig.V-1). To maintain the compatibility with the existing CANDU-6 reactor systems, the basic overall dimensions of T43 fuel bundle are the same as those of the reference 37-element bundle.

The small-diameter elements for the outer ring show a slightly eccentric welding-point between the endcap and the endplate, compared to the reference 37-element fuel bundle. This ensures that the T43 fuel bundle is geometrically compatible with the side stop/separator assembly of the CANDU-6 fueling machine (Fig.V-2).

The optimization of fuel element design is presented in Table V-1.

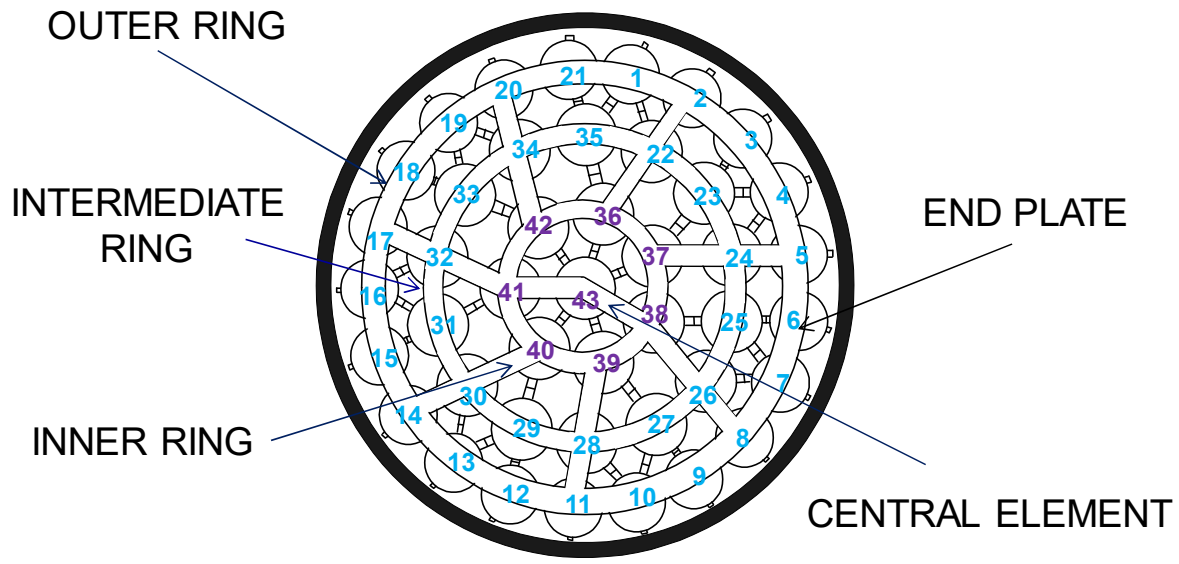

FIG.V-1. T43 fuel bundle geometry.

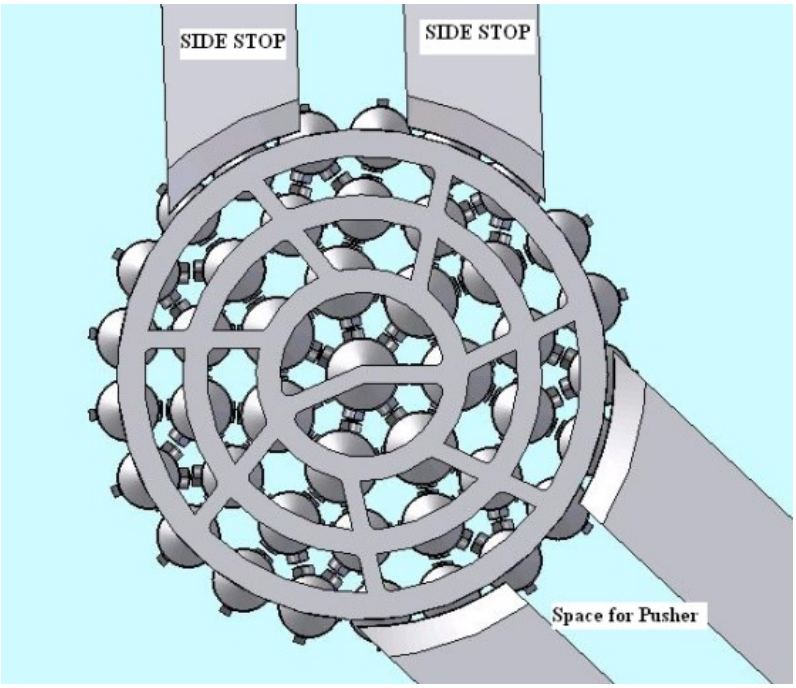

FIG.V-2. Interface between T43 fuel bundle and CANDU-6 Fueling Machine Components.

V-2.2. Endcap to sheath resistance welding

Resistance welding refers to a group of welding processes that produce coalescence of two surface where heat to form the weld is generated by the resistance of a welding current through the work pieces. Some factors influencing heat or welding temperatures are the portions of the work pieces, the electrode material, electrode geometry, mechanical clamping force of the electrodes, weld current and weld time, etc.

TABLE V-1. DESIGN SOLUTIONS FOR HIGH BURNUP FUEL ELEMENTS

Design solution	***Specific design objectives for extended discharge burnup***
- Decreasing of sheath diameter	Decreasing of fuel element linear power and average fuel temperature
- Increasing of initial pellet grain size	Ensuring that fission gas release is within acceptable limits
- Increasing the pellet dish volume - Increasing the pellet land width - Increasing the pellet chamfer	Minimization of the local strain in the sheath ridges and reduction of SCC failure susceptibility in power ramps
- Increasing the axial gap	Accommodation of axial fuel stack expansion
- Increasing the graphite layer thickness	Reduction of SCC failure susceptibility

The favorable features of resistance welding are:

- avoiding a large melting at the joint between the cladding and the endcap, and leading to the dynamic recrystalization with a finer structure;
- small heat affected zone;
- virtually guaranteed freedom for contamination;
- the use of weld condition monitoring as an on-line inspection technique.

The drawbacks of the welding method are:

- the external weld flash should be removed by machining;
- the quality of resistance welding is difficult to be assessed without non-destructive technique. Therefore, the quality of the welds is mainly based on operational experience combined with sample weld testing and destructive examination;
- cleanliness of the components being welded and the accuracy of machining in the weld preparation are important contributors to the weld quality.

The stress and strain distributions in the weld endcap-cladding region are influenced by pellet and cladding deformations in radial and axial direction and the interaction between them. The weld region has been modelled using the finite element method based on the image of metallographic samples obtained from manufacturing (for thin and thick elements) over design drawing (see Fig.V-3).

Stress and strain analyses were performed using ANSYS 7.1 code, especially taking into account of the residual stresses caused by welding. Power history with a simple ramp was considered for the analysis (Fig.V-4). ROFEM code was used to generate load conditions during the ramp (Fig.V-5). The values of the loads used in the analysis reflected the worst conditions that could exist during the irradiation of the fuel element in the power reactor.

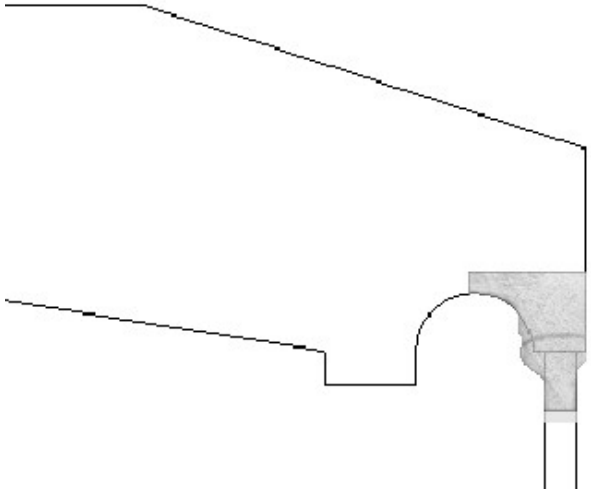

FIG.V-3. Illustration of s section through resistance welding end closure (after removing the outside weld flash).

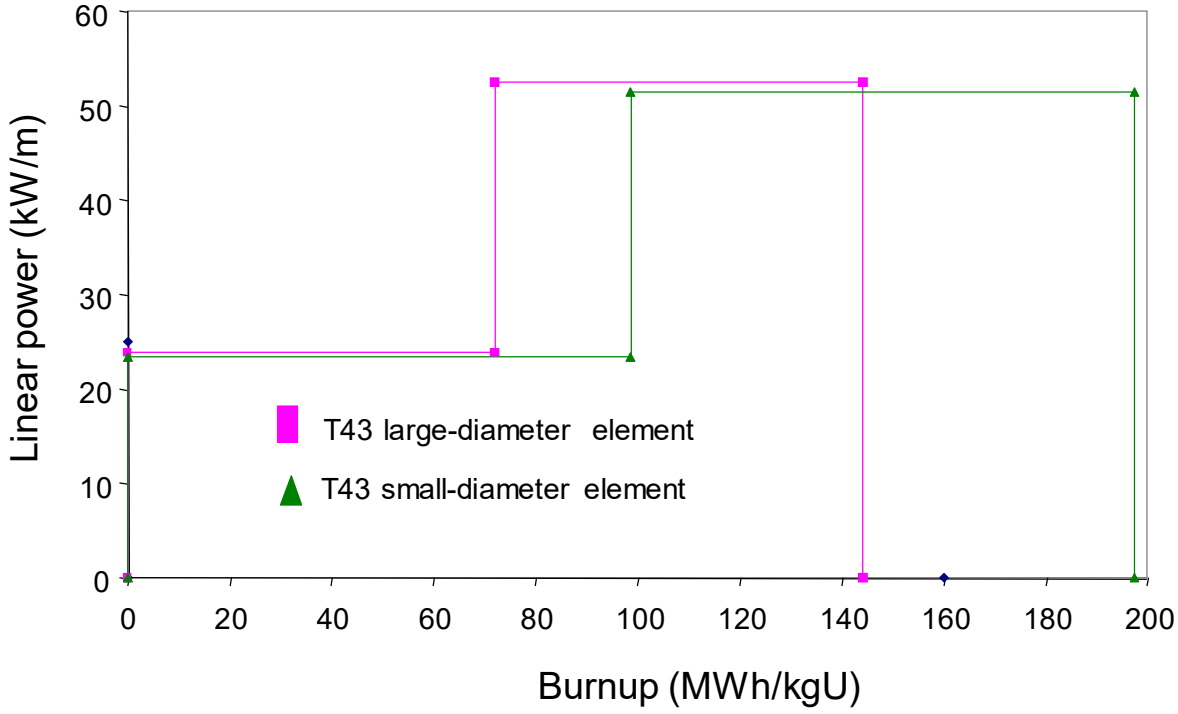

FIG.V-4. Power histories.

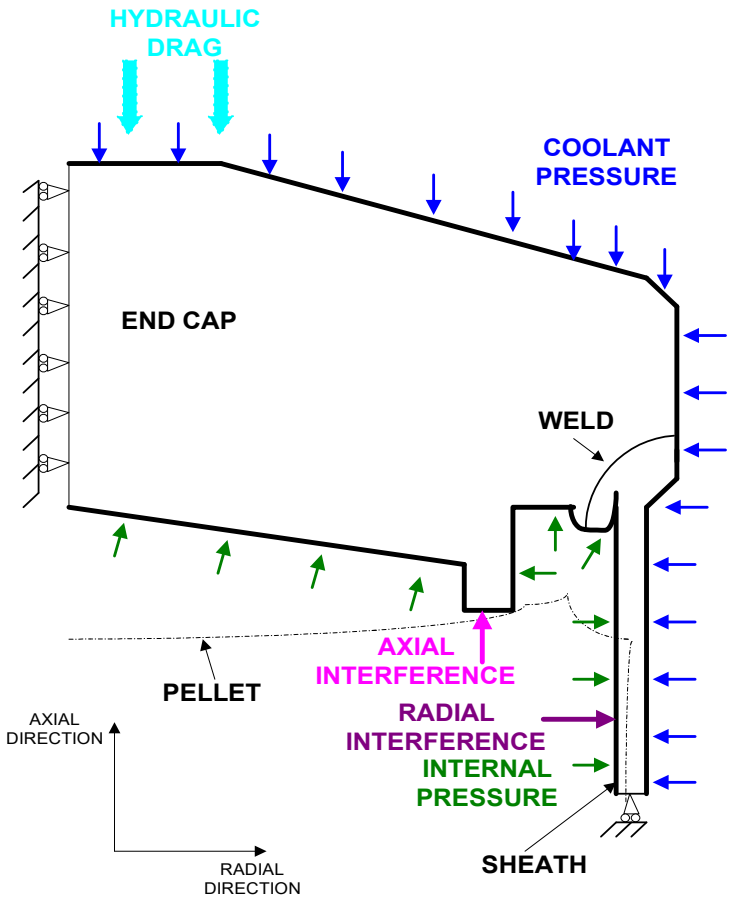

FIG.V-5. Weld geometry near the endcap and load conditions.

The equivalent stress and equivalent plastic deformation were analyzed for both outer-ring element (small-diameter fuel element) and inner-ring element (large-diameter fuel element). Figures V-6 and V-7 and Figures V-8 and V-9 show von Misses equivalent stress and von Misses equivalent plastic strain, respectively, for the outer-ring element.

In general, the stress and strain distributions were similar for both types of fuel elements. During the welding process the maximum stress was obtained on the outer surface of sheath in the region where the temperature was low and where the stress of the corresponding material from that area was small (~ 200 MPa, while 0.2% yield strength was around 380 MPa). In the weld region the stress was smaller, but a plastic deformation occurred (0.2% yield strength for the material in the weld region which has a high temperature was lower than that of the surrounding regions). After material cooling the weld region remained the most stressed zone due to the residual stresses (around 1.3 for the reference CANDU fuel, 1.7% for the inner-ring element of the T43 bundle and 1.4% for the outer-ring element of the T43 bundle). The maximum value occurred in the curvature region located on the outer surface of the cladding. There was a plastic deformation in the welded zone, but its value was relative low belonging to the range 0.5 – 0.7 %.

After the weld flash was removed, no significant changes for either the stress (slightly lower value) or the deformations were predicted. During irradiation, no significant changes was also observed (the material remained in the elastic domain). By comparison, the distributions of stress and strain presented here for the fuel elements of the T43 fuel bundle were smaller than the distributions of stress and strain obtained for the fuel elements of the reference 37-element fuel bundle under the same operating conditions.

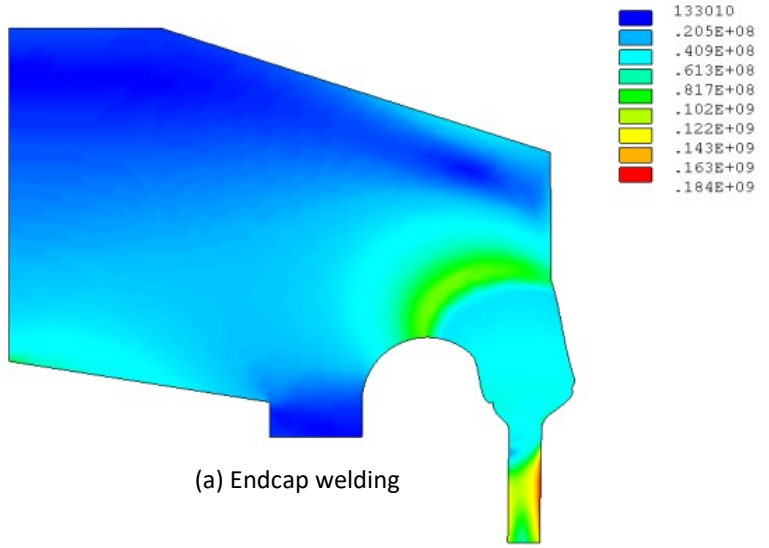

(a) Endcap welding

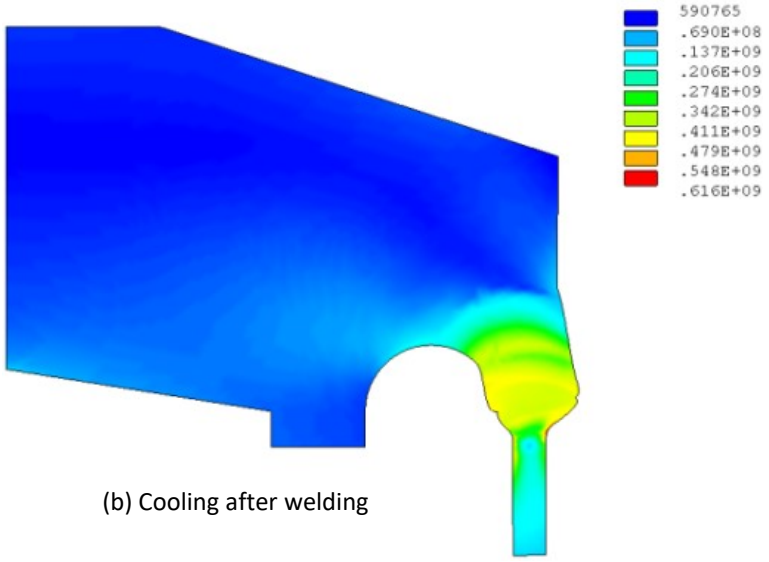

(b) Cooling after welding

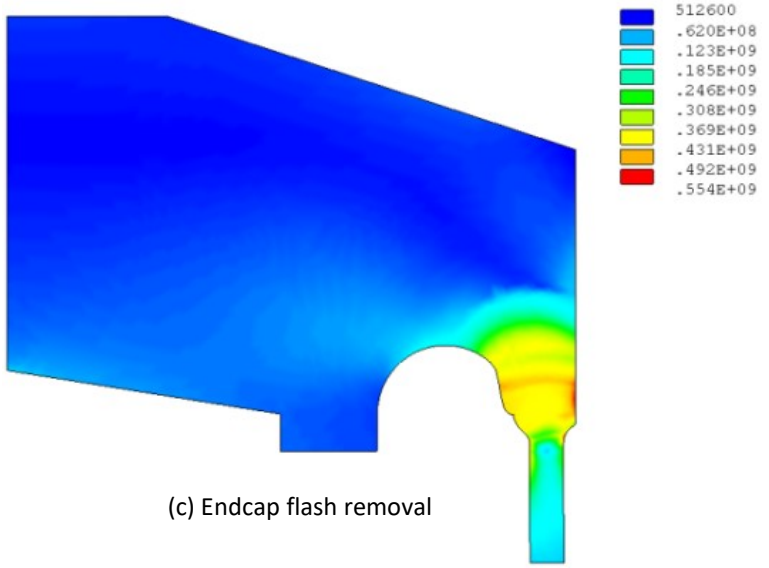

(c) Endcap flash removal

FIG.V-6. Equivalent von Misses stress at the weld region of the outer-ring element, at various stages from welding to flash removal.

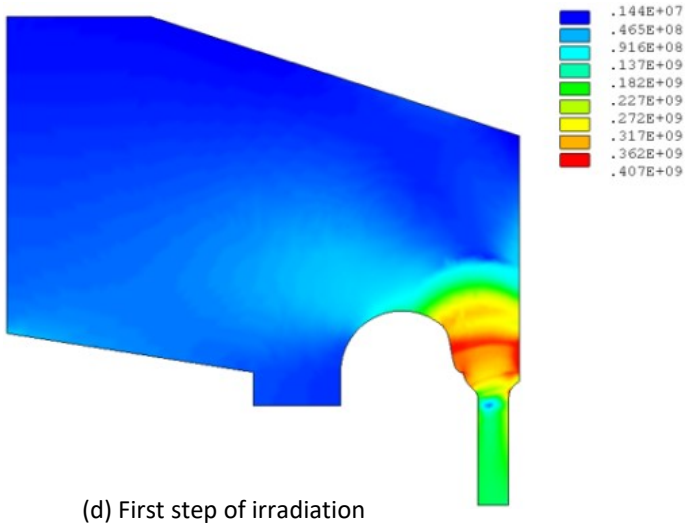

(d) First step of irradiation

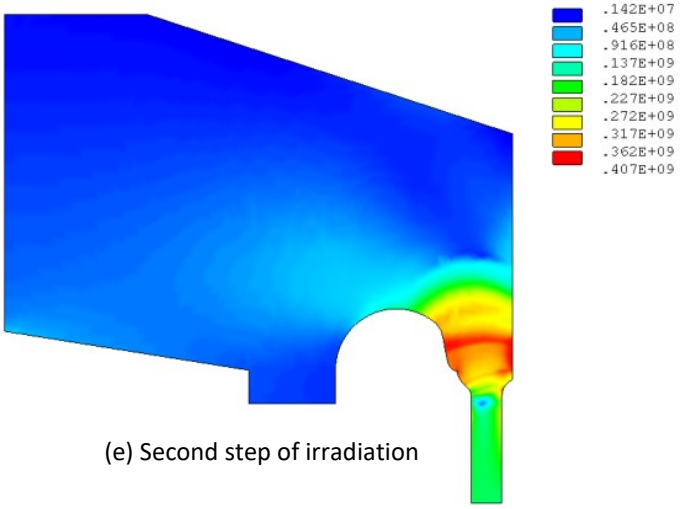

(e) Second step of irradiation

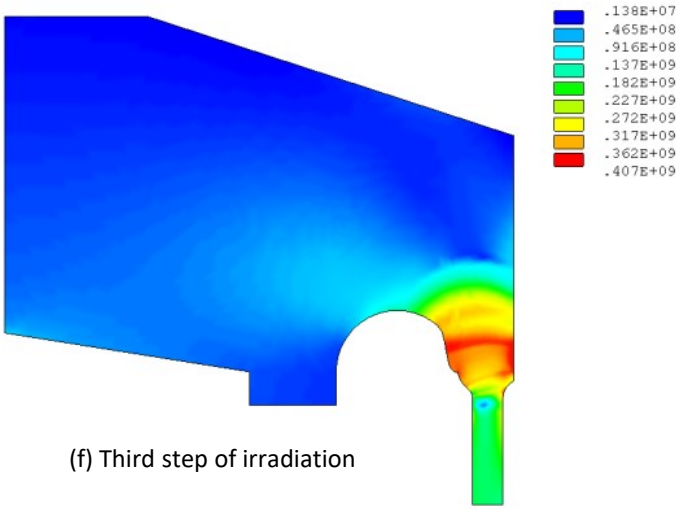

(f) Third step of irradiation

FIG.V-7. Equivalent von Misses stress at the weld region of the outer-ring element, at various stages from the first step of irradiation to the third step of irradiation.

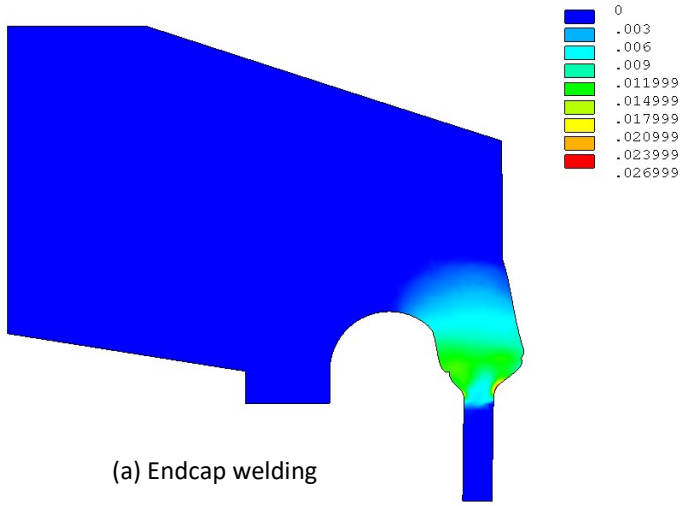

(a) Endcap welding

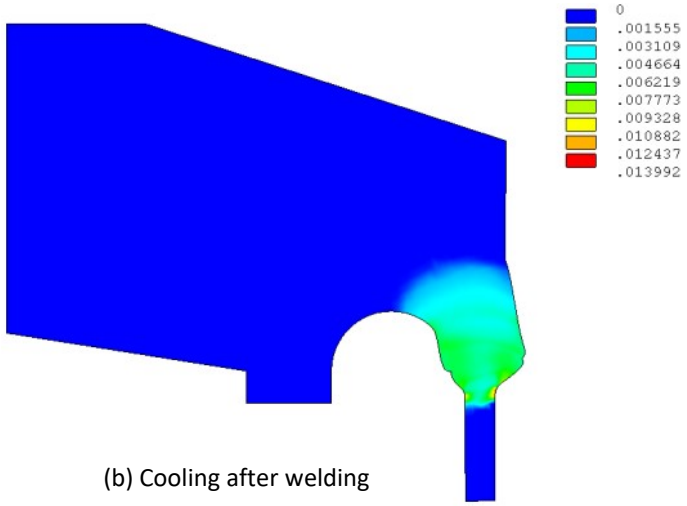

(b) Cooling after welding

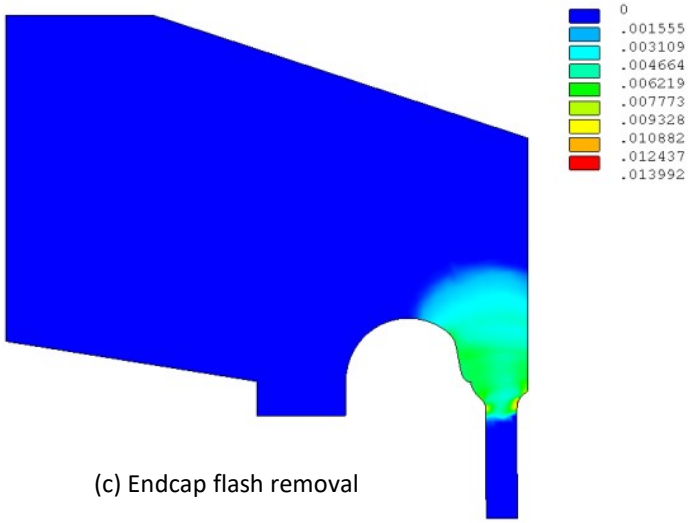

(c) Endcap flash removal

FIG.V-8. Equivalent von Misses plastic deformation at the weld region of the outer-ring element, at various stages from welding to flash removal.

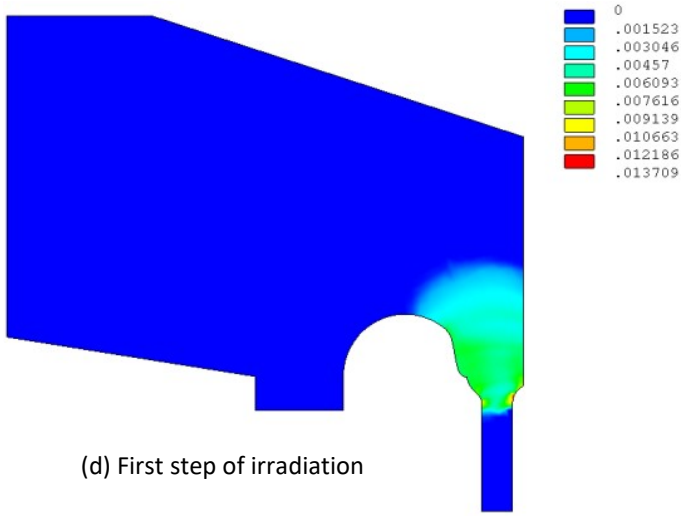

(d) First step of irradiation

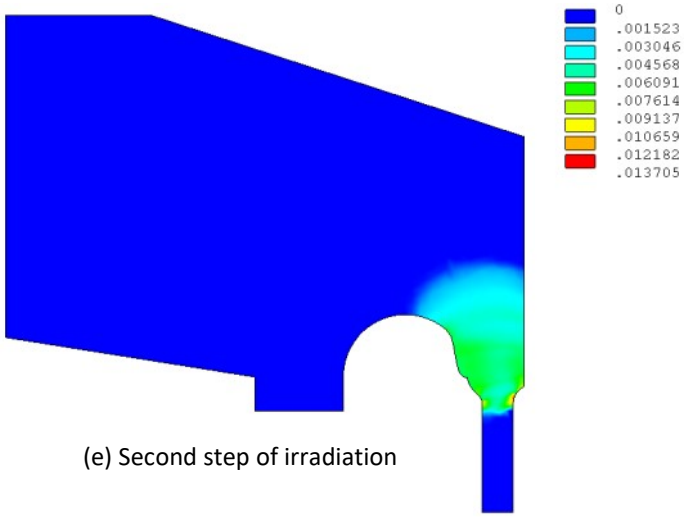

(e) Second step of irradiation

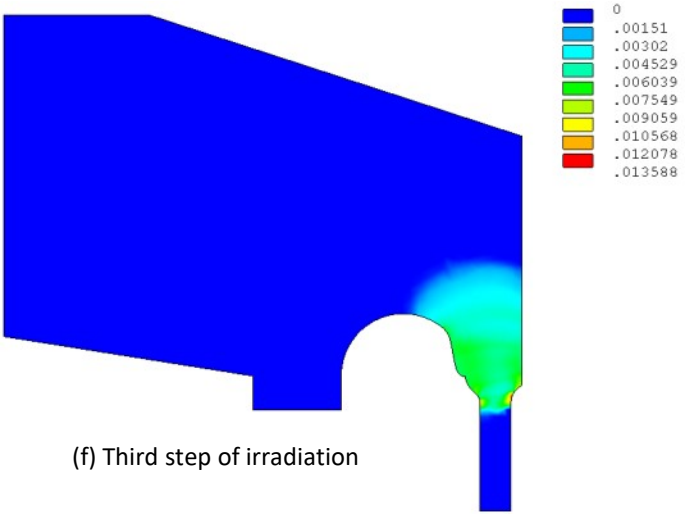

(f) Third step of irradiation

FIG.V-9. Equivalent von Misses plastic deformation at the weld region of the outer-ring element, at various stages from the first step of irradiation to the third step of irradiation.

V-3. REACTOR PHYSICS STUDIES CONCERNING T43 FUEL BUNDLE

The following studies addressed the proposed T43 fuel bundle [V-2]–[V-4], to identify proper ranges of manufacturing features that can ensure better economic and safety aspects. Known manufacturing uncertainties were taken into account, as well as some abnormal operating conditions.

V-3.1. Neutronic determination

This Section is intended to assess by calculation the economic and safety features of a T43 experimental fuel element that contain $(Th,U)O_2$ pellets.

Some difficulties were expected to occur during pellet fabrication, due to relatively high sintering temperature (>1800ºC), since the hyperfine mixing at molecule level is required for uranium and thorium oxide solutions co-precipitation; therefore, theoretical density of the fuel pellet was below 10 g/cm^3; actual theoretical densities were 9.0, 9.2, 9.4 and 9.6 g/cm^3. The enrichments used in the calculations were 5, 6, 7, 8, 9 and 10 wt.% U-235, while the Th/U weight ratios were 1.5, 1.857 and 2.333 (corresponding to 60/40, 65/35 and 70/30 % heavy element share respectively). The overall U-235 contents in the bundle ranged from 1 wt.% to 4 wt.% [V-5].

All the fuel elements in the bundle were considered to have the same pellet compositions, regardless their position in the bundle.

A simplified 2-D cell model was built using DRAGON, consisting of fuel bundle, coolant, pressure tube, annular gas (CO_2), calandria tube and moderator (Fig.V-10).

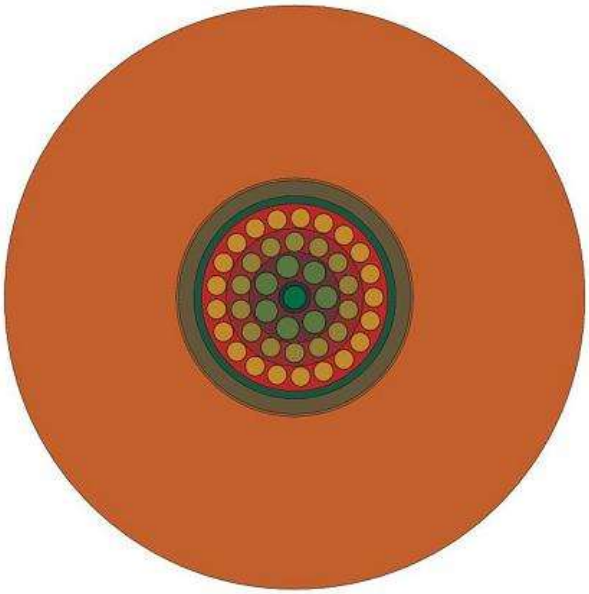

FIG.V-10. CANDU cell with T43 bundle (DRAGON plot).

An infinite lattice of such 2-D cells was assumed, as well as infinitely long bundles, therefore no neutron leakage was taken into account (reflective boundary condition at cell frontier) [V-6], [V-7].

The maximum burnup (B_{max}) was defined as the maximum burnup value for which the cell still remains critical. Encouraging results (B_{max} > 20 000 MWd/tHE, i.e. at least three times the usual maximum burnup for CANDU) were obtained for LEU enrichment ≥ 6 wt.% U-235, regardless the pellet density or Th/U ratio.

Radial power distribution can be considered a key safety parameter, since an unbalanced distribution may lead to uneven fuel sheath stress and thus to fuel failure. A Power Peaking Factor (PPF) can be defined for each fuel element to express its contribution to the bundle power output.

$$PPF_i = w_i \times V / (N_i \times v_i)$$

where:

w_i is the fraction of the bundle power generated in ring i, with $w_1+w_2+w_3+w_4 = 1$,
N_i is the number of fuel elements in ring I,
v_i is the volume of a fuel element in ring I,
V is the bundle fuel volume.

Volume weighting is only applicable for fuels having the same compositions throughout the bundle; in the case of the bundles having different pellet compositions in different fuel rings, the fission rates should be used instead.

PPF = 1 indicates a uniform power distribution. For the fuel bundles with natural uranium oxide, $PPF_{1, 2}$ and $_3$ are less than 1, while PPF_4 is about 1.1.

Using LEU+Th fuel instead of NU does not improve the radial power distribution, as seen in Fig.V-11. Two T43 fuel elements were presented: #14 (40% LEU+60% Th, 6 wt% U-235 in LEU, pellet density of 9 g/cm^3) and #55 (30% LEU+70% Th, 5 wt.% U-235 in LEU, pellet density of 9.6 g/cm^3).

The void effect, defined as the reactivity effect following a loss of coolant, is a key safety indicator. The coefficient of void reactivity, CVR, expresses this effect [V-8].

For modeling purposes, it was assumed that losing a certain amount of coolant will result in preserving its volume and reducing its density. Considering a homogenous coolant was certainly a simplifying assumption, but the overall results were satisfactory. For fuel bundles containing natural uranium, the CVR is positive: about 17/19 mk for C37 fuel at the beginning of life (DRAGON/WIMS estimates) and 18/20 mk for C43 fuel at the beginning of life and also 8.5/7.3 mk for C37 and 9/7.4 mk for C43 at the end of life. Fuel containing LEU+Th also has positive CVR (slightly smaller for fresh T37/T43 bundles than for the C37/C43, while T37 and T43 bundles at maximum burnup exhibit larger CVR than the corresponding C bundles).

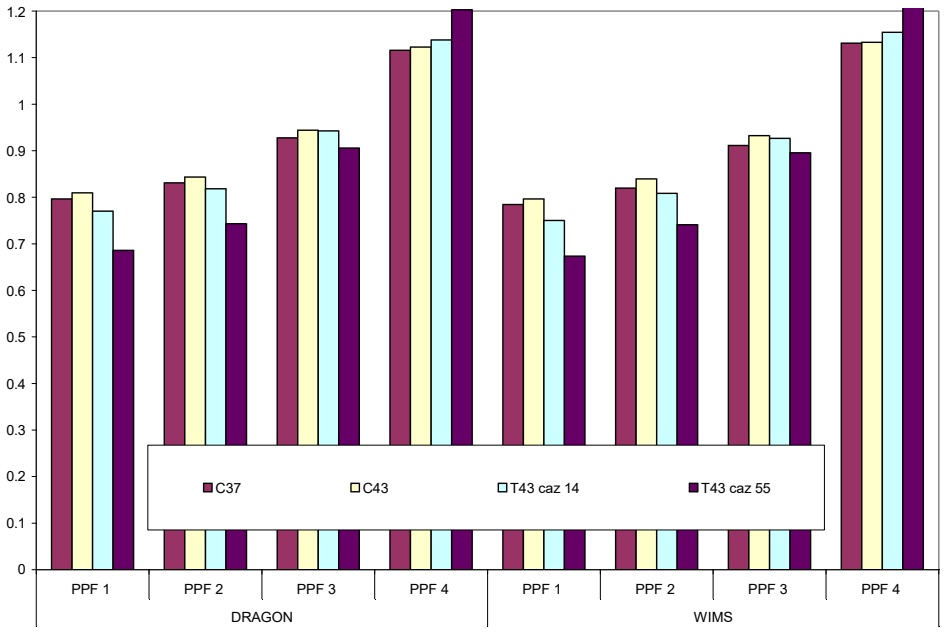

FIG.V-11. Power peaking factors at maximum burnup (DRAGON-WIMS calculations).

V-3.2. Core-follow burnup calculations for Thorium-Uranium mixed oxide fuel designs

The Thorium-Uranium mixed oxide fuel configurations have been preliminarily analyzed in [V-8]. Based on those analyses, two cases have been selected, case 4 and Case 64. Fuel compositions for two selected cases are presented in Table V-2.

TABLE V-2. THORIUM-URANIUM MIXED OXIDE FUEL CONFIGURATIONS.

Case # in [V-9]	*U-235/total U ratio*	*UO_2 (%)*	*ThO_2 (%)*	*Th/U ratio*	*Fuel density (g/cm^3)*
4	5	40	60	1.5	9.6
64	8	30	70	2.33	9.6

Linear element powers are represented as a function of burnup, and compared with the failure thresholds (red curve) for both cases (Fig.V-12 for case 4 and Fig.V-13 for Case 11) [V-9]. Although the failure threshold curve is for NU fuel, it is used here for the thorium-uranium mixed oxide fuel designs. In order to avoid possible conditions for fuel failure, the maximum linear power and power boost of the fuel element should not exceed both failure threshold curves [V-10]. The maximum linear powers have not exceeded the threshold values for both cases.

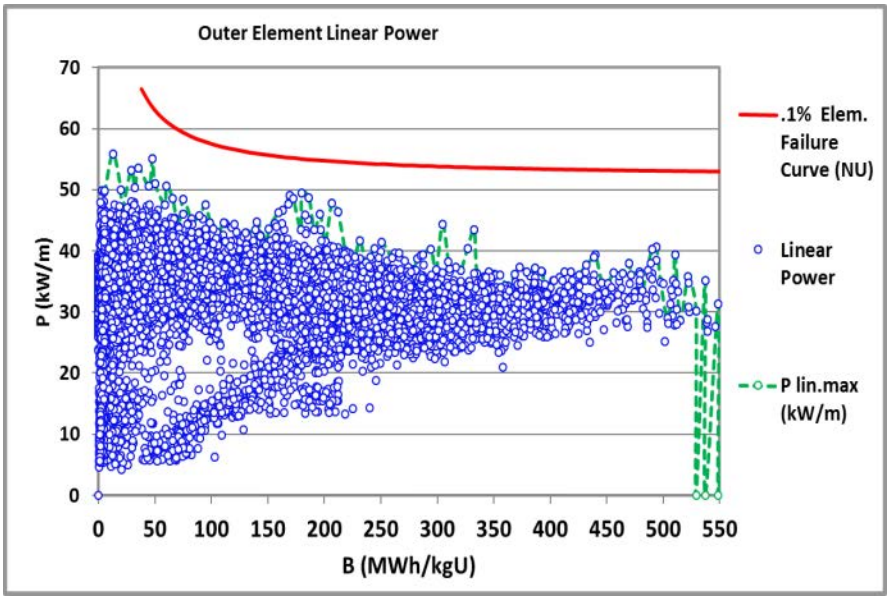

FIG.V-12. Outer element linear power (Case 4, see Table V-2 for fuel compositions).

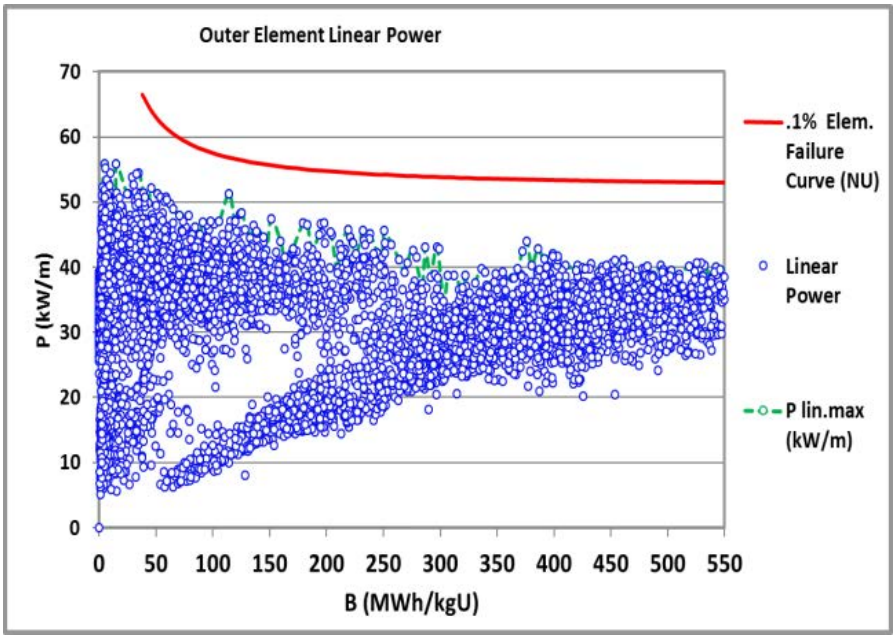

Fig.V-13. Outer element linear power (Case 64, see Table V-2 for fuel compositions).

Table V-3 shows a summary of the core-follow analysis for both cases. A significantly lower fuel bundle consumption is revealed by the thorium-uranium mixed oxide configurations (Case #4 and #64) face to that of NU. This leads logically, to an increased average burnup with benefits on the fuelling machine burden and on the nuclear radioactive waste generation. Also, in spite of some minor overrides of the license limit for bundle power, the element linear powers and power boosts for Th-U fuel configurations are a bit lower face to those of NU, this resulting in a lower fuel failure likelihood.

TABLE V-3. CORE-FOLLOW PARAMETERS

Parameter	*Case 4 (5% U-235, Th/U=1.5)*	*Case 64 (8%U-235, Th/U=2.33)*	*NU*
FPD	950	950	950
Bundle consumption	5176	2520	16240
Bundles / FPD	5.4	2.6	17.1
Average burnup (MWd/kg-HE)	13.9	17.0	6.0
Maximum bundle power (kW)	1080	1,089	914
Maximum channel power (kW)	7264	7112	7100
Maximum element linear power (kW/m)	55.9	55.8	56.4
Maximum element linear power boost (kW/m)	36.5	35.4	38.2

In conclusion, the thorium-uranium mixed oxide fuel configurations taken into consideration perform well in a CANDU 6 reactor with economic and operational benefits. Also, based on the core-follow simulations there is no fuel failure expected more than in the case of NU.

V-4. IRRADIATION OF TEST FUEL ELEMENTS A23

The test fuel element containing mixed oxide of thorium and uranium pellets (A23) was irradiated in a material test reactor. A fuel element containing only UO_2 pellets (5% U-235 enrichment) (A24) was also irradiated under similar conditions at the material test reactor [V-11]. Figure V-14 shows the test fuel elements assembly.

FIG.V-14. Test fuel elements (A23 + A24).

Relevant references for A23 include the following:

- manufacturing report [A-12];
- irradiation test report [A-13];
- PIE report [A-14];
- performance analysis by use of a computer code [A-15].

The following is a summary of manufacturing information for A23 test fuel element:

- the element was manufactured to comply with technical specifications and design according to procedures established for CANDU 6 fuel manufacturing;
- $(Th,U)O_2$ fuel pellets had a composition of 5% UO_2 (90 % enriched with U-235);
- sintered density of $(Th,U)O_2$ fuel pellets was 9.7 g/cm^3;
- fuel cladding was made of Zircaloy-4;

- the test fuel element was compatible with the irradiation device.

The element achieved a maximum linear power of about 33 kW/m (in the pre-ramp period) and 50.9 kW/m (in the ramp period). Corresponding to this power history, the maximum discharge burnup, achieved after 6184 effective hours of irradiation, was 189.2 MWh/Kg-HE (see Table V-4).

TABLE V-4. TEST FUEL ELEMENT POWER HISTORY

Experimental element	*Linear Power [kW/m]*		*Discharge Burnup [MWh/kg-HE]*
	Pre-ramp conditions	*Ramp (for 7 days)*	
A23	33	51	189.2

The irradiation data (power and burnup) has been collected using a specific data acquisition system during the entire test period. The irradiation history of the A23 test fuel element is shown in Fig.V-15. Some details for the power ramp included:

- power increase: 0.025 kW/m per minutes;
- maximum linear power: 51 kW/m;
- dwell time at the ramp terminal level: 7 days;
- coolant chemistry: no change from the pre-ramp period.

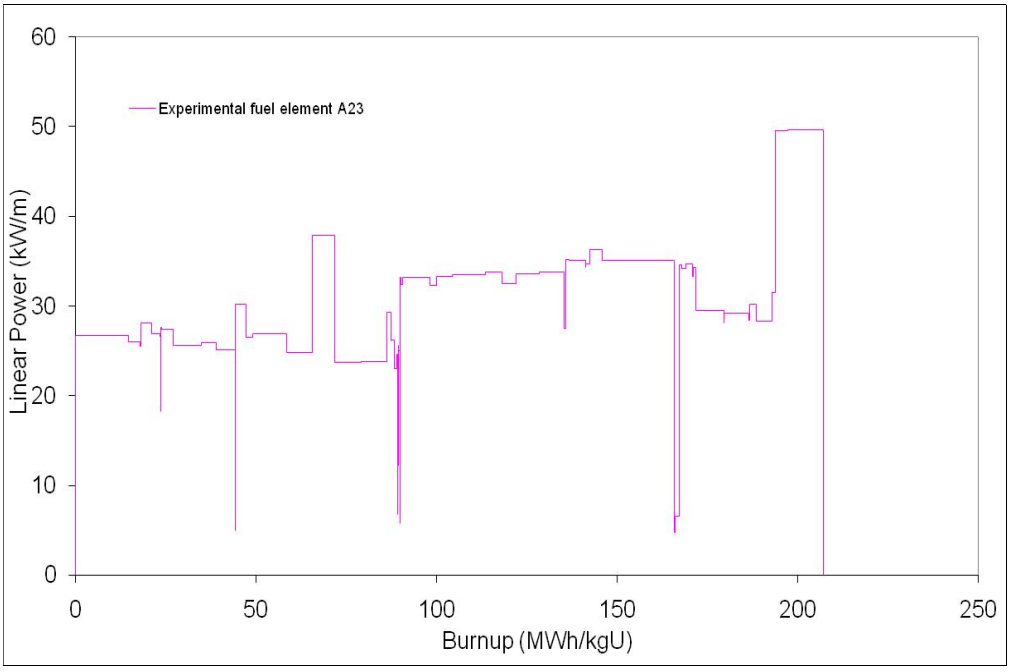

FIG.V-15. Irradiation history for the A23 test fuel element.

The visual examination [V-11] showed neither failures nor damage in the fuel element. Along, the entire length of the fuel element, circumferential ridges and distinct ridges at both ends near endcaps could be observed (Fig.V-16). Before the irradiation, the outer mean diameter was 13.054 mm. After irradiation the mean value increased to 13.167 mm. Some non-destructive examination results are presented in Table V-5.

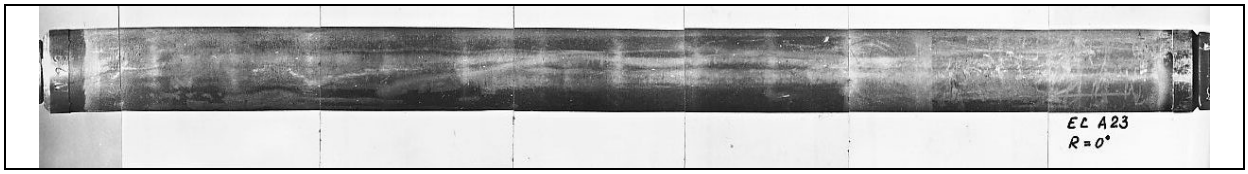

FIG.V-16. A23 test fuel element after irradiation.

TABLE V-5. POST-IRRADIATION MEASUREMENTS

Element	*Element Bow (mm)*	*Axial Elongation (mm)*	*Sheath Oxide Layer (µm)*		*Residual Sheath Strain* (%)*		*Ridge Height* (µm)*	*Gas Released Volume** (cm^3)*
			Outside	*Inside*	*Mid Pellet*	*Pellet Interface*		
A23	0.08	0.12	3-9	1-4	0.6	0.9	30	5.5

*Average value at the middle length region/ ** STP = Standard Temperature and Pressure

Ceramographic investigation of the grain size in sintered thorium pellets [V-10] needs appropriate surface preparation of the pellets. Conventional etching methods involve either chemical or thermal etching techniques being unsuitable for surface etching of irradiated thorium fuel. Transverse sections at the A23 element mid plane are presented in Fig.V-17. The thorium nuclear fuel is chemically stable and therefore it is very difficult to see the grain growths. The central zone of irradiated $(Th,U)O_2$ fuel pellets varied between 6.0 and 6.2 mm (Fig.V-17 (b)) at the section cut around 13.16 mm from the endcap.

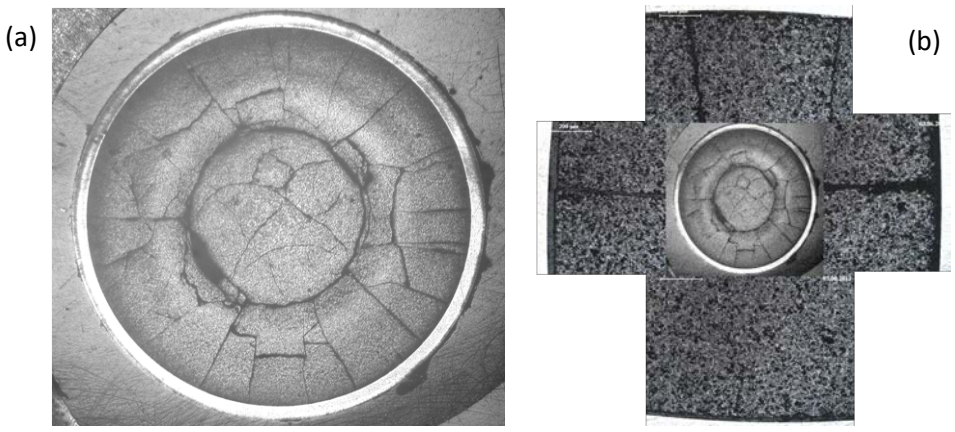

FIG.V-17. Micro structural features of the A23 element (transverse section): (a) Transverse section near the middle length of the element, (b) Detail in middle part of the transverse.

The computer code used to simulate this experiment was ROFEM, a modified version of the code used for thorium and uranium mixed oxides fuel. The improvements were implemented by INR Pitesti - Nuclear Fuel Performance Group. Some modifications within the fuel, include: theoretical density, melting temperature, thermal expansion, thermal conductivity, densifications, grain growth law and fission gas release were implemented.

Analyses on temperature (Fig.V-18), fission gas released (Fig.V-20), internal pressure (Fig.V-22), stress and strain deformation (e.g. Fig.V-19, Fig.V-21, Fig.V-23) were performed. Fuel temperature is the dominant parameter affecting most aspects of nuclear fuel element performance. It controls fuel expansion, fission product release and swelling; both processes are primary contributors to the stress and propensity for failure of the sheath.

For this stage of the ROFEM code development, the comparison between the experimental measurements and the calculated results showed a good agreement, the model used for the determination of grain growth law have been ameliorated.

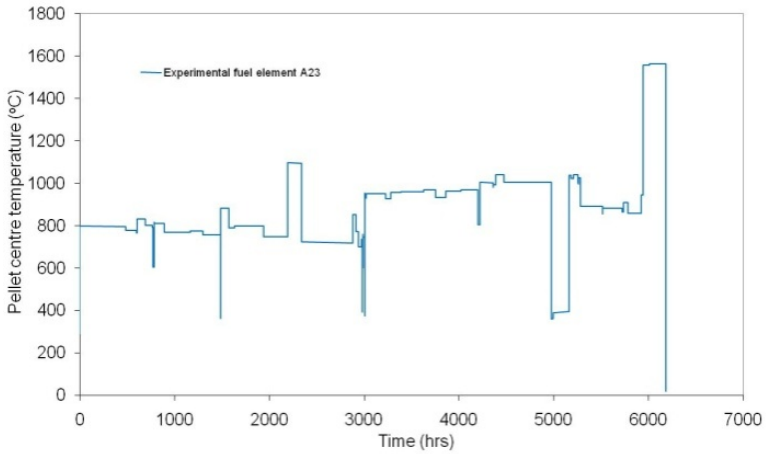

FIG.V-18. Fuel pellet centreline température.

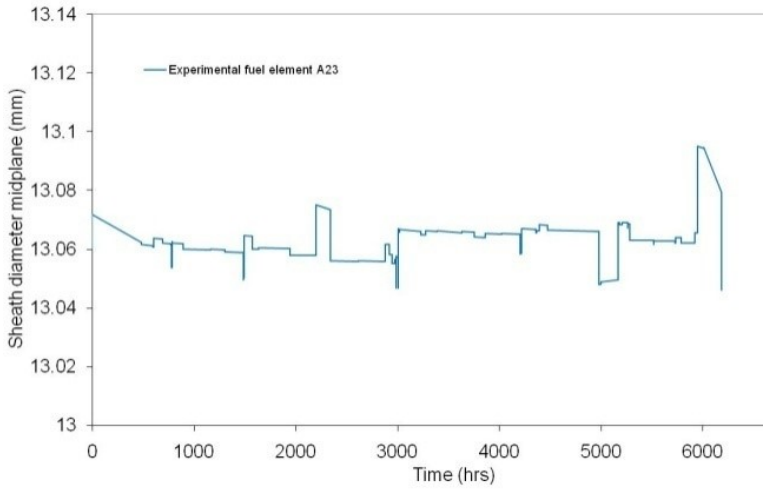

FIG.V-19. Sheath diameter at pellet mid-plane.

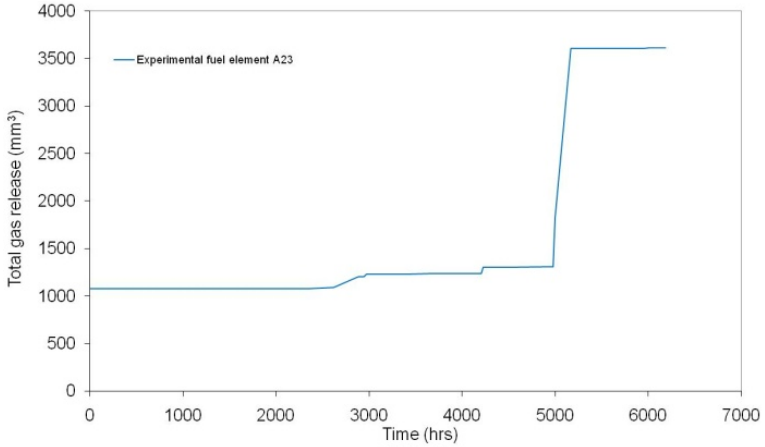

FIG.V-20. Total fission gas released.

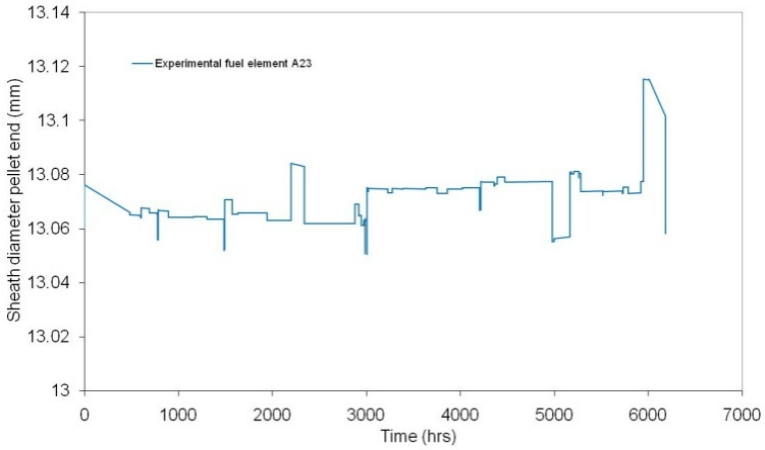

FIG.V-21. Sheath diameter at pellet end.

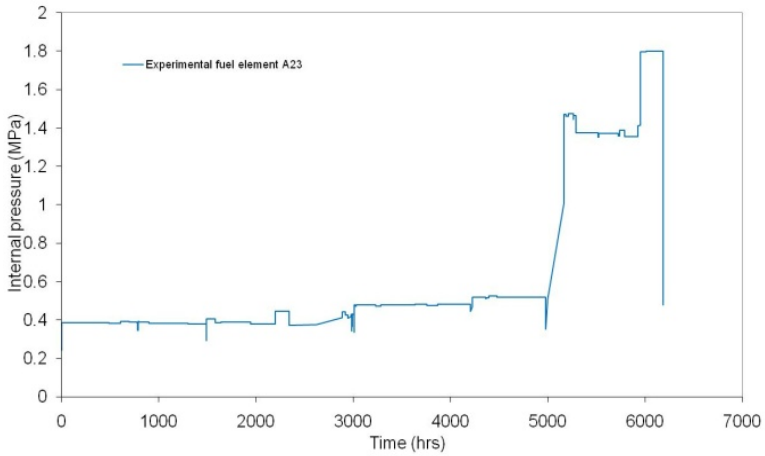

FIG.V-22. Internal gas pressure.

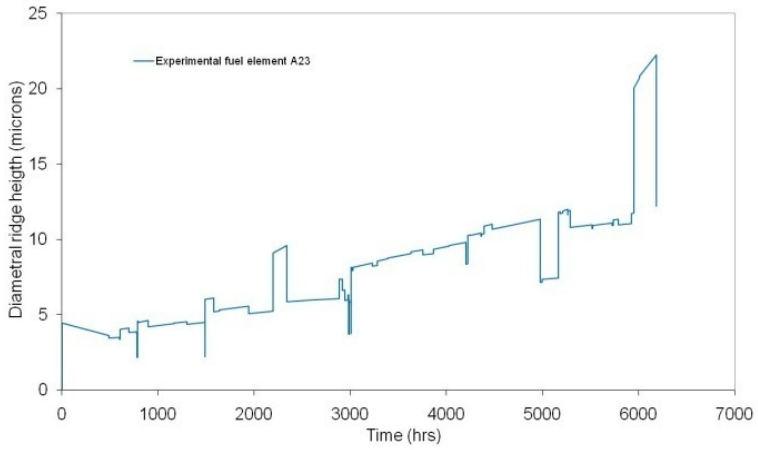

FIG.V-23. Diametral ridge height.

V-5. SUMMARY AND CONCLUSIONS

The following conclusions were reached:

- In this cycle the burnup is increased by trading off the conversion rate. The thorium is enriched with U-235 to achieve a better burnup. The main advantage of this type of fuel cycle comes from the burning of U-235 followed by U-233 build-up and, as U-233 is a better fissile material than U-235. The T43 bundle reactivity decreases with burnup more gradually than the one corresponding to 37R with NU or SEU. This means that the same discharge burnup, or even a better one, can be reached in the thorium cycle than in the uranium one, using the same initial U-235.

- The fuel discharge burnup is expected to be more than 20 MWd/kg-HE.

- The final plutonium inventory should be as low as possible. This point is very important for waste non-proliferation.

- The chain reaction is expected to be self-sustaining by U-233 build-up.

- The present design of T43 fuel bundle containing mixed oxide of thorium and uranium is one of the best option to move from ahead the actual natural uranium CANDU fuel to a next stage with a lot of benefits.

- Thorium has a low solubility, which makes irradiated thorium based fuels attractive for direct waste disposal.

ACKNOWLEDGEMENTS

This Research Contract was led by Chief Scientific Investigator, G. Olteanu of INR, Romania.

REFERENCES

[V-1] OLTEANU, G., Nuclear Fuel Bundle with 43 Elements Dedicated to APHWR, Report 9995, Institute for Nuclear Reactor (INR), Romania.

[V-2] International Atomic Energy Agency, Thorium Fuel Cycle- Potential Benefits and Challenges, TECDOC-1450, IAEA, Vienna (2005).
[V-3] International Atomic Energy Agency, Thorium Fuel Utilization. Options and Trends, TECDOC-13190, IAEA, Vienna (2002).
[V-4] ZHANG, Z., KURAN, S., "Status of Development of Thorium Fuel Cycle in CANDU Reactors", paper presented at the 4th Reuse International Workshop, Toronto, Canada, 2010.
[V-5] MARGEANU, C.A., RIZOIU, A., New Perspective on Using Thorium-Based Fuel in CANDU Reactors, Journal of Nuclear Research and Development **5** (2016) 35.
[V-6] DUMITRACHE, I., RIZOIU, A., Benchmark Problem for a CANDU6 Lattice Cell, Repor, 5933/2000, INR (2000).
[V-7] MARLEAU, G., Using of the T37 Bundle Fueled with Thorium-Uranium Mixed Oxide to Increase the Economic Performances of a CANDU Reactor, Report IR-11329, INR, Romania (2017); in Romanian.
[V-8] NEACSA, R., RIZOIU, A., PRISECARU, I., Improving CANDU Performance by Using Uranium-Thorium Mixed Oxide Fuel, Kerntechnik **83** (2018) 106.
[V-9] PRODEA, I., Irradiation Histories Generation using The DIREN Program for Thorium-based fuel. Comparison to The Case of Natural Uranium, Report IR-10719, INR, Romania (2015); in Romanian.
[V-10] PENN, W.J., WOOD, J.C., LO, R.K., CANDU Fuel Power ramp Performance Criteria, Nuclear technology **34** (1977) 249.
[V-11] OLTEANU, G. et al, Technical Specification for A23 and A24 Fuel Element Irradiation in Capsule C1 of TRIGA Research Reactor, Report 2247/1987, INR, Romania (1987).
[V-12] VALAN, V., Manufacturing of A23 - A24 Fuel Elements, Report 2307/1988, INR, Romania (1988).
[V-13] DRAGOMIRESCU, C., Irradiation of A24-A24 Fuel Elements, Report 2608/1988, INR, Romania (1988).
[V-14] PARVAN, M. et al, Post-Irradiation Examination Results for A23 and A24 Experimental Fuel Elements, Report 2758/1989, INR, Romania (1989).
[V-15] OLEANU, G., IONESCU, D.V., ROMAN, M.R., PARASCHIV, A., Romanian Irradiation Experiment on AHWR Type Fuel Elements Containing Mixed Oxide of Thorium and Uranium Pellets, Paper presented at Thorium Energy Conferences, Mumbai, India, 2015.
[V-16] IONESCU, D.V. et. al, Improvement of ROFEM Fuel Behavior Code for Simulation the Comportment of Mixed Oxide of Thorium and Uranium Fuel, Report 10000/2013, INR, Romania (2013).

ABBREVIATIONS

BARC	Bhabha Atomic Research Centre.
BNA	Burnable neutron absorber.
CANDU	Canada deuterium.
CHF	Critical heat flux.
CNEA	National Commission on Atomic Energy, Argentina.
CRP	Coordinated research project.
CVR	Coolant void reactivity.
EFP	End flux peaking.
FGR	Fission gas release.
FPD	Full power day.
HE	Heavy element.
I-SCC	Iodine induced stress corrosion cracking.
INR	Institute for Nuclear Reactor, Romania.
KAERI	Korea Atomic Energy Research Institute.
LER	Linear element rating.
LHGR	Linear heat generation rating.
LOCA	Loss of coolant accident.
LTA	Lead test assembly.
LWR	Light water reactor.
LZC	Liquid zone controller.
MOX	Mixed oxide.
NPP	Nuclear power plant.
NU	Natural uranium.
NUE	Natural uranium equivalent.
PCI	Pellet-cladding interaction.
PHWR	Pressurized heavy water reactor.
PIE	Post-irradiation examination.
SCC	Stress corrosion cracking.
SEU	Slightly enriched uranium.
37R	Reference 37-element fuel bundle.

CONTRIBUTORS TO DRAFTING AND REVIEW

ALVAREZ, L.	National Commission on Atomic Energy, Buenos Ares, Argentina
BASAK, U.	International Atomic Energy Agency
CHAN, P.	Royal Military Collage of Canada, Kinston, Ontario, Canada
OLTEANU, G.	Institute for Nuclear Reactor, Romania
PARK, J-H.	Korea Atomic Energy Research Institute, Taejon, Republic of Korea
SIM, K.	International Atomic Energy Agency
SINGH, J.	Bhabha Atomic Research Centre, Mumbai, India

Research Coordinated Meetings

Vienna, Austria, 8-10 October 2014
Buenos Aires, Argentina, 3-6 May 2016
Vienna, Austria, October 31-November 3, 2017

Consultancy Meeting

Vienna, Austria, 13-15 March 2018

IAEA
International Atomic Energy Agency

No. 25

ORDERING LOCALLY

In the following countries, IAEA priced publications may be purchased from the sources listed below or from major local booksellers.

Orders for unpriced publications should be made directly to the IAEA. The contact details are given at the end of this list.

CANADA

Renouf Publishing Co. Ltd

22-1010 Polytek Street, Ottawa, ON K1J 9J1, CANADA
Telephone: +1 613 745 2665 • Fax: +1 643 745 7660
Email: order@renoufbooks.com • Web site: www.renoufbooks.com

Bernan / Rowman & Littlefield

15200 NBN Way, Blue Ridge Summit, PA 17214, USA
Tel: +1 800 462 6420 • Fax: +1 800 338 4550
Email: orders@rowman.com Web site: www.rowman.com/bernan

CZECH REPUBLIC

Suweco CZ, s.r.o.

Sestupná 153/11, 162 00 Prague 6, CZECH REPUBLIC
Telephone: +420 242 459 205 • Fax: +420 284 821 646
Email: nakup@suweco.cz • Web site: www.suweco.cz

FRANCE

Form-Edit

5 rue Janssen, PO Box 25, 75921 Paris CEDEX, FRANCE
Telephone: +33 1 42 01 49 49 • Fax: +33 1 42 01 90 90
Email: formedit@formedit.fr • Web site: www.form-edit.com

GERMANY

Goethe Buchhandlung Teubig GmbH

Schweitzer Fachinformationen
Willstätterstrasse 15, 40549 Düsseldorf, GERMANY
Telephone: +49 (0) 211 49 874 015 • Fax: +49 (0) 211 49 874 28
Email: kundenbetreuung.goethe@schweitzer-online.de • Web site: www.goethebuch.de

INDIA

Allied Publishers

1st Floor, Dubash House, 15, J.N. Heredi Marg, Ballard Estate, Mumbai 400001, INDIA
Telephone: +91 22 4212 6930/31/69 • Fax: +91 22 2261 7928
Email: alliedpl@vsnl.com • Web site: www.alliedpublishers.com

Bookwell

3/79 Nirankari, Delhi 110009, INDIA
Telephone: +91 11 2760 1283/4536
Email: bkwell@nde.vsnl.net.in • Web site: www.bookwellindia.com

ITALY

Libreria Scientifica "AEIOU"

Via Vincenzo Maria Coronelli 6, 20146 Milan, ITALY
Telephone: +39 02 48 95 45 52 • Fax: +39 02 48 95 45 48
Email: info@libreriaaeiou.eu • Web site: www.libreriaaeiou.eu

JAPAN

Maruzen-Yushodo Co., Ltd

10-10 Yotsuyasakamachi, Shinjuku-ku, Tokyo 160-0002, JAPAN
Telephone: +81 3 4335 9312 • Fax: +81 3 4335 9364
Email: bookimport@maruzen.co.jp • Web site: www.maruzen.co.jp

RUSSIAN FEDERATION

Scientific and Engineering Centre for Nuclear and Radiation Safety

107140, Moscow, Malaya Krasnoselskaya st. 2/8, bld. 5, RUSSIAN FEDERATION
Telephone: +7 499 264 00 03 • Fax: +7 499 264 28 59
Email: secnrs@secnrs.ru • Web site: www.secnrs.ru

UNITED STATES OF AMERICA

Bernan / Rowman & Littlefield

15200 NBN Way, Blue Ridge Summit, PA 17214, USA
Tel: +1 800 462 6420 • Fax: +1 800 338 4550
Email: orders@rowman.com • Web site: www.rowman.com/bernan

Renouf Publishing Co. Ltd

812 Proctor Avenue, Ogdensburg, NY 13669-2205, USA
Telephone: +1 888 551 7470 • Fax: +1 888 551 7471
Email: orders@renoufbooks.com • Web site: www.renoufbooks.com

Orders for both priced and unpriced publications may be addressed directly to:

Marketing and Sales Unit
International Atomic Energy Agency
Vienna International Centre, PO Box 100, 1400 Vienna, Austria
Telephone: +43 1 2600 22529 or 22530 • Fax: +43 1 2600 29302 or +43 1 26007 22529
Email: sales.publications@iaea.org • Web site: www.iaea.org/books

19-00151

International Atomic Energy Agency
Vienna
ISBN 978–92–0–101319–4
ISSN 1011–4289